

Contents

1	Introduction.	1
1.1	Electron emission.	2
1.1.1	Kinetic electron emission.	2
1.1.2	Potential electron emission.	3
1.1.3	Many body excitations.	4
1.2	Resonant charge transfer during sputtering.	4
1.3	Structure of the thesis.	5
2	Basic theory of Auger and resonant charge transfer processes.	7
2.1	Hagstrum Theory of Auger Neutralization.	10
2.1.1	AN Transition rate.	12
2.1.2	Ion survival and neutralization probabilities.	18
2.1.3	Escape probability for an excited electron from the target.	21
2.1.4	Kinetic Energy Distributions for a static ion.	23
2.1.5	Effects that broaden the pure spectrum.	26
2.1.6	Kinetic Energy Distributions for a moving ion.	29
2.1.7	Conclusions on the Hagstrum model.	31
2.2	Developments of AN Theory.	32
2.2.1	“Magical” Energy.	33
2.2.2	Open problems	35
2.3	Resonant ionization mechanism in sputtering of metals.	35
2.3.1	TDAN Hamiltonian for scattering	38

2.3.2	TDAN Hamiltonian for sputtering	41
2.3.3	Sroubek's temperature model.	46
2.3.4	Quasi molecular interactions in sputtering.	48
3	Generalized Hamiltonian	51
3.1	Hamiltonian for one-electron tunneling.	51
3.1.1	The surface potential	54
3.1.2	Metal States	57
3.1.3	Atomic Potential	60
3.1.4	Atomic States	62
3.1.5	Image potential	66
3.1.6	Field Operator: selection of a truncated basis	68
3.1.7	Second quantized Hamiltonian for resonant electron transfer . . .	71
3.2	Hamiltonian for one and two-electron processes.	74
3.2.1	Electron screening.	74
3.2.2	Second quantized two-electron potential: collective excitations . .	76
3.2.3	Total Hamiltonian	78
3.3	Parametric time-dependence	78
4	Applications and results.	83
4.1	Fermi's golden rule formulation.	83
4.2	Experimental distribution.	89
4.3	Results compared with experimental spectra and with other models. . . .	90
4.4	Resonant charge transfer: spectral method.	95
4.5	Resonant charge transfer: wave packet propagation method.	103
5	Conclusions.	111
	Bibliography	117

Introduction.

The thesis deals with electronic processes induced at solid surfaces by localized, non adiabatical sources, such as slowly moving monoatomic particles or suddenly switched on localized states. In particular, ions beams of low impact kinetic energy (of the order or less than 1 keV) are considered. The main motivation of our study is that slow ions reflecting from (or within) a solid target provide a unique source for electronic excitations confined just to the surface region, making the related spectroscopies very surface sensitive tools to study solids. Besides, particles sputtered from surface carry with them precious information about the bulk structure of target. Several questions of both fundamental and practical interest are involved, concerning the ionization/neutralization of projectiles, the mechanisms of electron and photon emission, and the characteristics of sputtered particles from the solid.

Two main features are typical of ion-surface processes: (i) the change of charge in the projectile and (ii) the emission of particles by surface, i.e., electrons, atoms or photons. Our interest will be concerned with two cumbersome phenomena that have attracted much theoretical and experimental interest during the last thirty years. One is ion induced electron emission from metal surfaces and the other is secondary ion formation during sputtering of metals.

1.1 Electron emission.

Inelastic ion-surface collisions leading to electron emission are often accompanied by other processes like backscattering, sputtering and desorption. A widely used case-study is electron emission from alkali metal targets, following neutralization of slow projectiles of noble gases. This phenomenon generally involves three main steps, namely, excitation, transport, and escape of an electron through the surface of the sample. The first step is classified according to the kind of energy that the projectile provides to the excited electron. Indeed, a heavy projectile can excite the particle above the vacuum level either by kinetic or potential energy transfer. Therefore, two ejection mechanisms are established: one is known as “*Kinetic Electron Emission*” (KEE) and the other is called “*Potential Electron Emission*” (PEE). From the analysis of the spectrum of ejected electron, one can obtain essential information either on density of states of the target or on the effect of the projectile motion.

1.1.1 Kinetic electron emission.

KEE [1] was originally thought as a mechanism for electron excitation caused by direct binary collision with the incident ion, that penetrates the surface of the sample; target electrons close to the Fermi-level can be thought as free electrons, which are, then, ejected if the center of mass kinetic energy of the projectile is larger than the surface work function [2]. Excited electrons can, in turn, generate secondary excited electrons in a cascade multiplication. However, if the projectile is a low energy ion, most of the primary excited electrons do not have enough energy to excite other electrons above the vacuum level. In practice, only those electrons directly excited by ion contribute to the electron energy spectrum.

Another emission channel, subject to a threshold impact energy, was addressed to electron promotion in close atomic collisions [3]. The process occurs when the inner shells of the incoming ion, forming a transient molecule with a target atom, are promoted in energy. Then, some electrons of the projectile can occupy the outer shells, which are totally or partly empty and the promoted electrons can be directly excited above the

vacuum level. The vacancies left in the inner shells are most probably filled via an Auger transition, i.e., an electron of the outer shells can hop to an inner vacancy and the energy released can be sufficiently high to eject another electron, whose emission energy is related to energy difference between the active shells.

A third mechanism, called “*surface-assisted Kinetic Electron Emission*” (sKEE) has been recently proposed in experiments of slow ions impact on metal surfaces at normal or near normal incidence [4]. In this mechanism, for which no threshold impact energy is required, nonadiabatic excitations are allowed by a kind of localization or confinement of valence electrons by the surface potential.

1.1.2 Potential electron emission.

PEE [5, 6, 7] basically involves Auger-type processes, where the incoming ion, of sufficiently high ionization energy, is neutralized before hitting the surface of the target [8]. Accordingly, the energy released in the process is converted into electron excitation, which occurs when the ion is in the neighborhood of the surface. This explains why an Auger transition is practically unaffected by the scattering at the surface of the target. Besides, electron emission can occur only if the energy of the excited electron is greater than a threshold energy that depends either on the work function (ϕ) of the surface or on the ionization energy (I) of the impinging particle. Indeed, the ion-surface interaction modifies the energies of the projectile levels. Thus, if I' is the corrected ionization energy for an ion at atomic distances from the sample, PEE requires $I' > 2\phi$.

Auger transition are two-electron processes occurring in several forms, according to the origin of the electrons: in Auto-Ionization (AI), both participating electrons belong to the projectile; on the other hand, if one of the two electrons initially occupies a projectile level, and the other one lies in a valence state the target, the resulting process is called Auger de-excitation (AD); finally, in Auger neutralization (AN), the two active electrons originate from the valence band of the target.

PEE can be also induced by a resonant, one-electron tunneling from an occupied level of the valence band and an excited level of the incoming ion; in this case the projectile de-excites via AD [9].

1.1.3 Many body excitations.

Simple metals, as Aluminum or Magnesium, can also convert a part or the whole of the potential energy, released by projectile neutralization, into many body excitations. One of these is the excitation of a surface plasmon whose decay mostly occurs by energy transfer to a single valence electron (*plasmon-assisted neutralization*). The process requires the neutralization energy to exceed the plasmon energy, thus, slow He^+ and Ne^+ projectiles can excite the surface plasmon of Al and Mg, while Ar^+ ions cannot [10, 11]. Another form of collective response of the metal target is the singular behavior of electrons at the Fermi level, due to the abrupt change of charge of the projectile, which causes permanent deformations in the conduction band. So called shake-up electrons originate both from the electronic structure of the conduction band and the Pauli principle. Their signature, observed in experiments of Ar^+ impact on Al surfaces, is the exponential tailing of the kinetic energy distributions of ejected electrons [12].

1.2 Resonant charge transfer during sputtering.

When an atomic beam impinges upon a metal surface, the resonant coupling between some localized levels of the projectile and the continuous spectrum of conduction states, leads to the possibility of electron transfer between sputtered atom and the surface. The basic approach to the problem was given by the time dependent Anderson-Newns (TDAN) Hamiltonian [13], in which a single atomic state interacts with an (infinitely) broad band of states through one-body hopping potentials.

In the last decades, some theoretical and experimental studies have suggested the existence of other ionization mechanisms not included in the basic TDAN Hamiltonian. The main ionization channel, predominating at higher emission energies ($\gtrsim 100$ eV) is

well described by resonant tunneling of the electron between the outgoing atoms and the metal surfaces [14]. The other, observed at lower emission energies ($\lesssim 40$ eV), is suggestive of some form of surface excitation [16]. It was explained with a model accounting for the quasi-molecules transiently formed between the secondary emitted atoms and their nearest-neighbor substrate particles, put in motion by the collision cascade generated by the primary ion beam [17]. More recent studies have demonstrated that the resonant charge transfer is significantly affected by the crystal symmetry of the surface. In particular, the existence of a projected band gap along the surface normal of the crystal, partially prevents the penetration of electrons normal to the surface, which is the favored direction in atom-surface charge transfer processes [18, 19].

1.3 Structure of the thesis.

The thesis is structured in three main parts. In the first one, we describe the basic models for electron emission and charge transfer during ion-surface interaction.

In the second part, we present a formalism which allows to derive a generalized Hamiltonian, that includes Auger neutralization and resonant charge transfer processes, as well as many-body electron excitations.

In the third part, we apply the formalism to calculate: (1) the kinetic energy distribution of emitted electrons excited by Auger neutralization of Ar^+ ions on Al(111) surface; (2) the negative ionization probability for the negative ions of Silver and Gold ejected from their elemental surfaces.

Finally, in the last chapter, we discuss future developments and applications of the approach to different projectile/target combinations, with particular attention to nanostructured targets.

Chapter 2

Basic theory of Auger and resonant charge transfer processes.

When a positively charged, monoatomic ion beam slowly approaches a metal surface, non radiative charge-transfer processes occur that neutralize the incident particles to their ground state. An initial classification of these processes can be given according to whether the transferred electrons lose energy or not.

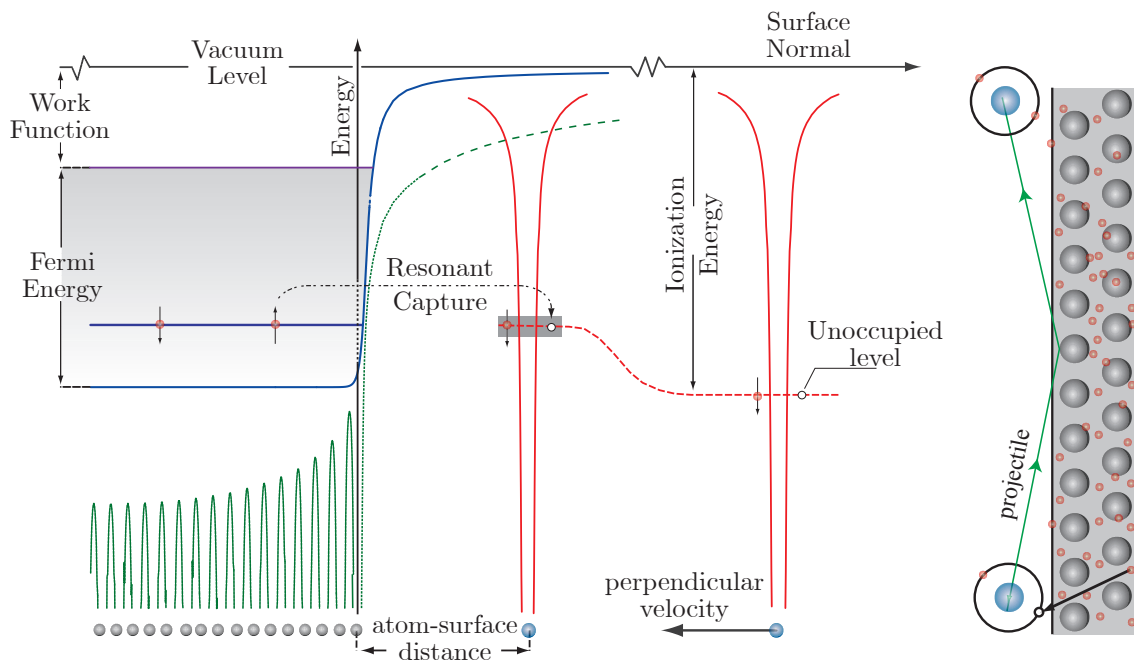


Figure 2.1: Resonant neutralization of a slow ion at a metal surface

If they do not, that is, in the case of a single charge exchange transition, if the initial and final states of the electron are degenerate in energy, the process is known as **resonant neutralization** (RN). Then, for an electron to be resonantly captured by the projectile, there must be an unoccupied atomic level degenerate with an occupied metal state (Fig. 2.1). A similar mechanism occurs when an atom of the sample is ejected by the collision cascade generated by the incident beam. The outgoing, secondary particle can be, accordingly, ionized positively or negatively.

If the impinging ion has only one active level with a large ionization potential, compared to the surface work function, resonant transitions are forbidden. In this case, nonradiative, **Auger-type processes** occur that simultaneously neutralize the ion and excite a second electron, which may be emitted into vacuum. As we shall see, the kinetic-energy distribution of these ejected electrons contains spectroscopic information concerning the electronic structure in the surface region of the solid.

It should be noticed that both resonant and non resonant transitions are fast relative to the time (about 10^{-11} s) during which the atom is in contact with the electrons of the solid before it has collided with the surface.

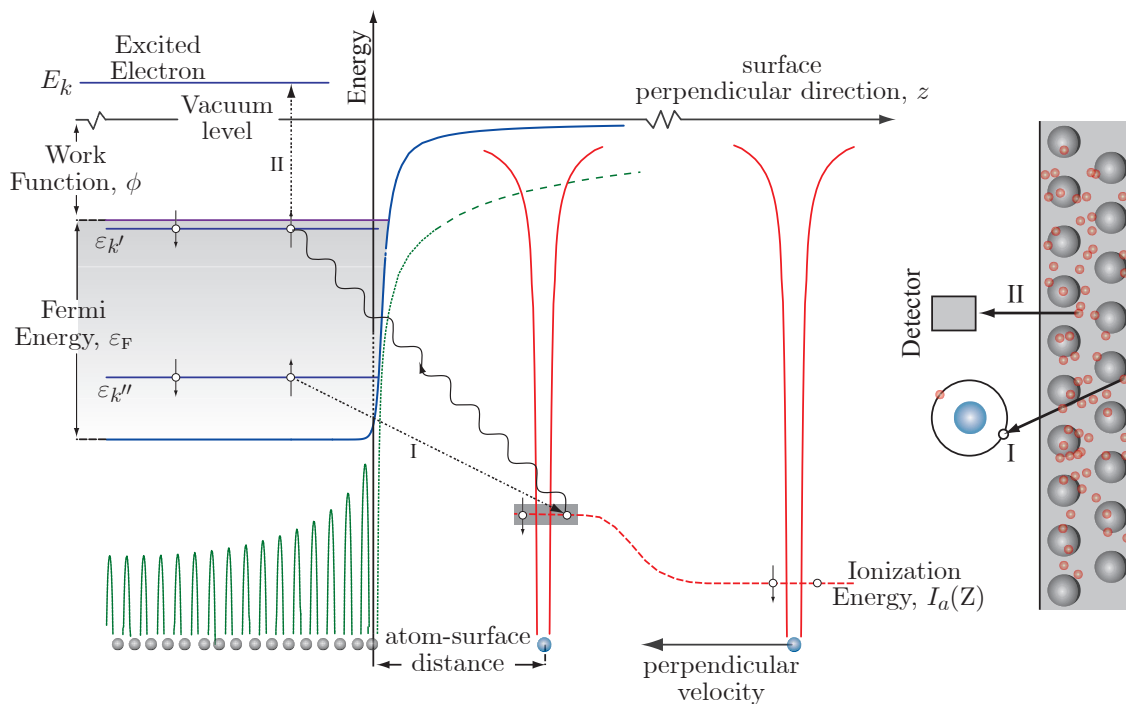


Figure 2.2: Auger neutralization of a slow ion at a metal surface

Auger electron emission can be further classified on the basis of the mechanisms that convert the potential energy released during ion neutralization into electron excitation. In **Auger neutralization** (AN), shown in Fig. 2.2, two electrons, in the filled valence band of the metal, interact when the incoming ion is just outside the metal surface, exchanging energy and momentum. One electron, the neutralizing electron, tunnels through the potential barrier into the potential well, presented by the ion, and drops to the vacant atomic ground level (transition I, in Fig. 2.2). The energy released in this transition is taken up by the second interacting electron which now may have sufficient energy to escape from the metal (transition II, in Fig. 2.2). Both transitions I and II can take place anywhere within the filled valence band so that the ejected electrons have a range of energies rather than one specific energy.

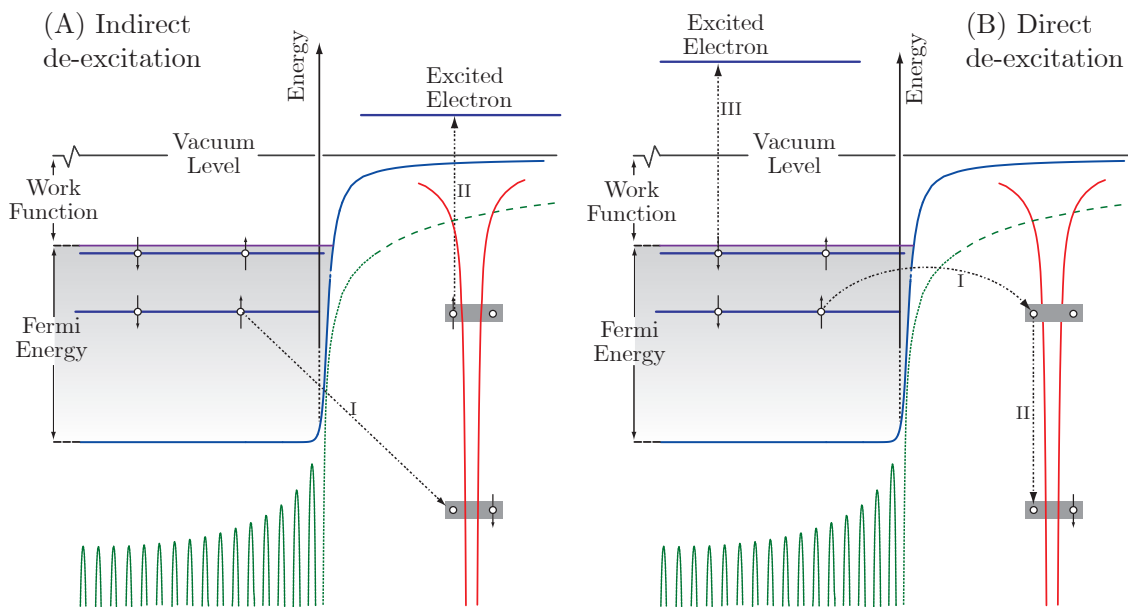


Figure 2.3: Direct and indirect de-excitation following resonant neutralization of a slow ion at a metal surface

Indirect Auger de-excitation (AD) occurs when the projectile approaches the surface into an excited state. Then, a valence electron from the surface tunnels to the unoccupied ionic ground state (transition I in Fig. 2.3(A)) and the excited electron of the projectile is ejected (transition II in Fig. 2.3(A)). **Direct Auger de-excitation** follows resonant neutralization of the projectile (transition I in Fig. 2.3(B)) into an excited state (RN+AD): the ion decays from his excited state emitting an electron (transitions II and III in Fig. 2.3(B)).

Auger neutralization and de-excitation processes are in competition: the occurrence of one mechanism in preference to another depends either on the surface work function or on the energies of the projectile levels near surface. For example, in experiments of 100 – 1000 eV-Ar⁺ ions bombarding Al samples PEE is almost entirely due to AN processes [12, 19]. In fact although, far from the surface the energies of lowest excited states of Ar are nearly degenerate with the Fermi energy of Al, the interaction with the surface yields a positive shift of about 1 – 2 eV, making negligible the probability for RN+AD processes.

The first part of this chapter is devoted to the theory that explains electron emission from a solid surface, following Auger neutralization (AN) of an incident ion: there, will be described a model due to H. D. Hagstrum [8] which allows to identify the broadening of the kinetic energy distributions of ejected electrons. The second part concerns the problem of secondary ion formation during sputtering. In particular, we discuss the problem of resonant charge transfer between the ejected atom and the surface. Following the seminal works of Sroubek [15, 16], we introduce the general Anderson-Newns Hamiltonian as starting point. Then, we obtain an expression for the rate of positive ionization as a function of the ion velocity.

2.1 Hagstrum Theory of Auger Neutralization.

Before Hagstrum, it was only known that electrons can be ejected from metal surfaces by slow ions. It was Olifant [20], in the late 20's, who first observed that when positive ions of He were incident on a Mo target, the ions were neutralized and electrons given off. Subsequently, Olifant and Moon [21] used a resonant tunneling mechanism to explain the effect. During 1930s-1950s, Massey [22], Shekhter [23] and, then, Cobas and Lamb, suggested a two-stage process, i.e., resonant neutralization followed by Auger de-excitation.

In his pioneering papers [25], Hagstrum took into account the following aspects never treated in earlier theories:

- initial-state lifetime and nonadiabatic excitation of electrons from the filled band into states above the Fermi level from which they can participate to the Auger process;
- dependence of the matrix elements of the electron-electron interaction on the angle formed by the excited electron’s velocity with the surface normal;
- probability that an excited electron can escape from the surface;
- variation of the energy level(s) of the impinging ion and of the surface parameters as the projectile approaches the surface;
- final-state lifetime of the target/projectile system;

El.	ε_F (eV)	ϕ (eV)	El.	ε_F (eV)	ϕ (eV)
Cu	7.23	4.4	Ag	5.49	4.3
Na	3.24	2.35	Au	5.53	4.3
Cs	1.59	1.81	Fe	11.1	4.31
W	5.00	5.2	K	2.12	2.22
Al	11.7	4.08	Pb	9.47	4.25

Table 2.1: Theoretical Fermi energies (ε_F), calculated from a free electron gas model, and experimental work functions (ϕ), measured by x-ray photoemission spectroscopy, for some common metals.

Hagstrum also discussed the role of resonant charge transfer processes, in order to determine the relative strength of the AN and RN+AD mechanisms. Finally, He was concerned with the competition of another mechanism for electron emission, due kinetic energy transfer from the impinging ion to the ejected electron. Hagstrum demonstrated that Auger processes, induced by slow, noble gas ions, occur with higher probability on the inward trip of the particle toward the surface, at a distance where processes involving kinetic energy can be neglected. Indeed later studies [12, 19, 11] showed that electrons ejected via kinetic energy transfer from the incident beam have a sharp spectrum, peaked at kinetic energies below ~ 1 eV.

The Hagstrum's model is based on the determination of the distribution of emitted electrons N vs their kinetic energy E_k , following the neutralization of the impinging ion. A smooth and structureless metal surface is considered, with the properties attributed to an atomically clean polycrystalline surface, i.e., Fermi Energy ε_F , measured from the bottom of the conduction band, work function ϕ and conduction band width $\varepsilon_0 = \varepsilon_F + \phi$. The values used for ε_F and ϕ , reported in table 2.1 for most common metals, are either calculated or derived from experiments [26, 27]

2.1.1 AN Transition rate.

We consider an AN process, as schematized in Figs. 2.2 and 2.4, where $\varepsilon_{k'}$ and $\varepsilon_{k''}$ are the initial energies, relative to the vacuum level, of the emitted and neutralizing electrons that occupy the valence states $|k'\rangle$ and $|k''\rangle$, respectively.

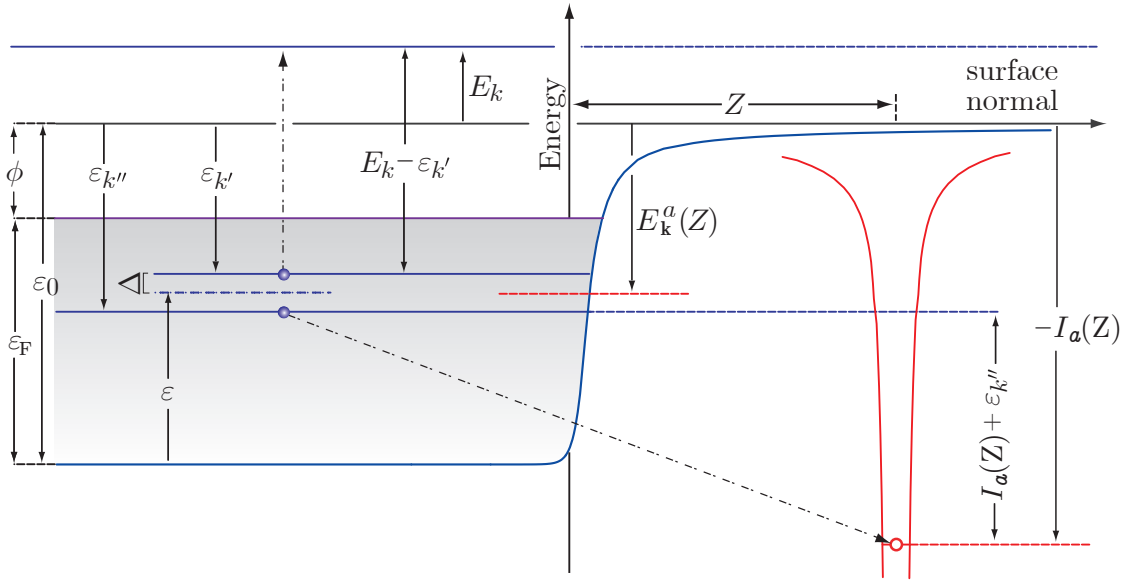


Figure 2.4: Energies involved in the Hagstrum's model for AN

The incoming ion, at distance Z , has an empty state $|a(Z)\rangle$ with energy $\varepsilon_a(Z)$, measured from the vacuum level, and ionization energy $I_a(Z) = -\varepsilon_a(Z)$. Neutralization occurs by tunneling of a valence electron, which releases an energy equal to $\varepsilon_{k''} + I_a(Z)$. By conversion into $E_k - \varepsilon_{k'}$, the energy is provided to another valence electron that can escape the metal and be detected in the state $|k'\rangle$, with kinetic energy E_k . Energy

conservation implies that the initial energy of the system equals its final energy, i.e.,

$$\varepsilon_{k''} + \varepsilon_{k'} = E_k - I_a(Z), \quad (2.1)$$

which means that the kinetic energy of the emitted electron in the vacuum is

$$E_k = \varepsilon_{k'} + \varepsilon_{k''} + I_a(Z). \quad (2.2)$$

The maximum kinetic energy available to an excited electron requires that both participating electrons, in their initial states, lie at the Fermi level:

$$E_{\text{max}} = -2\phi + I_a(Z). \quad (2.3)$$

Thus, for an electron to be excited above the vacuum level E_{max} needs to be positive, i.e., $I_a(Z) > 2\phi$.

It follows that the many body Hamiltonian, \mathcal{H}_{AN} , for ion-induced Auger electron emission depends parametrically on the ion-surface distance and involves a set of Fermion operators related to: the ion state ($c_a(Z)$, $c_a^\dagger(Z)$), the valence states ($c_{k'}$, $c_{k''}$, $c_{k'}^\dagger$, $c_{k''}^\dagger$) and the continuous states above the vacuum level (C_k , C_k^\dagger). The two-electron, Auger potential is specified by the matrix elements $V_{ak''}^{kk'}(Z)$ that, in the simplest case, may be represented by a screened Coulomb potential,

$$V_{ak''}^{kk'}(Z) = \langle a(Z) | \langle k | \frac{\exp(-\mu |\hat{r}_1 - \hat{r}_2|)}{|\hat{r}_1 - \hat{r}_2|} | k' \rangle | k'' \rangle, \quad (2.4)$$

of inverse screening length μ and in atomic units (that will be used henceforward). Neglecting the superposition of atomic and metal states, we can write

$$\mathcal{H}_{\text{AN}} = \mathcal{H}_0 + \mathcal{V}_{\text{AU}} \quad (2.5a)$$

$$\mathcal{H}_0 = \varepsilon_a(Z) c_a^\dagger(Z) c_a(Z) + \sum_{k'} \varepsilon_{k'} c_{k'}^\dagger c_{k'} + \sum_k E_k c_k^\dagger c_k \quad (2.5b)$$

$$\mathcal{V}_{\text{AU}} = \sum_{k,k',k''} V_{ak''}^{kk'}(Z) c_k^\dagger c_a^\dagger(Z) c_{k'} c_{k''}. \quad (2.5c)$$

The total transition rate for AN of an ion, when its distance (Z) from the surface is frozen, can be calculated from the (time independent) Fermi's golden rule as:

$$\frac{1}{\tau}(Z) \propto \sum_f |V_{fi}(Z)|^2 \delta(E_f(Z) - E_i). \quad (2.6)$$

The latter involves an initial state $|i\rangle$, with the target in its ground state and the projectile positively charged, and a group of final states $\{|f(Z)\rangle\}$, with an excited electron above the Fermi level and the projectile neutralized. In eq. (2.6), $V_{fi}(Z) = \langle f(Z)|\mathcal{V}_{\text{AU}}|i\rangle$ is the matrix element of the many body electron-electron potential and the Dirac δ -function ensures energy conservation. Ignoring collective excitations in the many electron system, we can write

$$\frac{1}{\tau}(Z) \propto \sum_k \sum_{k'k''} \left| V_{ak''}^{kk'}(Z) \right|^2 \delta(E_k - I_a(Z) - \varepsilon_{k'} - \varepsilon_{k''}). \quad (2.7)$$

This relationship is simplified when we express it in the “continuous limit”, that is: we transform the summations over the electron momenta (k , k' and k'') into integrals over energies (E_k , $\varepsilon_{k'}$ and $\varepsilon_{k''}$) and solid angles (Ω_k , $\Omega_{k'}$ and $\Omega_{k''}$),

$$\begin{aligned} \frac{1}{\tau}(Z) &\propto \int d^2\Omega_k \int d^2\Omega_{k'} \int d^2\Omega_{k''} \int_{-\phi}^{\infty} dE_k \rho(E_k) \int_{-\varepsilon_0}^{-\phi} d\varepsilon_{k'} \rho_c(\varepsilon_{k'}) \\ &\times \int_{-\varepsilon_0}^{-\phi} d\varepsilon_{k''} \rho_c(\varepsilon_{k''}) \left| V_{ak''}^{kk'}(Z) \right|^2 \delta(E_k - I_a(Z) - \varepsilon_{k'} - \varepsilon_{k''}), \end{aligned} \quad (2.8)$$

via the density of final excited states $\rho(E_k)$ and the densities of initial valence states $\rho_c(\varepsilon_{k'})$, $\rho_c(\varepsilon_{k''})$. The integration limits in eq. (2.8) are established from the condition that thermal interactions can be neglected; therefore, at the absolute zero, the excited electron has an energy above the Fermi level and that the initial electronic states lie within the Fermi surface.

A further clarification of the essential features of the process is achieved by averaging out the angular dependence of the matrix element (2.4) on the initial states. To do so, we need to evaluate the double angular integral

$$W_a^k(\varepsilon_{k'}, \varepsilon_{k''}; Z) = \int d^2\Omega_{k'} \int d^2\Omega_{k''} \left| V_{ak''}^{kk'}(Z) \right|^2, \quad (2.9)$$

which turns out to be a very hard task to be performed analytically. Hagstrum did not attempt a first principle calculation of (2.9), but, on experimental bases, he separated “the magnitude of the matrix element, as a function of the distance of the atomic particle from the surface, and its dependence upon the angle between the excited electron’s velocity and the surface normal”. Thus, he proposed the factorization

$$W_a^k(\varepsilon_{k'}, \varepsilon_{k''}; Z) = F(\varepsilon_{k'}, \varepsilon_{k''}; Z) p_{\theta_k}(E_k), \quad (2.10)$$

where the unknown dependence of the matrix element on the initial state energies, as well as on the projectile-surface distance, is contained in $F(\varepsilon_{k'}, \varepsilon_{k''}; Z)$. The other factor in eq. (2.10), namely $p_{\theta_k}(E_k)$, labels the probability density that an excited electron, with momentum k and energy E_k , has the solid angle Ω_k . Due to the symmetry of the problem- and to the choice of an ideal flat surface- the matrix element (2.10) does not depend on the azimuthal angle of the excited electron momentum. This implies that the quantity

$$dP_{\theta_k}(E_k) = 2\pi p_{\theta_k}(E_k) \sin \theta_k d\theta_k \quad (2.11)$$

is the probability that the momentum k , at the fixed energy E_k , lies on the lateral surface of a cone forming an angle in the interval $(\theta_k, \theta_k + d\theta_k)$, with the surface normal.

Now, for every kinetic energy E_k , the probability that the electron momentum lies within the entire solid angle is 1, then, the total transition rate (2.8) can be rewritten as

$$\begin{aligned} \frac{1}{\tau}(Z) &\propto \int_{-\phi}^{\infty} dE_k \rho(E_k) \int_{-\varepsilon_0}^{-\phi} d\varepsilon_{k'} \rho_c(\varepsilon_{k'}) \\ &\times \int_{-\varepsilon_0}^{-\phi} d\varepsilon_{k''} \rho_c(\varepsilon_{k''}) F(\varepsilon_{k'}, \varepsilon_{k''}; Z) \delta(E_k - I_a(Z) - \varepsilon_{k'} - \varepsilon_{k''}). \end{aligned} \quad (2.12)$$

We can, thus, introduce the characteristic function

$$S_a(E_k; Z) = \int_{-\varepsilon_0}^{-\phi} d\varepsilon_{k'} \rho_c(\varepsilon_{k'}) \int_{-\varepsilon_0}^{-\phi} d\varepsilon_{k''} \rho_c(\varepsilon_{k''}) \quad (2.13)$$

$$\times F(\varepsilon_{k'}, \varepsilon_{k''}; Z) \delta(E_k - I_a(Z) - \varepsilon_{k'} - \varepsilon_{k''}), \quad (2.14)$$

which allows to express eq. (2.12) in the form:

$$\frac{1}{\tau}(Z) \propto \int_{-\phi}^{\infty} dE_k \rho(E_k) S_a(E_k; Z). \quad (2.15)$$

The physical interpretation of $S_a(E_k; Z)$ is straightforward: it gives a measure of the number of electrons excited to a state $|k\rangle$ of energy $E_k > \phi$, provided that the incident ion has not been neutralized before reaching the distance Z . More importantly, multiplying (2.13) with the density of final excited states, and normalizing the resulting expression to unity, we get

$$p_{\text{EX}}(E_k; Z) = \frac{\rho(E_k) S_a(E_k; Z)}{\int_{-\phi}^{\infty} dE_k \rho(E_k) S_a(E_k; Z)}, \quad (2.16)$$

which denotes the probability density, per unit energy, for an AN transition with the ion state empty at distance Z .

In order to get a closer insight into the effect of (2.13), we define a new set of energy variables,

$$\varepsilon = \frac{\varepsilon_{k'} + \varepsilon_{k''}}{2} + \varepsilon_0, \quad \Delta = \frac{\varepsilon_{k'} - \varepsilon_{k''}}{2}, \quad E_k^a(Z) = \frac{E_k - I_a(Z)}{2}, \quad (2.17)$$

with the physical interpretation shown in Fig. 2.4. The transformation yields

$$\begin{aligned} S_a(E_k; Z) = & \left[\int_0^{\frac{\varepsilon_{\text{F}}}{2}} d\varepsilon \int_{-\varepsilon}^{\varepsilon} d\Delta + \int_{\frac{\varepsilon_{\text{F}}}{2}}^{\varepsilon_{\text{F}}} d\varepsilon \int_{\varepsilon - \varepsilon_{\text{F}}}^{\varepsilon_{\text{F}} - \varepsilon} d\Delta \right] \delta(E_k^a(Z) - \varepsilon + \varepsilon_0) \\ & \times \rho_c(\varepsilon + \Delta - \varepsilon_0) \rho_c(\varepsilon - \Delta - \varepsilon_0) F(\varepsilon + \Delta - \varepsilon_0, \varepsilon - \Delta - \varepsilon_0; Z). \end{aligned} \quad (2.18)$$

If we also neglect the variation of the matrix element (2.10), with either $\varepsilon_{k'}$ or $\varepsilon_{k''}$, by approximating

$$F(\varepsilon_{k'}, \varepsilon_{k''}; Z) \approx F_0(Z), \quad (2.19)$$

we obtain

$$S_a(E_k; Z) = 2 F_0(Z) A(\omega)|_{\omega=E_k^a(Z)} \quad (2.20)$$

where we are left with the so called *Auger Transform*:

$$A(\omega) = \int_0^{\omega+\varepsilon_0} d\Delta \rho_c(\omega + \Delta) \rho_c(\omega - \Delta) \quad \text{if } 0 < \omega + \varepsilon_0 < \frac{\varepsilon_F}{2}, \quad (2.21a)$$

$$= \int_0^{-\phi-\omega} d\Delta \rho_c(\varepsilon - \Delta) \rho_c(\varepsilon + \Delta) \quad \text{if } \frac{\varepsilon_F}{2} < \omega + \varepsilon_0 < \varepsilon_F, \quad (2.21b)$$

which turns out to be the self-convolution of the one electron density of occupied states of the conduction band. From this relationship, we see that both the total rate

$$\frac{1}{\tau}(Z) \propto F_0(Z) \int_{-\phi}^{\infty} dE_k \rho(E_k) A(E_k^a(Z)), \quad (2.22)$$

and the probability density

$$p_{\text{EX}}(E_k, Z) = \frac{\rho(E_k) A(E_k^a(Z)) \Theta(E_k + \phi)}{\int_{-\phi}^{\infty} dE_k \rho(E_k) A(E_k^a(Z))}, \quad (2.23)$$

depend on the product of the self-folded density of populated states, below the Fermi level, and the density of excited states, above the Fermi level.

We can focus on (2.23), remarking that

$$dP_{\text{EX}}(E_k, Z) = p_{\text{EX}}(E_k, Z) dE \quad (2.24)$$

can be, indeed, interpreted as an excitation probability once we are sure that the ion state $|a(Z)\rangle$ is unoccupied. To do so, we need to include in the calculation the probability

$$dP_{\text{N}}(Z, v_{\perp}) = p_{\text{N}}(Z, v_{\perp}) dZ \quad (2.25)$$

that the incoming ion, of constant velocity v_{\perp} , perpendicular to the surface plane, undergoes Auger neutralization in the distance interval $(Z, Z + dZ)$. It follows that the kinetic energy distribution of electrons excited by AN is

$$N_{\text{I}}(E_k) = N_0 \int_0^{\infty} dZ p_{\text{N}}(Z, v_{\perp}) p_{\text{EX}}(E_k, Z), \quad (2.26)$$

with N_0 a normalization constant.

In order to determine the distribution of ejected electron, we have to consider that not all excited electrons are actually emitted from the sample. In fact, every surface has its own transmission function, i.e., the fraction of excited electrons, with kinetic energy E_k , that escape the surface barrier. In Hagstrum's model, such a quantity is evaluated by

$$T(E_k) = 2\pi \Theta(E_k) \int_0^{\theta_c} d\theta_k \sin \theta_k p_{\theta_k}(E_k), \quad (2.27)$$

where $\theta_c = \theta_c(E_k)$ is the maximum value of θ_k for which an excited electron is ejected. Since $p_{\text{EX}}(E_k, Z)$ does not depend on Ω_k , by eq. (2.26) and eq. (2.27) the kinetic energy distribution of emitted electrons is:

$$N(E_k) = T(E_k) N_1(E_k) \quad (2.28)$$

Summing up, we have seen that AN is specified by the total rate (2.22) and the distribution of emitted electrons (2.23). These quantities are modeled by: (i) the absolute square of the matrix elements of the Auger potential (2.10), yielding the characteristic function (2.13), (ii) the ion neutralization probability (2.25) and the transmission function (2.27).

2.1.2 Ion survival and neutralization probabilities.

Based on experimental evidences [8], Hagstrum observed that (2.22) has the exponential dependence

$$\frac{1}{\tau}(Z) = \omega_0 \exp(-\gamma Z), \quad (2.29)$$

where $\omega_0 = \exp(\gamma Z_0)/\tau_0$ contains the AN transition rate

$$\frac{1}{\tau_0} = \frac{1}{\tau}(Z_0) = F_0(Z_0) \int_{-\phi}^{\infty} dE_k \rho(E_k) S(E_k^a(Z_0)) \quad (2.30)$$

for a projectile at the distance of closest approach to surface, Z_0 , and

$$\gamma = \frac{1}{Z - Z_0} \ln \left(\frac{\tau}{\tau_0}(Z) \right) \quad (2.31)$$

depends on the decay of the electronic wave function from the valence band, outside the surface. Indeed (2.30) can be estimated by fitting with experiments, while the inverse length (2.31) takes typical values in the range $\gamma = 2 - 5 \text{ \AA}^{-1}$.

Let us consider an ion moving perpendicularly to the surface with a constant velocity v_\perp that is small with respect to the Fermi velocity $v_F = \sqrt{2\varepsilon_F}$. We can interpret the quantity $dZ/(\tau(Z)v_\perp)$ as the probability that the ion, moving with speed v_\perp through the element dZ at Z , will undergo an AN transition. Hence, the probability that the incoming ion will reach the distance Z without being neutralized, from an infinite distance toward the surface, is:

$$p_s(Z, v_\perp) = \exp \left[- \int_Z^\infty \frac{1}{\tau(Z')} \frac{dZ'}{v_\perp} \right]. \quad (2.32)$$

Here, the subscript s stands for “survival”, thus, that the probability that the ion survives neutralization, from $Z' = \infty$ to $Z' = Z$, and undergoes an AN transition in the space dZ , is:

$$p_N(Z, v_\perp) dZ = p_s(Z, v_\perp) \frac{dZ}{\tau(Z)v_\perp} = \frac{1}{\tau(Z)v_\perp} \exp \left[- \int_Z^\infty \frac{1}{\tau(Z')} \frac{dZ'}{v_\perp} \right]. \quad (2.33)$$

If we, now, replace the transition rate with eq. (2.29), in eqs. (2.32) and eq. (2.33), we obtain

$$p_s(Z, v_\perp) = \exp \left(- \frac{e^{-\gamma(Z-Z_0)}}{\gamma v_\perp \tau_0} \right) = \exp \left(- \frac{\omega_0}{\gamma v_\perp} e^{-\gamma Z} \right) \quad (2.34)$$

and

$$p_N(Z, v_\perp) = \frac{e^{-\gamma(Z-Z_0)}}{v_\perp \tau_0} \exp \left(- \frac{e^{-\gamma(Z-Z_0)}}{\gamma v_\perp \tau_0} \right) = \frac{\omega_0 e^{-\gamma Z}}{v_\perp} \exp \left(- \frac{\omega_0}{\gamma v_\perp} e^{-\gamma Z} \right). \quad (2.35)$$

Fig. 2.5 shows both probability distributions (2.34) and (2.35), together with the neutralization distance

$$Z_m = Z_0 + \frac{1}{\gamma} \ln \left(\frac{1}{\gamma v_{\perp} \tau_0} \right), \quad (2.36)$$

where $P_N(Z, v_{\perp})$ is maximum, which has the same order of the mean distance of neutralization.

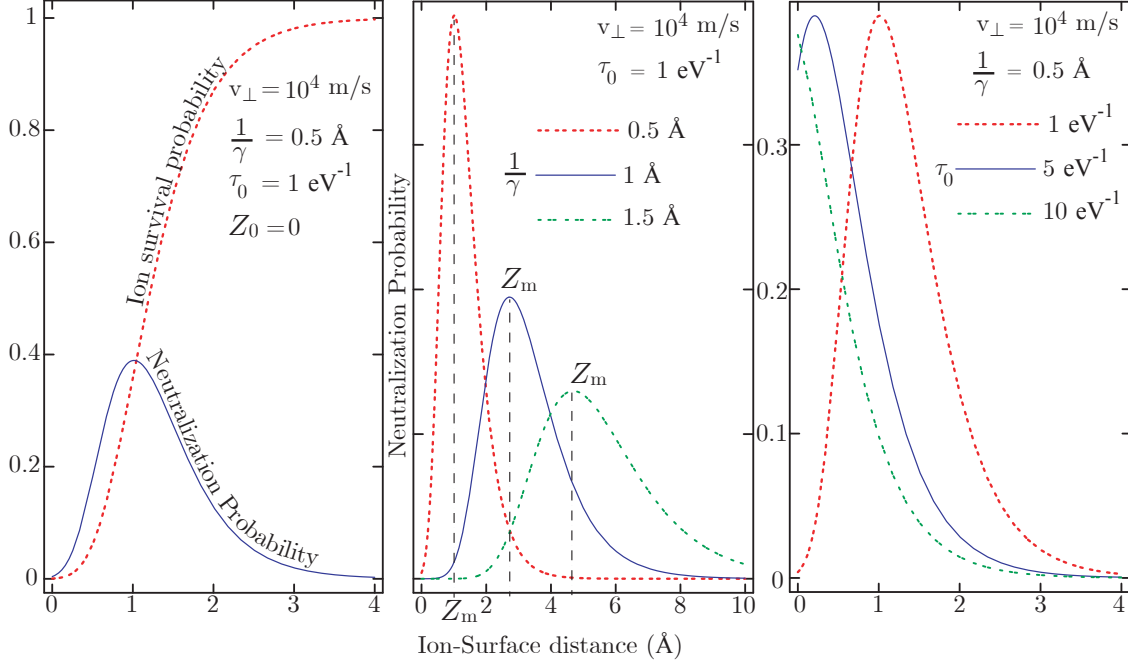


Figure 2.5: Ion survival (2.34) and neutralization (2.35) probability distributions, for different values of the input parameters γ , τ_0 .

Assuming that the transition rate (2.29) holds also for distance of closest approach $Z_0 = 0$, we have

$$\int_{Z_0}^{\infty} p_N(Z, v_{\perp}) dZ = 1 - p_s(Z_0, v_{\perp}) = 1 - \exp \left(-\frac{1}{\alpha v_{\perp} \tau_0} \right). \quad (2.37)$$

Such an integral is of great interest because it specifies the probability the ion is neutralized during his whole inward trip towards the surface. If we consider slow ions, from eq. (2.37), we also have:

$$\lim_{v_{\perp} \rightarrow 0} \int_{Z_0}^{\infty} p_N(Z, v_{\perp}) dZ = 1 \quad (2.38)$$

This means that the probability that AN occurs for very slow ions, while they are approaching the surface, is very close to unity.

2.1.3 Escape probability for an excited electron from the target.

In deriving eq. (2.27), we mentioned that of all electrons excited by AN only a part has enough energy to leave the metal. This is because, the electron momentum of an excited electron, within the target, is refracted, outside the surface, by the surface barrier. The latter can be approximated, in the simplest case, to a step potential of height $-\varepsilon_0$ along the surface perpendicular coordinate. Specifically, if k is the electron momentum inside the metal and k' is the electron momentum outside the solid, in the refraction process, the parallel component of the momentum (to the surface) is conserved, i.e., $k_{\parallel} = k'_{\parallel}$. On the other hand, for the perpendicular components we have

$$k_{\perp} = k \cos \theta_k, \quad k'_{\perp} = k' \cos \theta_{k'}, \quad (2.39)$$

where θ_k is the incidence angle and $\theta_{k'}$ the refraction angle, relative to the surface normal. Refraction at the surface is such that:

$$\frac{k'^2_{\perp}}{2} = \frac{k^2_{\perp}}{2} - \varepsilon_0 \quad (2.40)$$

If we substitute eq. (2.39) into eq. (2.40) we obtain

$$\frac{k'^2}{2} \cos^2 \theta_{k'} = \frac{k^2}{2} \cos^2 \theta_k - \varepsilon_0 \Rightarrow (\varepsilon_k - \varepsilon_0) \cos \theta_{k'} = \varepsilon_k \cos^2 \theta_k - \varepsilon_0. \quad (2.41)$$

meaning that an electron is allowed to leave the metal only if $\theta_{k'} < \frac{\pi}{2}$, i.e.,

$$\theta_k < \theta_c = \arccos \sqrt{\frac{\varepsilon_0}{\varepsilon_k}}, \quad (2.42)$$

θ_c being the maximum value of the incidence angle for electron emission to occur. The simplest a priori assumption that one can make about $p_{\theta}(\varepsilon_k)$, in eq. (2.10), is that the

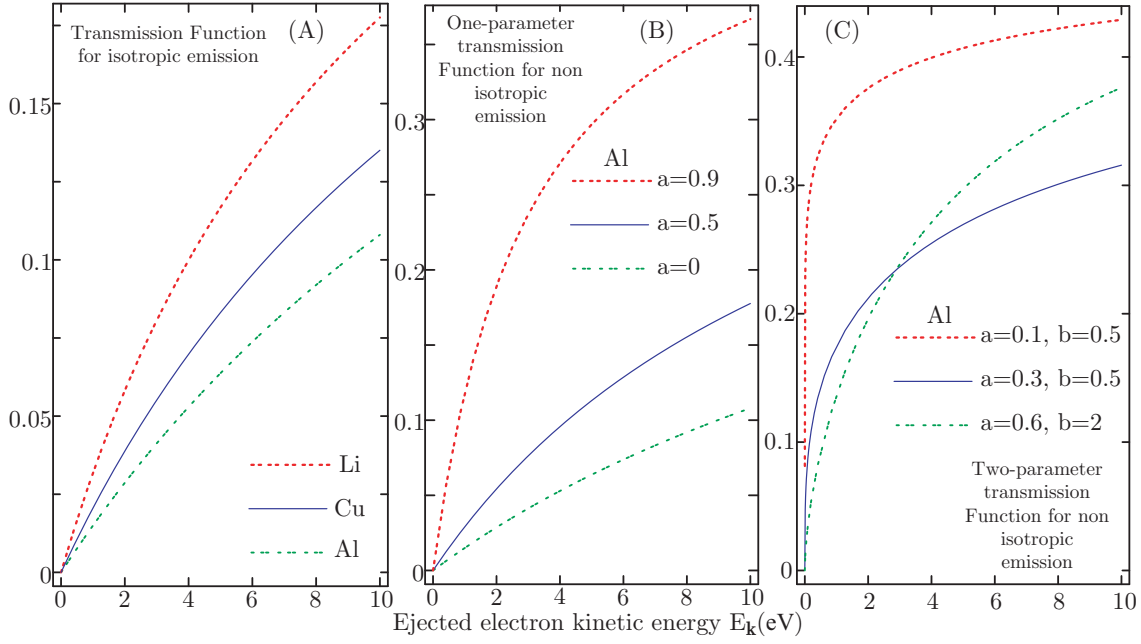


Figure 2.6: Transmission functions in the case of isotropic (2.43) and non isotropic emission (2.44), (2.45)

angular distribution is isotropic, i.e., $p_\theta(\varepsilon_k) = 1/(4\pi)$. So, we can integrate eq. (2.27), obtaining:

$$T(\varepsilon_k) = \frac{1}{2} \left(1 - \sqrt{\frac{\varepsilon_0}{\varepsilon_k}} \right) \Theta(\varepsilon_k - \varepsilon_0). \quad (2.43)$$

This transmission function, shown in Fig. 2.6(A), allows a very small number of emitted electrons, for different ion-surface combinations. This suggests that the angular distribution function is not spherical. Several hypothesis have been made about the elliptic nature of $P_\theta(\varepsilon_k)$, leading to different expressions for the transmission function. For example, in

$$T(\varepsilon_k) = \frac{1}{2} \left[\frac{1 - \sqrt{\frac{\varepsilon_0}{\varepsilon_k}}}{1 - a\sqrt{\frac{\varepsilon_0}{\varepsilon_k}}} \right] \Theta(\varepsilon_k - \varepsilon_0), \quad (2.44)$$

the parameter a is such that, for $a = 0$, eq. (2.44) equals eq. (2.43), while, for $0 < a < 1$, as shown in Fig. 2.6(B), the transmission function allows a larger number of electrons than eq. (2.43) to be emitted at very low energies. There are transmission function with

two parameters, like

$$T(\varepsilon_k) = \frac{1}{2} \left[1 - \left(\frac{\varepsilon_0}{\varepsilon_k} \right)^b \right]^a \Theta(\varepsilon_k - \varepsilon_0), \quad (2.45)$$

in which $b > 0$ and $0 < a < 1$ (see Fig. 2.6(C)). Nevertheless the parameters in eqs. (2.44) and (2.45) need to be determined by fitting with the experiments

2.1.4 Kinetic Energy Distributions for a static ion.

As a first step towards a quantitative study of AN, we analyze the form of the kinetic energy distributions of emitted electrons due to “pure” AN, i.e., the distributions obtained by neglecting the variation of the ion energy levels near the surface of the target, as well as the finite lifetime of initial and final states. This distribution function, denoted $N_0(\varepsilon_k)$, is determined from eq. (2.28) as

$$N_0(\varepsilon_k) = T(\varepsilon_k) N_I^0(\varepsilon_k), \quad (2.46)$$

in which $N_I^0(\varepsilon_k)$ is the “pure spectrum” of excited electrons. The latter is obtained from eq. (2.26), under the condition that the ionization energy of the ion is fixed to a distance Z_* , of the order of Z_m (eq. (2.36)). This means that the ion is assumed to stand still and

$$N_I^0(\varepsilon_k) = N_0 p_{\text{EX}}(\varepsilon_k, Z_*) \lim_{v_{\perp} \rightarrow 0} \int_0^{\infty} dZ p_N(Z, v_{\perp}) = N_0 p_{\text{EX}}(\varepsilon_k, Z_*). \quad (2.47)$$

A simple model for the conduction band of a metal target involves either a constant or a parabolic density of states [8, 25]; in the first case, introducing an energy variable, ε , measured from the bottom of the conduction band, we have $\rho_c(\varepsilon) = \beta_1$, corresponding to the Auger Transform

$$A_1(\varepsilon) = \beta_1^2 \varepsilon^2, \quad \text{for } 0 < \varepsilon < \frac{\varepsilon_F}{2}, \quad (2.48a)$$

$$= \beta_1^2 (\varepsilon_F - \varepsilon) \quad \text{for } \frac{\varepsilon_F}{2} < \varepsilon < \varepsilon_F; \quad (2.48b)$$

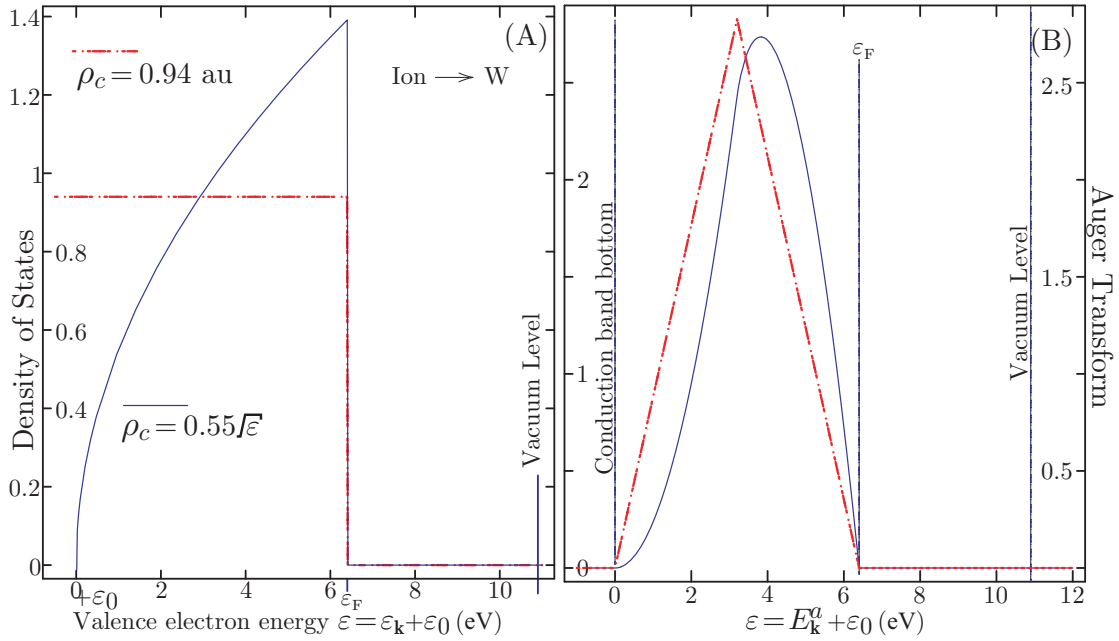


Figure 2.7: (A) Density of valence states and (B) Auger Transform for a singly charged ion impinging on a W surface (specified by parameters $\beta_1 = 0.94$ au and $\beta_2 = 0.55$ au)

in the second case, from $\rho_c(\varepsilon) = \beta_2\sqrt{\varepsilon}$, we get

$$\begin{aligned}
 A_2(\varepsilon) &= \frac{\pi\beta_2^2}{4}\varepsilon, \quad \text{for } 0 < \varepsilon < \frac{\varepsilon_F}{2}, & (2.49a) \\
 &= \frac{\beta_2^2}{2} \left[\varepsilon^2 \sin^{-1} \left(\frac{\varepsilon_F}{\varepsilon} - 1 \right) + 2(\varepsilon_F - \varepsilon) \sqrt{\varepsilon\varepsilon_F - \varepsilon_F^2} \right] \quad \text{for } \frac{\varepsilon_F}{2} < \varepsilon < \varepsilon_F. & (b)
 \end{aligned}$$

In this way, we have introduced another fitting parameter, β_1 or β_2 , to account for the effect of the surface on the electronic structure of the target, while, for the density of final states, we use the free-electron gas law: $\rho(\varepsilon_k) = \sqrt{\varepsilon_k}$. The two assumptions (2.48) and (2.49) leads to different pure spectra, shown in Fig. 2.8(A), for a positive ion impinging on a Tungsten surface. With the transmission function (2.43), the corresponding kinetic energy distributions of ejected electrons have the shape reported in Fig. 2.8(B).

The same distributions are calculated and compared with experiments of 130 eV Ar^+ impact on Al polycrystalline surface [12], Fig. (2.9): we immediately notice the absence of tails in the theoretical distributions. They exhibit an abrupt cut at the value of maximum energy of the emitted electrons, i.e., $E_{\text{max}} = -2\phi + I_a(Z_*)$ (eq. (2.3)). Moreover, the experimental distributions show a dependence on the ion impact velocity, which underlies

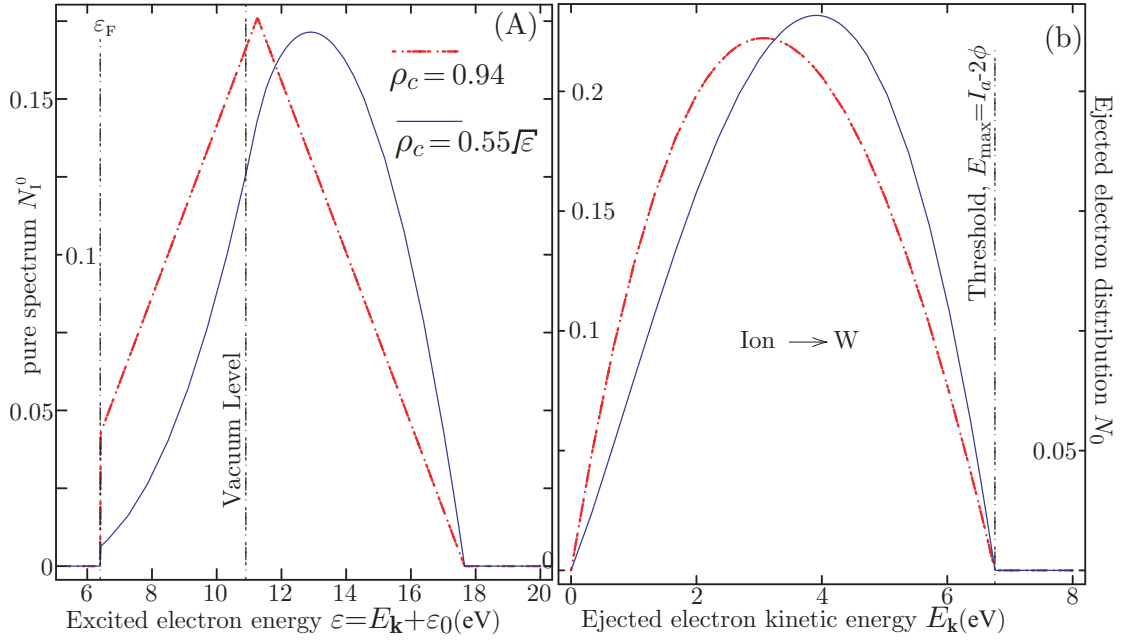


Figure 2.8: (A) pure spectrum and (B) kinetic distribution of ejected electrons for a singly charged ion impinging on a W surface (specified by parameters $\beta_1 = 0.94$ au and $\beta_2 = 0.55$ au)

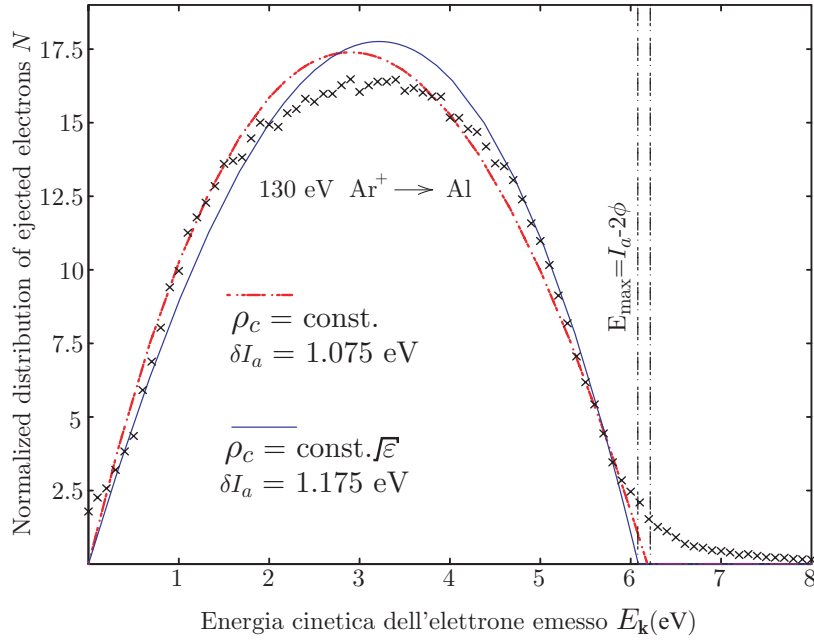


Figure 2.9: Pure spectrum vs Kinetic energy distribution of ejected electrons from a polycrystalline Al surface, bombarded with 130 eV Ar^+ ions. Theoretical calculations are derived from eqs. (2.48) and (2.49).

a sort of broadening mechanism. In other words, it seems that the experimental spectra

can be obtained from the theoretical pure spectrum by convolution with a broadening function whose width depends on the ion impact velocity.

2.1.5 Effects that broaden the pure spectrum.

For a complete understanding of AN, we need to estimate the source and magnitude of the energy broadenings inherent in the process. Hagstrum's based his analysis on experiments of electron emission from both metal (Ni) and semiconducting (Ge) surfaces bombarded very slow positive ion beams (4 – 100 eV Ne^+).

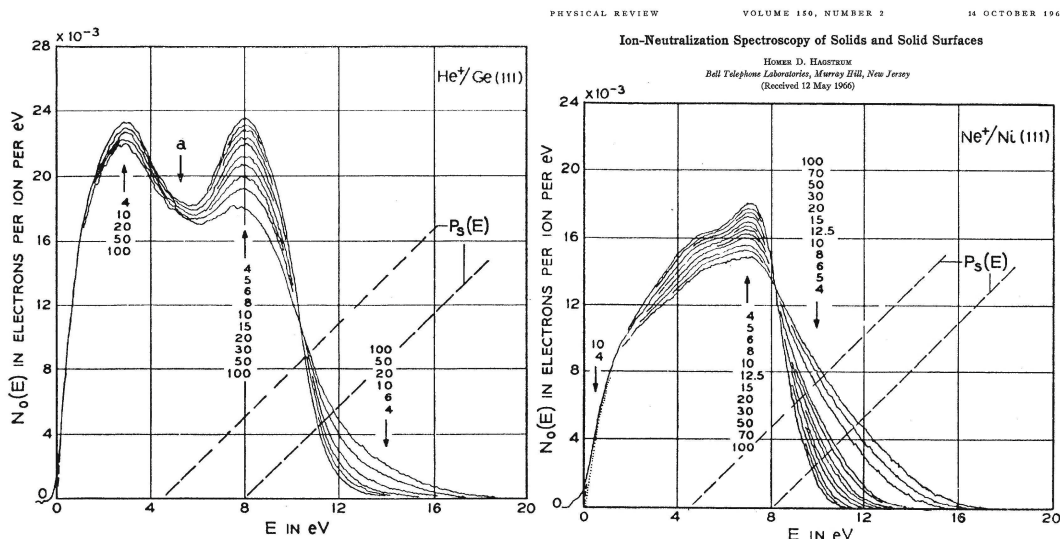


Figure 2.10: Experimental Kinetic energy distributions for He^+ ions incident on atomically clean Ge(111) and Ni(111). Incident ion impact energies, in electron volts, are indicated in sequence at three points on the curves. The level $N_0(E) = 1.5 \times 10^{-3}$ electrons/ion/eV is indicated by the line $a - a$.

From the observation that the tails of the experimental curves became wider with increasing the impact energy of the projectile (Fig. 2.10), he distinguished velocity dependent and velocity independent types of broadening, resulting from [8, 25]: (i) initial state lifetime, (ii) final state lifetime, (iii) shift in atomic energy level(s) near the surface, (iv) variation of impact parameter at the surface and (v) nonadiabatic excitation of electrons in the solid induced by the ion motion. The only significant static broadening was attributed to the final state lifetime.

In other terms, the distributions of ejected electrons are broadened by those dynamical features, concerning both the incident ion beam and the surface of the sample, that are outside the Fermi Golden rule formulation (eq. (2.6)) used to construct the pure spectrum (eq. (2.47)).

We have already seen that the main contributions to the initial state lifetime is brought by the ion neutralization probability (eq. (2.35)); thus, a measure of the initial state lifetime broadening **(i)**, denoted $\Delta_i(v_\perp)$, is given by the Heisenberg uncertainty principle, which, using eqs. (2.29)-(2.36), is written

$$\Delta_i(v_\perp) \sim \frac{1}{\tau(Z_0)} = \gamma v_\perp. \quad (2.50)$$

In Hagstrum's experiments (Fig. 2.10), Δ_i is of the order of 0.1 – 1 eV, for impact velocities in the range 0.5 – 10 au.

The final state lifetime broadening **(ii)**, denoted Δ_f , is due to the holes left in the band of the solid and increases with increasing their energies towards the Fermi level. It can be estimated from mean free paths of hot electrons in solids and takes values in the range $\Delta_f = 0.01 - 0.1$ eV for most metals and semiconductors [8].

Level shift broadening **(iii)** comes about because the energy of the projectile level has the form:

$$\varepsilon_a(Z) = -I_a + \delta\varepsilon_a(Z), \quad (2.51)$$

where I_a is the ionization energy of the unperturbed ion, infinitely distant from the target, and $\delta\varepsilon_a(Z)$ is the correction due to the ion-surface interaction. Much theoretical effort has been devoted to the determination of $\delta\varepsilon_a(Z)$ [8, 28, 29], which, for sufficiently large Z , can be interpreted as the response of a classical conductor to either electron or nuclear charges in the projectile. Indeed, $\delta\varepsilon_a(Z)$ contains two main components: one, denoted $\delta\varepsilon_a^{\text{IM}}(Z)$, is due to the Coulombic image force of attraction for the positive ion, yielding the classical potential $-1/(4Z)$, and the other, $\delta\varepsilon_a^{\text{EX}}(Z)$, is caused by the repulsion resulting from interpenetration of the electron clouds of the projectile, with the target atoms, and the Pauli principle. Hagstrum approximated $\delta\varepsilon_a^{\text{IM}}(Z) \approx -1/(4Z)$ and

used $\delta\varepsilon_a^{\text{EX}}(Z) = B_I^0 \exp(-b_I(Z - Z_c))$ to represent the effect of the repulsive electron-electron interaction between the ion and an atom of the crystal. He further assumed $b_I \sim 5 \text{ \AA}^{-1}$, $B_I^0 \sim 0.05 \text{ eV}$, for all monovalent ions and neutral atoms, and defined $Z_c = R_I + a/2$, sum of the particle's radius and half lattice constant of the metal, as the distance at which the atomic particle touches the metal surface [8]. These considerations lead to the function

$$\delta\varepsilon_a(Z) = -\frac{1}{4Z} + B_I^0 \exp(-b_I(Z - Z_c)) \quad (2.52)$$

shown in Fig. (2.11) for different projectile ions.

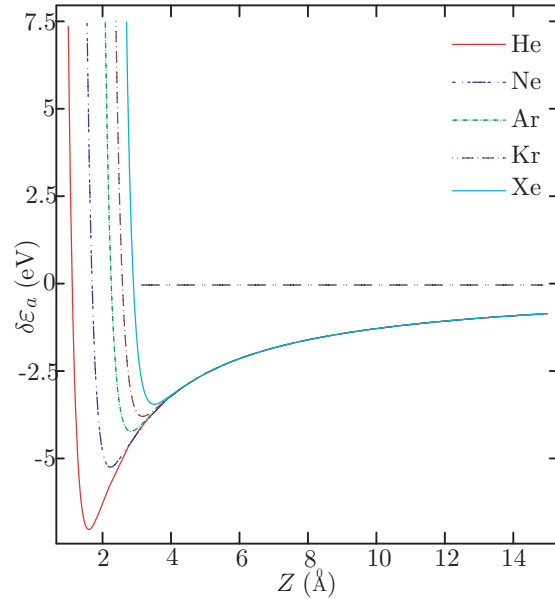


Figure 2.11: Energy shift (2.52), due to the interaction of He^+ , Ne^+ , Ar^+ , Kr^+ and Xe^+ ions with a clean Al(111) surface: the contribution of the image potential, $-1/(4Z)$ is the same for all projectiles, while the repulsive term changes with the projectile radius.

Another source of broadening (iv) is the variation in the surface parameters, with the decrease of the projectile target distance. Its magnitude, Δ_s , is basically due to the surface roughness, which means that either the work function ϕ or the ion energy $\varepsilon_a(Z)$ are not constant over the surface of the target. Many experiments [8] tell us that Δ_s affects the low kinetic energy region of the spectrum ejected electrons for incoming ions of impact energy larger than $\sim 100 \text{ eV}$, at nearly normal incidence. At lower impact

energy, this type of broadening can be treated as a correction to the final state lifetime broadening, yielding $\Delta_f + \Delta_s \sim 0.1$ eV.

Finally, the projectile motion in the neighborhood of the target causes deformations in the surface band structure, which are more significant for metal surfaces where non adiabatic electron-hole pairs are created at the Fermi energy. A rough estimation of the effect yields a non adiabatic broadening (\mathbf{v}) of the form $\Delta_n(v_\perp) \sim v_\perp/d$, where d is the average screening length of target electrons to the potential of the moving ion. In a metal sample, we can take $d \sim 0.5$ Å, yielding $\Delta_n \sim 0.2$ eV for 4 eV He⁺ ions and $\Delta_n \sim 3$ eV for 1 keV He⁺ ions. This means that Δ_n should be comparable in magnitude to Δ_i .

2.1.6 Kinetic Energy Distributions for a moving ion.

We proceed now to include specifically in the theory those effects which broaden the energy distribution function (2.47). Substituting eq. (2.23) into eq. (2.26), and using eq. (2.17), the internal distribution of excited electrons, by a moving ion, is written:

$$N_1(E_k) = N_0 \rho(E_k) \Theta(E_k + \phi) \frac{\int_0^\infty dZ p_N(Z, v_\perp) A\left(\frac{E_k + \varepsilon_a(Z)}{2}\right)}{\int_{-\phi}^\infty dE_k \rho(E_k) A\left(\frac{E_k + \varepsilon_a(Z)}{2}\right)}, \quad (2.53)$$

in which the broadening due to atomic level shifting (iii), discussed in the previous subsection, is already included in $\varepsilon_a(Z)$, via eqs. (2.51) and (2.52). The easiest way to account for the other sources of broadening is to consider that the elemental Auger transition, for which $\varepsilon_{k'}$, $\varepsilon_{k''}$ - in eqs. (2.18) and (2.21)- and Z have specific values, results in excited electrons whose energies may be taken to be distributed according to the Lorentzian function

$$B(\delta E_k, v_\perp) = \frac{1}{\delta E_k^2 + \Gamma(v_\perp)^2}, \quad (2.54)$$

with half width at half maximum (HWHM)

$$\Gamma(v_\perp) = \Delta_f + \Delta_i(v_\perp) + \Delta_s(v_\perp) + \Delta_n(v_\perp) \approx \Gamma_0 + \Lambda_0 v_\perp. \quad (2.55)$$

Indeed experiments performed with slow ions of impact energy below ≤ 200 eV have confirmed there is a linear law relating the width of the distribution function and the ion perpendicular velocity. Therefore, the broadened distribution of excited electrons is derived from the broadened Auger transform

$$A'(E_k, v_\perp) = \int_{-\infty}^{\infty} B(\delta E_k, v_\perp) A\left(\frac{E_k + \delta E_k + \varepsilon_a(Z)}{2}\right) d(\delta E_k), \quad (2.56)$$

as

$$N'_1(E_k) = N_0 \rho(E_k) \Theta(E_k + \phi) \frac{\int_0^\infty dZ p_N(Z, v_\perp) A'(E_k, v_\perp)}{\int_{-\phi}^\infty dE_k \rho(E_k) A'(E_k, v_\perp)}. \quad (2.57)$$

Finally the broadened distribution of ejected electron is:

$$N'(E_k) = T(E_k) N'_1(E_k). \quad (2.58)$$

An application this model is shown Fig. 2.12.

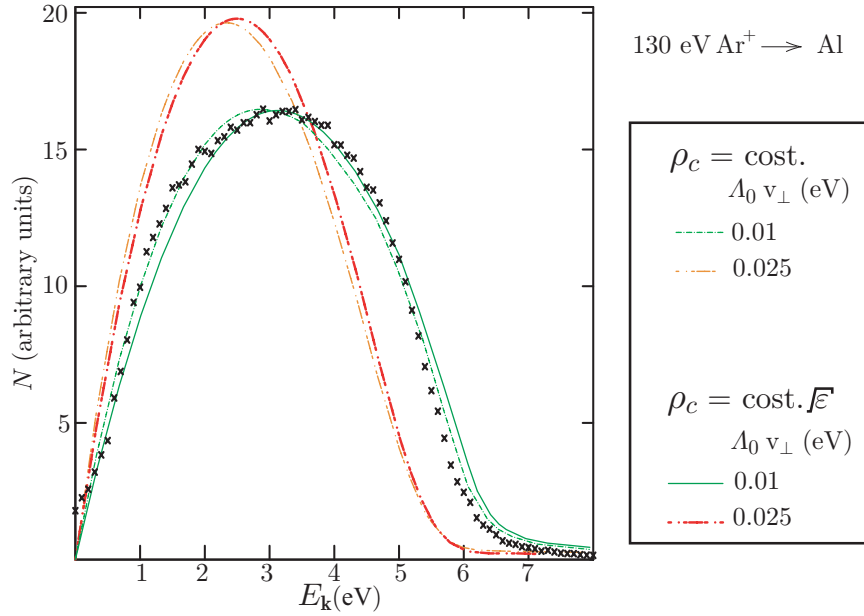


Figure 2.12: Kinetic energy distribution of ejected electrons from a polycrystalline Al surface, bombarded with 130 eV Ar⁺ ions. Data are compared with the calculations obtained from (2.57) with the Auger transforms of eqs. (2.48) and (2.49).

There, we report two types of distributions of emitted electrons from an Al surface, bombarded by 130 eV Ar⁺ ions;: one corresponds to the Auger transforms (2.48), where

a constant density of valence state has been assumed; the other is obtained from (2.49), where the density of valence state is proportional to $\sqrt{\varepsilon}$. In these spectra, we have used the neutralization probability (2.35), with $\omega_0 = 0.01 \text{ eV}^{-1}$ and $\gamma = \Lambda_0$. The transmission function is assumed to have the spherical form (2.43), while the broadening function (2.54), has no velocity independent broadening ($\Gamma_0 = 0$) and $\Lambda_0 v_\perp$ is set to 0.025 eV and 0.01 eV, respectively.

It is worthwhile noticing that Hagstrum worked out some simplifications on eqs. (2.56) and (2.57), by linearly expanding $\varepsilon_a(Z)$ around Z_m (eq. (2.36)) which leads to the replacement of $p_N(Z, v_\perp)$ and $B(\delta E_k, v_\perp)$ with two Gaussian functions of standard deviations σ_1 and σ_2 , respectively [8]. The approximation can be proved to be adequate only for very slow incoming ions (of impact kinetic energy $< 10 \text{ eV}$).

2.1.7 Conclusions on the Hagstrum model.

The model presented so far is suitable for studying the basic properties of electron emission from clean metal surfaces due to AN of slow, monoatomic and singly charged ions. Its final goal is the determination of the distribution function (2.58) that, because of the two-electron nature of the process, results the determination of the following quantities:

1. Matrix elements $V_{ak'k'}^{kk'}(Z)$ of the electron-electron repulsion between intimal and final states (2.4);
2. Density of valence electron states $\rho_c(\varepsilon_{k'})$ and $\rho_c(\varepsilon_{k''})$, yielding the Auger transform (2.21);
3. Density of excited electron states $\rho(\varepsilon_k)$;
4. Energy of the atomic level $\varepsilon_a(Z)$, including the shift brought by the ion-surface interaction (2.51);
5. Neutralization probability $p_N(Z, v_\perp)$, well approximated by the rate equation (2.35);

6. Transmission function $T(E_k)$, for both isotropic (2.43) and non-isotropic (2.44)-(2.45) ejection.
7. Broadening function $B(\delta E_k, v_\perp)$ for the effects (i)-(v), listed in § 2.1.5.

We conclude this section by observing that the Hagstrum’s model is still considered as a reference point for more self-consistent treatments of Auger neutralization. The key quantity of the approach is the selfconvolution of the density of states of the valence band of the target, which qualitatively reproduces many experimental results.

2.2 Developments of AN Theory.

The crucial assumption leading to the Hagstrum’s construction of the spectrum of ejected electron is related to the treatment of the matrix element of the electron-electron interaction (2.4). Indeed, eq. (2.21) was widely used throughout the 1970s-1980s to analyze Auger processes from simple metals (see, for example, Ref. [30]). Nevertheless, Hagstrum himself [25] tried to improve the crude approximation (2.19) by combining eqs. (2.18) and (2.56) into the convolution of two “transition densities”, denoted U_1 and U_2 , that contain the either the matrix elements (2.10) or the broadening corrections (2.54):

$$A''(E_k, Z) = \int_{\max(\varepsilon_0 - \phi, \varepsilon_a(Z) + E_k)}^{\min(-\phi, \varepsilon_a(Z) + E_k)} U_1(\omega) U_2(\varepsilon_a(Z) + E_k - \omega) d\omega. \quad (2.59)$$

Such a relations is still used in the determination of the spectrum of ejected electrons from metal, semiconductors and biological materials (see, for example, Ref. [31] and Ref. [32]). A similar approach, proposed by Appelbaum and Hamann [33], leads to the following improvement of eq. (2.13):

$$S'_a(E_k; Z) = \int_{-\varepsilon_0}^{-\phi} d\varepsilon_{k'} \rho_c(\varepsilon_{k'}) \int_{-\varepsilon_0}^{-\phi} d\varepsilon_{k''} \rho_c(\varepsilon_{k''}) \quad (2.60)$$

$$\times \frac{\gamma_{k'k''}^a(Z) F(\varepsilon_{k'}, \varepsilon_{k''}; Z)}{(E_k - I_a(Z) - \varepsilon_{k'} - \varepsilon_{k''})^2 + \gamma_{k'k''}^a(Z)^2}, \quad (2.61)$$

in which the δ -function is replaced with a Lorentzian that accounts for the broadening mechanisms of each elemental AN transition; nevertheless in Ref. [33] actual calculations were carried out under the same approximations of the basic Hastrum's model.

2.2.1 “Magical” Energy.

More recently, Monreal and coworkers [34, 35, 36] have reconsidered the transition rate (2.8), by removing the approximation (2.10) and defining a corrected (2.13) in the form:

$$S_a''(E_k, \Omega_{\text{IN}}; Z) = \int d^2\Omega_{k'} \int d^2\Omega_{k''} \int_{-\varepsilon_0}^{-\phi} d\varepsilon_{k'} \rho_c(\varepsilon_{k'}) \int_{-\varepsilon_0}^{-\phi} d\varepsilon_{k''} \rho_c(\varepsilon_{k''}) \quad (2.62)$$

$$\times \left| V_{ak''}^{kk'}(Z) \right|^2 \delta(E_k - I_a(Z) - \varepsilon_{k'} - \varepsilon_{k''}), \quad (2.63)$$

with Ω_{IN} the solid angle of the excited electron momentum within the solid. This, let us correct the excitation probability (2.16),

$$p_{\text{EX}}(E_k, \Omega_{\text{IN}}; Z) = \frac{\rho(E_k) S_a''(E_k, \Omega_{\text{IN}}; Z)}{\int_{-\phi}^{\infty} dE_k \rho(E_k) S_a''(E_k, \Omega_{\text{IN}}; Z)}, \quad (2.64)$$

and rewrite the total transition rate (2.8) as

$$\frac{1}{\tau}(Z) \propto \int_{\Omega_{\text{IN}}} d^2\Omega_{\text{IN}} \int_{Z_0}^{\infty} dZ p_{\text{N}}(Z, v_{\perp}) p_{\text{EX}}(E_k, \Omega_{\text{IN}}; Z), \quad (2.65)$$

where no hypothesis has been made on the functional dependence of $p_{\text{N}}(Z, v_{\perp})$. Now, we introduce the number of excited electron in the metal per unit energy and per unit of solid angle

$$\frac{dN_{\text{I}}}{d^2\Omega_{\text{IN}}} = \int_{Z_0}^{\infty} dZ p_{\text{N}}(Z, v_{\perp}) p_{\text{EX}}(E_k, \Omega_{\text{IN}}; Z) \quad (2.66)$$

and we include the effect of the surface barrier via a transmission function $T(E_k, \Omega_{\text{OUT}})$ that depends either on the Kinetic energy of the ejected electron or on the solid angle Ω_{OUT} , formed by the electron momentum outside the solid. It follows that the distribution

of ejected electrons, per unit energy and unit solid angle, reads

$$\frac{dN}{d^2\Omega_{out}} = T(E_k, \Omega_{OUT}) \frac{d^2\Omega_{IN}}{d^2\Omega_{OUT}} \frac{dN_I}{d^2\Omega_{IN}}. \quad (2.67)$$

If we integrate eq. (2.67) over the external hemisphere, we obtain the distribution of emitted electrons, per unit energy

$$N(E_k) = \int_0^{2\pi} d\phi_{OUT} \int_0^{\pi/2} d\theta_{OUT} \sin\theta_{OUT} T(E_k, \Omega_{OUT}) \frac{d^2\Omega_{IN}}{d^2\Omega_{OUT}} \frac{dN_I}{d^2\Omega_{IN}} \quad (2.68)$$

The broadening function (2.54) applies to the Auger transform (2.62) yielding the convolution product

$$S'''(E_k, \Omega_{IN}; Z) = \frac{\Gamma(v_{\perp})}{\pi} \int_{-\infty}^{\infty} \frac{S''_a(E_k + \delta E_k, \Omega_{IN}; Z)}{(\delta E_k^2 + \Gamma(v_{\perp})^2)} d(\delta E_k), \quad (2.69)$$

that, substituted into eq. (2.64) in spite of $S''_a(E_k, \Omega_{IN}; Z)$, produces the broadened internal distribution of excited electron $N'_I(E_k)$, as in (2.57). Using the convolution theorem, we re-express (2.69) in the time domain

$$S'''(E_k, \Omega_{IN}; Z) = \int_{-\infty}^{\infty} \tilde{S}''_a(t, \Omega_{IN}; Z) e^{iE_k t - \Gamma(v_{\perp})|t|} \frac{dt}{2\pi}, \quad (2.70)$$

where $\tilde{S}''_a(t, \Omega_{IN}; Z)$ is the Fourier transform of (2.62). Next, we expand (2.70) in Taylor series for small v_{\perp} , i.e., for small $\Gamma(v_{\perp})$, to write

$$S'''(E_k, \Omega_{IN}; Z) = S''(E_k, \Omega_{IN}; Z) - \Gamma(v_{\perp}) S_d(E_k, \Omega_{IN}; Z) + o(\Gamma(v_{\perp})^2), \quad (2.71)$$

where a new function

$$S_d(E_k, \Omega_{IN}; Z) = \int_{-\infty}^{\infty} \frac{dt}{2\pi} |t| \tilde{S}''_a(t, \Omega_{IN}; Z) e^{iE_k t} \quad (2.72)$$

$$= \text{Pr} \left[\int_{-\infty}^{\infty} \frac{dS''(E'_k, \Omega_{IN}; Z)}{dE'_k} \frac{dE'_k}{E'_k - E_k} \right] \quad (2.73)$$

has been introduced. We observe that the E_k -integral of $S_d(E_k, \Omega_{IN}; Z)$ vanish; then, $S_d(E_k, \Omega_{IN}; Z)$ changes its sign at least once, i.e., its value must be 0 somewhere, at a

certain energy $E_k = E_k^*$ where the broadened spectrum coincide with the pure spectrum, i.e.,

$$S'''(E_k^*, \Omega_{\text{IN}}; Z) \approx S''(E_k^*, \Omega_{\text{IN}}; Z) + o(\Gamma(v_{\perp})^2). \quad (2.74)$$

The existence of E_k^* , known as “*Magic Energy*”, is clearly shown in Fig. 2.10 as an intersection point for all curves.

2.2.2 Open problems

A delicate issue is the accurate determination of the total rate for AN, underlying the ion neutralization probability $p_N(Z, v_{\perp})$: models have been proposed to define the form of the Auger potential beyond the constant screening approximation of eq. (2.4). Among these, we would like to mention refs. [9, 37, 35, 38, 34], where the effect of spin correlations in He^+ projectiles has been studied.

Another fundamental point is related to the many body nature of the electron-electron interaction in a many electron system. As discussed in § 1.1.3, several evidences, both theoretical and experimental, have supported the hypothesis that noble gas ion neutralization, at simple metal surfaces, can activate a collective behavior in the conduction electrons [10, 11, 12]. A theoretical model accounting for these features will be presented in chapter 3, while in chapter 4, we shall provide a detailed description of ion induced many-body shake up [12, 19].

2.3 Resonant ionization mechanism in sputtering of metals.

We have already mentioned that during atom-surface collisions, a variety of events occur leading to the ejection of secondary electrons, secondary target atoms, and photons. It is called sputtering the mechanism through which a target emits particles, after ion bombardment. In order for a sputtering event to take place, part of the kinetic energy

of the impinging particle must be transferred to target particles, that only subsequently may leave the target as sputtered particles [39, 40, 41, 42]. One of the most studied process is resonant charge transfer (RCT) between an atomic particle and the target surface. Atomic particles of the first surface layers receive an impulse from the “collisional cascade”, generated by the incident beam, and are, thus, ejected in different charge states with different probabilities. In contrast, the incident projectile approaches a well defined surface in a well prepared state, colliding with the target, and it moves outward in a range of ionized states with different probabilities. What differentiates the two phenomena is the kinetic energy region over which they occur. Scattered particles move faster than secondary emitted ones.

In Fig. 2.1, we have shown a process of resonant capture, when the impinging, singly charged projectile is scattered as a neutral atom. A complementary process is resonant ionization, occurring when a neutral projectile is positively ionized, during the interaction with the surface. In case of scattering, the resonant tunneling of electrons between an electronic orbital of the projectile and the conduction band of metal is the dominant charge exchange mechanism. In case of sputtering, and generally at kinetic energies of about 1 – 30 eV, we need to include surface excitations as another (indirect) resonant charge exchange mechanism in competition with the direct one. The clarification of the physical origin of the ionization of an atom leaving a metal surface has been a topic of great interest for many years. The matter is that knowledge of the positive and negative ionization probability is a prerequisite for quantitative interpretation of various surface experimental methods based on the sputtering processes, as SIMS. Another important clue is that the energy spectrum of secondary ions is related to the adsorption energy of the surface.

Resonant charge exchanges can also produce negative ions either in projectiles or in secondary atoms. At short distances from the surface ionization is no longer possible because the image interaction pulls the affinity level down. On the other hand, excited levels are promoted while the ion is approaching the surface. So at distances small enough from surface, resonant ionization is favored if the excited atomic state is opposite to the unfilled level of the solid [5, 43]

In general, when an atom is near a surface, it can interact electronically with the substrate, so that its localized states are not anymore stationary states. This is due to electron tunneling between the atom and the metal. The “true” eigenfunctions of the system are indeed linear combinations of the unperturbed eigenfunctions of the free atom and of the unperturbed metal. Shifts in the atomic levels are caused either by the electron-electron or by the ion-electron interactions, which makes the formalization of a self-consistent method unpracticable.

A basic model was developed by Newns [13], who adapted the Anderson theory [13] of magnetic impurities in metals to describe chemisorption processes on solid surfaces. The resulting Hamiltonian,

$$\mathcal{H}_{\text{TDAN}}(t) = \varepsilon_a(t)c_a^\dagger(t)c_a(t) + \sum_k \varepsilon_k c_k^\dagger c_k + \sum_k [V_{ak}(t)c_a^\dagger c_k + \text{H.C.}], \quad (2.75)$$

is known as the time dependent Anderson-Newns Hamiltonian (TDAN). It allows to study either positive or negative ionization of an atom, with one active level $\varepsilon_a(t)$, specified by the fermion operators $c_a(t)$, $c_a^\dagger(t)$, which moves in the neighborhood of a metal target. The substrate has a wide spectrum of energies $\{\varepsilon_k\}$, represented by the fermion operators $\{c_k\}$, $\{c_k^\dagger\}$, so that any localized electronic excitation created by the atomic motion spreads very quickly into the substrate, on a time scale which is inversely proportional to the bandwidth. It is assumed that resonant tunneling of electrons between the adatom and the substrate band is the dominant charge exchange mechanism, thus, the interaction is characterized by the one-electron hopping integrals $V_{ak}(t)$. A further limitation requires the kinetic energy of the moving particle to be in the intermediate range (eV to keV), which makes it possible to treat the adatom trajectory classically, yielding the parametric time-dependence in (2.75). The aim of the model is to find the deviations from adiabaticity, i.e. the fraction of the minority charge states of the atom at the end of the interaction process.

The ionization probability of a sputtered atom depends on the dynamics of the atom leaving the surface and on the electronic structure of the adatom surface system. Sroubek was among the first scientists who adapted the TDAN model to describe low energy charge transfer in secondary atomic emission from sputtered metals [15]. To did so,

he neglected the effect of the collision cascade on the periodic atomic structure of the surface and treated the hopping interaction, in (2.75), as a small perturbation. Several improvements were proposed by Brako and Newns [44, 45, 46], and, then, by Norskov and Lundqvist [14], who kept the full strength of the perturbation and focussed on the slowly varying time-dependence of $\mathcal{H}_{\text{TDAN}}(t)$ in the time-scale of electronic transitions. It turned out that the experiments involving moving particles of kinetic energies typically larger than ~ 50 eV were correctly reproduced [47, 48, 49]; on contraire, the TDAN model failed to explain the detailed mechanism of secondary ion formation at energies below ~ 30 eV [13, 46, 50, 51, 52]. It was Sroubek again who proposed a substrate-excitation model to explain the low velocity regime of secondary ion emission [16]: the theory is based on the assumption that the electrons in the collision cascade region are excited to the empty states, of energy ε_k , above the Fermi level of the target, with a probability $e^{-\varepsilon_k/k_B T_s}$, in which T_s is the effective “electronic temperature” on the collision cascade region. Subsequently, Sroubek and Fine [53], used a promotion mechanism to explain electron emission from bombarded solids.

Successive efforts on the emission of secondary ions were devoted to include in the basic Anderson-Newns Hamiltonian the effects of electronic excitations, produced during sputtering. A first attempt in solving this problem was proposed by Sroubek and coworkers [54], who discussed the influence of a locally time dependent perturbation in the substrate. A more rigorous formulation was proposed in ref. [55], with the aid of retarded Green’s functions. In Ref. [56, 17, 57], it was presented a theory of positive resonant charge exchanges between sputtered atoms and metal surfaces. A generalized Anderson-Newns Hamiltonian was constructed, in which surface excitations occur as Quasi-Molecular correlations in the diatomic systems, formed transiently in the collision cascade, between secondary emitted atoms and their nearest neighbours substrate atoms. This model was extended later to negative ionization [58].

2.3.1 TDAN Hamiltonian for scattering

Resonant charge transfer in low energy ion scattering from a metal target can be described by a model theory [44, 51, 52] in which the metal is treated as a non-interacting

fermi gas of work function ϕ . The valence atomic state $|a(t)\rangle$, of energy $\varepsilon_a(t)$, is assumed to be non-degenerate during the ion motion. This localized level is broadened by the interaction with the metal state $|k\rangle$, of energy ε_k , through hopping potential $V_{ak}(t) = \langle a(t)|\hat{V}(t)|k\rangle$, where $\hat{V}(t)$ is the perturbation due to coupling of the atom with the metal. Time dependence of the atomic level and hopping potential comes from the motion of the atom outside the solid surface. With this assumption, the Hamiltonian of the system is the TDAN Hamiltonian (2.75).

The usual solution of $\mathcal{H}_{\text{TDAN}}(t)$ is based on the equation of motion method [51, 52]. In the Heisenberg representation, the destruction operators $c_a(t)$ and $c_k(t)$ evolve as

$$i\frac{d}{dt}c_a(t) = \varepsilon_a(t)c_a(t) + \sum_{\mathbf{k}} V_{ak}(t)c_k(t) \quad (2.76)$$

$$i\frac{d}{dt}c_k(t) = \varepsilon_k c_k(t) + V_{ka}(t)c_a(t) \quad (2.77)$$

with the boundary conditions $c_a(t_0) = c_a$ and $c_k(t_0) = c_k$, where the time t_0 refers to the system before the interaction ($t_0 \rightarrow -\infty$). The expectation value of the number operator $n_a(t) = c_a^\dagger(t)c_a(t)$ of the atomic level, in the remote future,

$$P_0 = \langle c_a^\dagger(\infty)c_a(\infty) \rangle, \quad (2.78a)$$

gives the charge in the atomic level after the atom has left the metal surfaces. Hence, it can be interpreted as an occupation probability for the atomic state. Conversely, the expectation value of the hole number operator $\bar{n}_a(t) = c_a(t)c_a^\dagger(t)$ yields

$$R_+ = 1 - \langle n_a(\infty) \rangle = \langle c_a(\infty)c_a^\dagger(\infty) \rangle, \quad (2.78b)$$

which can be interpreted as the ionization probability for the level.

Solving eq. (2.77) and substituting into eq. (2.76), we find

$$\begin{aligned} i\frac{d}{dt}c_a(t) &= \varepsilon_a(t)c_a(t) - i \lim_{t_0 \rightarrow -\infty} \sum_{\mathbf{k}} V_{ak}(t) \int_{t_0}^t e^{-i\varepsilon_k(t-t')} V_{ka}(t') c_a(t') dt' \\ &+ \lim_{t_0 \rightarrow -\infty} \sum_{\mathbf{k}} V_{ak}(t) e^{i\varepsilon_k(t-t_0)} c_k. \end{aligned} \quad (2.79)$$

Now, we observe that the hopping term $V_{ka}(t')$, in the t' -integral of eq. (2.79), is slowly varying on the time-scale of electronic transitions; in other words, it is nearly constant, with respect to the fast oscillating term $e^{-i\varepsilon_k(t-t')}$, for large time scales. On the other hand, the k -summation yields a quasi delta function of $t - t'$. This means that we can neglect the effect of the variation of the hopping interaction within in the time interval (t', t) , and approximate

$$V_{ka}(t') \approx V_{ka}(t) \quad \text{and} \quad c_a(t') \approx e^{i \int_{t'}^t d\tau \varepsilon_a(\tau)} c_a(t), \quad (2.80)$$

within the t' -integral. The latter, known as ‘‘semiclassical approximation’’ [50], let us reduce (2.79) into the integrable form

$$\left[i \frac{d}{dt} - \varepsilon_a(t) + i \Delta_a(t) \right] c_a(t) = \lim_{t_0 \rightarrow -\infty} \sum_k V_{ak}(t) e^{i\varepsilon_k(t'-t_0)} c_k, \quad (2.81)$$

where

$$\Delta_a(t) = \pi \sum_k |V_{ak}(t)|^2 \delta(\varepsilon_a(t) - \varepsilon_k) \quad (2.82)$$

can be interpreted as the lifetime broadening of the atomic level. Eq. (2.81) can be formally integrated and substituted in (2.78a). In this way, we arrive at the key-relationships of RCT:

$$\begin{aligned} \langle n_a(t) \rangle &= \langle n_a \rangle e^{-2 \int_{-\infty}^t \Delta_a(t') dt'} \\ &+ \sum_k \langle n_k \rangle \left| \int_{-\infty}^t dt' V_{ak}(t') e^{-i \int_t^{t'} d\tau [\varepsilon_a(\tau) - \varepsilon_k]} e^{-\int_t^{t'} d\tau \Delta_a(\tau)} \right|^2 \end{aligned} \quad (2.83a)$$

$$\begin{aligned} \langle \bar{n}_a(t) \rangle &= \langle \bar{n}_a \rangle e^{-2 \int_{-\infty}^t \Delta_a(t') dt'} \\ &+ \sum_k \langle \bar{n}_k \rangle \left| \int_{-\infty}^t dt' V_{ak}(t') e^{-i \int_t^{t'} d\tau [\varepsilon_a(\tau) - \varepsilon_k]} e^{-\int_t^{t'} d\tau \Delta_a(\tau)} \right|^2 \end{aligned} \quad (2.83b)$$

Eqs. (2.83) can be solved analytically, under hypersimplified models for the time dependence of the matrix elements of (2.75). For example, we can assume a rectilinear trajectory for the outgoing particle, with velocity v . Then, neglecting the initial occu-

pancy of the atomic state and taking [52, 51]

$$V_{ak}(t) = V_0 e^{-\gamma vt/2}, \quad \varepsilon_a(t) = \varepsilon_{a0}, \quad \Delta(t) = \Delta_0 e^{-\gamma vt}, \quad (2.84)$$

we get:

$$P_0 = \Theta(-\phi - \varepsilon_{a0}) + \frac{2}{\pi} \exp\left[\frac{-\pi |\phi + \varepsilon_a^0|}{\gamma v}\right] \text{sign}(-\phi - \varepsilon_{a0}), \quad (2.85a)$$

and

$$R_+ = \Theta(\varepsilon_{a0} - \phi) - \frac{2}{\pi} \exp\left[\frac{-\pi |\varepsilon_a^0 - \phi|}{\gamma v}\right] \text{sign}(\varepsilon_{a0} - \phi). \quad (2.85b)$$

2.3.2 TDAN Hamiltonian for sputtering

We consider a spinless system where an ejected atom has a valence (affinity) state $|a(t)\rangle$, of instantaneous energy $\varepsilon_a(t)$ and valence (affinity) energy $\varepsilon_{a\infty} = \varepsilon_a(t \rightarrow \infty)$. We assume the metal substrate, of work function $-\phi$, to be unaffected by the collision cascade leading to secondary atomic ejection, so that its conduction band is well described by the unperturbed states $\{|k\rangle\}$ and unperturbed energies $\{\varepsilon_k\}$.

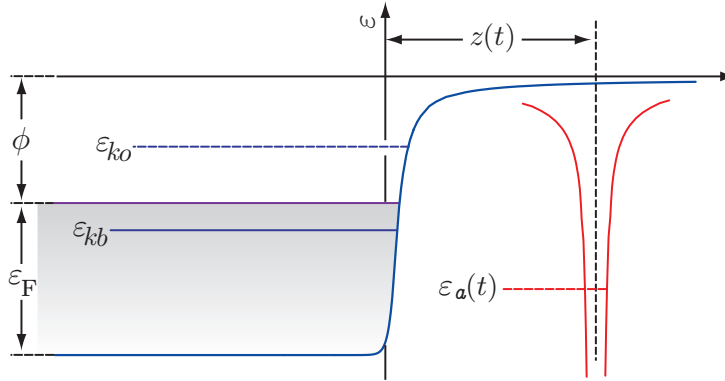


Figure 2.13: Energies of a metal-atom system used in the derivation of the eqs. (2.92).

We complete the TDAN Hamiltonian (2.75) by modeling the hopping integrals as in eq. (2.84): $V_{ak}(t) = V_0 e^{-\gamma vt}$, obtaining a function independent on substrate states. A first aim of the model is to calculate the projected density of states $\rho_a(t, \varepsilon_k)$ for the

ejected atomic orbital. Since sputtering is a rapid process, the projected density of states follows non-adiabatically the reference Hamiltonian (2.75). The consequence is a tail extending above the Fermi level. Ignoring thermal interactions, the probability that an atom is ionized is then

$$R_+ = \int_{-\phi}^{\infty} \rho_a(t \rightarrow \infty, \varepsilon_k) d\varepsilon_k, \quad (2.86)$$

while, the probability that it remains neutral reads

$$P_0 = \int_{-\infty}^{-\phi} \rho_a(t \rightarrow \infty, \varepsilon_k) d\varepsilon_k. \quad (2.87)$$

As a first step, the coupling terms (??) can be treated as small perturbations, and the electronic structure of the non interacting secondary atom/metal system can be reduced to the simplified energy-diagram shown in Fig. 2.13. In particular [15], we partition the metal states into two subsets, $\{|k_o\rangle\}$ and $\{|k_b\rangle\}$, of spectra $\{\varepsilon_{k_o}\}$ and $\{\varepsilon_{k_b}\}$, lying respectively above and below the Fermi level; neglecting thermal interactions, we observe that each state $|k_o\rangle$ is initially empty ($\varepsilon_{k_o} > -\phi$), while each state $|k_b\rangle$ is initially occupied ($\varepsilon_{k_b} \leq -\phi$). We further neglect the parametric time-dependence of the unperturbed part of (2.75), assuming that the atomic orbital is described by a stationary state $|a\rangle = |a(0)\rangle$ of energy $\varepsilon_{a0} = \varepsilon_a(0)$. Hence, we focus on a three level system containing the atomic orbital in interaction either with an empty or with an occupied metal states. The one-electron, time-dependent Hamiltonian, spanning (2.75), simplifies to

$$\begin{aligned} H_{ak_o k_b}(t) &= |a\rangle \varepsilon_a^0 \langle a| + |k_o\rangle \varepsilon_{k_o} \langle k_o| + |k_b\rangle \varepsilon_{k_b} \langle k_b| \\ &+ [V_{ak_o}(t) |a\rangle \langle k_o| + V_{ak_b}(t) |a\rangle \langle k_b| + \text{HC}]. \end{aligned} \quad (2.88)$$

This operator can be diagonalized at each instant of time, using adiabatic perturbation techniques: we consider the approximations

$$|\varepsilon_{a0} - \varepsilon_{k_o}| \gg |\varepsilon_{a0} - \varepsilon_{k_b}|, \quad |V_{ak}(t)| \ll |\varepsilon_{a0} - \varepsilon_{k_o}|, \quad \frac{\partial V_{ak}(t)}{\partial t} \ll (\varepsilon_{a0} - \varepsilon_{k_o})^2. \quad (2.89a)$$

necessary for the applicability of perturbation method. So we can keep only the linear terms in

$$B(t) = \frac{V_{ak}(t)}{(\varepsilon_{a0} - \varepsilon_{k_o})} \quad (2.90)$$

and the linear and quadratic terms in

$$A(t) = \frac{V_{ak}(t)}{\varepsilon_{a0} - \varepsilon_{k_b}} \quad (2.91)$$

to obtain the instantaneous eigenstates:

$$|k_0^A(t)\rangle = |k_0\rangle + B(t)|a\rangle, \quad (2.92a)$$

$$|k_b^A(t)\rangle = \left[1 - \frac{1}{2}A^2(t)\right]|k_b\rangle + A(t)|a\rangle - A(t)B(t)|k_0\rangle, \quad (2.92b)$$

$$|a^A(t)\rangle = \left[1 - \frac{1}{2}A^2(t)\right]|a\rangle + A(t)|k_b\rangle - \left[1 - \frac{1}{2}A^2(t)\right]B(t)|k_0\rangle. \quad (2.92c)$$

Now, in agreement with the adiabatic theorem [59], when we evaluate (2.92), in the long-time limit ($t \rightarrow \infty$), we find that the system retrieves its ground unperturbed state:

$$|k_0^A(\infty)\rangle \rightarrow |k_0\rangle, \quad |k_b^A(\infty)\rangle \rightarrow |k_b\rangle, \quad |a^A(\infty)\rangle \rightarrow |a\rangle. \quad (2.93)$$

Then, in order to find a non trivial solution at large times, we follow the leads of non adiabatic perturbation theory [60], to write

$$|k_0^N(\infty)\rangle = |k_0\rangle + |a\rangle \int_0^\infty dt \langle a^A(t) | \frac{\partial \mathcal{H}}{\partial t} | k_0^A(t) \rangle \frac{e^{i(\varepsilon_{k_o} - \varepsilon_{a0})t}}{\varepsilon_{k_o} - \varepsilon_{a0}} \quad (2.94)$$

$$+ |k_b\rangle \int_0^\infty dt \langle a^A(t) | \frac{\partial \mathcal{H}}{\partial t} | k_0^A(t) \rangle \frac{e^{i(\varepsilon_{k_o} - \varepsilon_{k_b})t}}{\varepsilon_{k_o} - \varepsilon_{k_b}}. \quad (2.95)$$

The probability that the atomic state is mixed into a metal state above the Fermi energy, at $t \rightarrow \infty$, is

$$P_{k_o} = |\langle a | k_0^N(\infty) \rangle|^2 = \left| \int_0^\infty dt \langle a^A(t) | \frac{\partial \mathcal{H}}{\partial t} | k_0^A(t) \rangle \frac{e^{i(\varepsilon_{k_o} - \varepsilon_{a0})t}}{\varepsilon_{k_o} - \varepsilon_{a0}} \right|^2 \quad (2.96)$$

and the projected density comes from the product of this quantity by the density of empty band states $\rho(\varepsilon_{k_o})$:

$$\rho_a(t \rightarrow \infty, \varepsilon_{k_o}) = \rho(\varepsilon_{k_o}) P_{k_o}. \quad (2.97)$$

Using the hopping matrix elements (??), eq. (2.96) reduces to

$$P_{k_o} = \left[1 - \frac{V_0^2}{(\varepsilon_{k_b} - \varepsilon_{a0})^2} \right] \gamma^2 v^2 \frac{V_0^2}{(\varepsilon_{k_o} - \varepsilon_{a0})^4} \quad (2.98)$$

and, neglecting the effect of the metal states below the Fermi level, we get:

$$P_{k_o} \approx \gamma^2 v^2 \frac{V_0^2}{(\varepsilon_{k_o} - \varepsilon_{a0})^4}. \quad (2.99)$$

Thus, the probability (2.86) becomes:

$$R_+ = \gamma^2 v^2 V_0^2 \int_{-\phi}^{\infty} \frac{\rho(\varepsilon_{k_o})}{(\varepsilon_{k_o} - \varepsilon_{a0})^4} d\varepsilon_{k_o}. \quad (2.100)$$

In the case when the atomic energy is resonant with the filled part of the conduction band, i.e., $\varepsilon_{a0} < -\phi$, we can estimate the effect of all initially occupied band states by the following considerations:

1. Each $|k_b\rangle$ is strongly coupled to the atomic state only if its energy is confined within the range

$$\varepsilon_{a0} - \Delta_{a0} \leq \varepsilon_{k_b} \leq \varepsilon_{a0} + \Delta_{a0}, \quad (2.101)$$

given by the width

$$\Delta_{a0} = \pi \rho(\varepsilon_{a0}) V_0^2 \quad (2.102)$$

of the projected density of states at $t = 0$; then, the number of states, below the Fermi energy, involved in the interaction with the atomic state is $\Delta N = \rho(\varepsilon_{a0}) \Delta_{a0}$.

2. The dependence on time of the Hamiltonian (2.75) has the characteristic scale $\tau = (\gamma v)^{-1}$, during which the atomic state is indistinguishable from a group of $\delta N = \delta_{a0} \rho(\varepsilon_{a0})$ states, within the energy interval $\delta_{a0} = 1/\tau = \gamma v$.
3. The ratio $\delta N/\Delta N$ gives a measure of the charge fraction that occupies the atomic state via resonant tunneling from the occupied metal states.

Therefore, the ionization probability (2.100) needs to be corrected as

$$R'_+ = \frac{\delta N}{\Delta N} R_+ = \frac{\gamma^3 v^3}{\pi \rho(\varepsilon_{a0})} \int_{-\phi}^{\infty} \frac{\rho(\varepsilon_{k_o})}{(\varepsilon_{k_o} - \varepsilon_{a0})^4} d\varepsilon_{k_o}. \quad (2.103)$$

Finally, approximating $\rho(\varepsilon_{k_o}) \approx \rho(\varepsilon_{a0})$, we get

$$R'_+ = \frac{\hbar^3 \gamma^3 v^3}{3\pi (-\phi - \varepsilon_{a0})^3}. \quad (2.104)$$

We notice that in the eq. (2.100), where we have neglected charge transfer processes via the occupied metal states, the ionization probability has a quadratic dependence either on the atomic velocity or on the coupling constant V . In contrast, eq. (2.104) shows a cubic dependence on the velocity and no dependence on V . This indicates that the final redistribution of electrons occurs at the time when the width of the projected density of states is close to the natural width δ_{a0} .

As for the validity of the theory, a crucial condition is that the effective atomic level ε_{a0} lies below the Fermi level. However, in many adatom-substrate systems the instantaneous energy $\varepsilon_a(t)$ crosses the Fermi energy, during the atomic motion. We can give a qualitative estimation of the effect of Fermi level crossing on eq. (2.104): in the system depicted in (2.13), the effective energy of the adatom is time dependent, while the hopping integral is time independent. At the time $t = 0$ the effective energy is just equal to the Fermi energy. We assume that the following expression:

$$\varepsilon_a(t) = (\varepsilon_{a0} + \phi) [1 - e^{-\gamma v t}] - \phi \quad (2.105)$$

holds. Working in the sudden approximation [60], we can give an idea of the number of states that do not follow the variations in (2.75) as the time proceeds. Two states,

separated in energy by the amount ω , do not change if the variations in the Hamiltonian occur in a time interval much shorter than $\tau = \omega^{-1}$. In the case depicted in (2.13), the atomic state energy coincides with the Fermi energy, while the state $|k_0\rangle$ is just below the Fermi surface. If the energy separation between the two states is an integer multiple n of the separation ω itself in a time interval smaller than ω^{-1} , then the state $|k_0\rangle$ remains unchanged, which implies

$$n\omega = (\varepsilon_{a0} + \phi) \left(\frac{\gamma_V}{\omega} \right). \quad (2.106)$$

Hence, the number of unchanged states is

$$\rho\omega = \left[(\varepsilon_{a0} + \phi) \frac{\gamma_V}{n} \right]^{1/2} \rho \quad (2.107)$$

and the probability for ion emission:

$$R_+'' = \frac{\rho\omega}{\rho\Delta_{a0}} = \left[(\varepsilon_{a0} + \phi) \frac{\gamma_V}{n\Delta_{a0}^2} \right]^{1/2}. \quad (2.108)$$

By this qualitative approach we can assert that the ionization probability goes as the square root of the emission velocity of sputtered, in the case of Fermi level crossing.

2.3.3 Sroubek's temperature model.

The considerations of the previous subsection suggest a power law dependence of the ionization probability on the ion emission velocity. Brako and Newns [44] showed that the TDAN model can be applied to the study of RCT in secondary atomic emission. This is because the incoming trajectory of a scattering atom is irrelevant to the final occupation/ionization probability of its valence state. In this respect, atoms reflected and ejected from a surface with the same kinetic energy should have the same charge state.

Indeed, Norskov and Lundqvist [14] used a formalism similar to the one leading to eq. (2.85), showing that probability for positive and negative ionization roughly follow

exponential laws

$$R_+ = e^{-(I-\phi)/cv} \quad \text{and} \quad R_- = e^{-(\phi-A)/cv}, \quad (2.109)$$

respectively, where c is a constant, ϕ is the substrate workfunction, and I and A are the ionization potential and the affinity energy of the atom. This trend is in contrast with the power law given by eq. (2.108).

A simple microscopic semi-phenomenological theory of ionization was proposed by in ref [16, 61]: the leading assumption is that the electrons, in the collision cascade region, are excited to the empty states, of energy ε_k , above the Fermi level of the target, with a probability $e^{-\varepsilon_k/k_B T_s}$, in which T_s is the effective “electronic temperature” of the collision cascade region. T_s is assumed to be an empirical parameter having a value between 1000 and 3000 K for clean metals. Another assumption is that T_s is constant during the ejection process and the ejected atoms interact with the excited target through the hopping integrals (??). The latter is taken to be proportional to the overlap of valence wave functions, then, the parameter γ is the average value of γ_a and γ_b , where γ_a and γ_b are defined from the valence wave functions of the ejected atom A and the target atom B , as

$$\psi_a \propto e^{-\gamma_a r}, \quad \psi_b \propto e^{-\gamma_b r} \quad (2.110)$$

The energy ε_a of the valence level of the ejected atom is time dependent, because depends from the distance from surface. Time development of the positive charge \bar{n}_a on the ejected atom satisfies the master equation

$$\frac{d\bar{n}_a}{dt} = -\frac{\bar{n}_a - \bar{n}_{a0}}{\tau} \quad (2.111)$$

where

$$\bar{n}_{a0} = \exp \left[\frac{\varepsilon_F - \varepsilon_a(t)}{k_B T_s} \right], \quad \tau = \frac{e^{2\gamma vt}}{2\Delta}, \quad (2.112)$$

and Δ is the half width of the level ε_a at the surface. The solution of eq. (2.111) for the positive ionization probability $R_+ = \bar{n}_a(\infty)$ is approximately given by

$$R_+ = \exp \left[\frac{\varepsilon_F - \varepsilon_a(t_0)}{k_B T_s} \right], \quad t_0 = \frac{1}{2\gamma} \ln \left(\frac{\Delta}{\gamma v} \right). \quad (2.113)$$

If we further approximate the energy $\varepsilon_a(t)$ with the relations

$$\varepsilon_a(t_0) = \begin{cases} \varepsilon_a(0) + [\varepsilon_a(\infty) - \varepsilon_a(0) \Gamma v t] & , t \leq \frac{1}{\Gamma v} \\ \varepsilon_a(\infty) & , t > \frac{1}{\Gamma v} \end{cases} \quad (2.114)$$

then, the ionization probability R_+ reads

$$R_+ = \exp \left[\frac{\varepsilon_F - \varepsilon_a(0)}{k_B T_s} \right] \exp \left\{ \frac{[\varepsilon_a(0) - \varepsilon_a(\infty)] \Gamma}{k_B T_s} \ln \left(\frac{\Delta}{\gamma v} \right) \right\}, \quad (2.115)$$

for $\Delta e^{-2\gamma/\Gamma} < \gamma v < \Delta$, and

$$R_+ = \exp \left[\frac{\varepsilon_F - \varepsilon_a(\infty)}{k_B T_s} \right] \quad (2.116)$$

for smaller value of γv . As shown in (2.115), the theory predicts a power law behavior of the ionization probability vs the inverse emission velocity, in contrast with the exponential behavior (2.85b) of the TDAN model. Indeed, some experiments seem to validate the behavior (2.115) at low emission velocities [47, 49].

2.3.4 Quasi molecular interactions in sputtering.

We have seen that at emission energies of the order of 10 eV, the basic hopping mechanism for positive ionization can be negligible with respect to surface-induced excitations. A possible way to treat such complicated effects, at a relatively simple level, is to represent surface excitations in terms of local, time dependent potentials, that induce multiple scattering processes in the metal band [54, 55]. An improved formulation uses a double localized level TDAN Hamiltonian, that includes the atomic orbitals of emitted atoms and their nearest neighbour substrate atoms, forming a QM during the first stages of the

emission process [56, 17]. With this mechanism, a band hole may be trapped into a transient molecular orbital (MO), which is promoted to the empty band levels. Then, a new ionization channel has been introduced, in which charge exchanges between sputtered atoms and the metal are mediated by a second localized level interacting resonantly with the continuum. This can be very important at low incident energies, when the QM has a longer average lifetime. The new Hamiltonian has the form

$$\begin{aligned} \mathcal{H}(t) = & \varepsilon_a(t) c_a^\dagger(t) c_a(t) + \varepsilon_m(t) c_m^\dagger(t) c_m(t) + \sum_{\mathbf{k}} \varepsilon_{\mathbf{k}} c_{\mathbf{k}}^\dagger c_{\mathbf{k}'} \\ & + \left[\sum_{\mathbf{k}} V_{ka}(t) c_k^\dagger c_a(t) + \text{HC} \right] + \left[\sum_{\mathbf{k}} V_{km}(t) c_k^\dagger c_m(t) + \text{HC} \right] \\ & + \sum_{\mathbf{k}} V_{kk'}(t) c_k^\dagger c_{k'}, \end{aligned} \quad (2.117)$$

where $\varepsilon_a(t)$ and $\varepsilon_m(t)$ are the atomic and QM energies; $V_{ka}(t)$ is the usual hopping interaction and $V_{km}(t)$ is the coupling between the QM orbital and a continuous state of metal. Finally, $V_{kk'}(t)$ is an intraband scattering potential. Working in the Heisenberg scheme, we have to solve the following equations of motion

$$i \frac{d}{dt} c_a(t) = \varepsilon_a(t) c_a(t) + \sum_{\mathbf{k}} V_{ak}(t) c_k(t) \quad (2.118)$$

$$i \frac{d}{dt} c_m(t) = \varepsilon_m(t) c_m(t) + \sum_{\mathbf{k}} V_{mk}(t) c_k(t) \quad (2.119)$$

$$i \frac{d}{dt} c_k(t) = \varepsilon_k c_k(t) + \sum_{\mathbf{k}'} V_{kk'}(t) c_{k'}(t) + V_{ka}(t) c_a(t) + V_{km}(t) c_m(t) \quad (2.120)$$

The former equations can be combined and iterated to give a formal result in terms of the unperturbed retarded Green's functions of the discrete and continuous states. Using the semiclassical approximation [50], the solution for destruction operator of the atomic-electron is [17]

$$\begin{aligned} c_a(t) = & \lim_{t_0 \rightarrow -\infty} \sum_{kk'} \int_{-\infty}^t dt' \exp \left[-i \int_{t'}^t d\tau [\varepsilon_a(\tau) + \Sigma_a(\tau)] \right] V_{ak}(t') \\ & \times e^{-i\varepsilon_k t'} \left[\delta_{kk'} - i \int_{-\infty}^{t'} dt'' e^{i(\varepsilon_k - \varepsilon_{k'})t''} T_{kk'}^m(\varepsilon_{k'}, t'') \right] e^{i\varepsilon_{k'} t_0} c_{k''}, \end{aligned} \quad (2.121)$$

where $T_{kk'}^m(\varepsilon, t)$ is a Brako and Newns instantaneous T matrix [44], that contains the effect of QM potential; the real and imaginary parts of $\Sigma_a(t)$ give respectively the instantaneous shift and broadening of the atomic level in the interaction with the QM.

Generalized Hamiltonian

In the previous chapter we considered some models about Auger neutralization and resonant charge transfer. These processes, involving charge exchanges between an ion and a solid, can be understood from the basic one-electron, and two-electron, interactions within the many electron system. In this chapter, we shall present the guidelines leading to the definition of a “universal” Hamiltonian which accounts for both Auger and resonant transitions.

The importance of a generalized Hamiltonian consists in having a first principle formalism to apply to the main interactions occurring when a many, mutually interacting electron system is simultaneously probed by a metal surface potential and a moving atomic potential. In the next chapter we will apply this formalism to Auger neutralization and to negative resonant ionization.

3.1 Hamiltonian for one-electron tunneling.

The tunneling of an electron between a moving ion and a homogeneous conductor is modeled by the first quantized, one-body Hamiltonian

$$\hat{H}_1[\mathbf{R}] = \frac{\hat{p}^2}{2} + \hat{V}_E[\mathbf{R}], \quad (3.1)$$

in which $\hat{\mathbf{p}}$ is the momentum operator, and $\hat{\mathbf{r}}$ the position operator, for the particle, while \mathbf{R} denotes the ion position vector relative to the surface plane. All information concerning the (classical) environment are contained into the effective pseudopotential function $V_E(\mathbf{r}, \mathbf{r}', \mathbf{R}) = \langle \mathbf{r} | \hat{V}_E[\mathbf{R}] | \mathbf{r}' \rangle$. This potential operator has the form

$$\hat{V}_E[\mathbf{R}] = \hat{V}_S + \hat{V}_A[\mathbf{R}] + \Delta\hat{V}_{AS}[\mathbf{R}], \quad (3.2)$$

where: (i) $V_S(\mathbf{r}) = \langle \mathbf{r} | \hat{V}_S | \mathbf{r} \rangle$ accounts for the surface barrier of the metal band; (ii) $\hat{V}_A[\mathbf{R}]$ denotes the central field operator of the ion at position \mathbf{R} ; (iii) $\Delta\hat{V}_{AS}[\mathbf{R}]$ describes the change of the surface potential due the ion charge [29, 82]. Eq. (3.2) can be used to study resonant exchange processes in ion-surface scattering, when the effect of the motion of target atoms upon the final charge state of the projectile is neglected. The approximation works quite well for projectiles of impact energies larger than 50 – 100 eV interacting with quasi free-electron targets. Fig. 3.1 shows a schematic diagram of the process taken from ref. [46]

However, at lower energies, say, below ~ 20 eV, the projectile spends much time, close to the target, electronically interacting with nearest neighbor substrate atoms. Such an effect significantly modifies the occupation/ionization probability of the atomic states of the scattering beam that can receive/cease electrons to the metal. A similar situation is offered by low energy, secondary atomic emission following the collision cascade generated by a keV-ion beam: ejected atoms exhibit quasi-molecular interactions with nearest neighbor substrate atoms, which strongly influences their final charge-states, as we shall see in the following chapter. In such cases, the easiest way to account for a moving surface is to consider: (a) the atom whose final charge state we want to investigate and (b) a substrate atom transiently forming a quasi-molecule with the former particle. Both particle are allowed to interact with the ideal substrate, therefore, the pseudo-potential (3.2) becomes:

$$\hat{V}_E[\mathbf{R}_a, \mathbf{R}_b] = \hat{V}_S + \hat{V}_{QM}[\mathbf{R}_a, \mathbf{R}_b] + \Delta\hat{V}_{QMS}[\mathbf{R}_a, \mathbf{R}_b], \quad (3.3)$$

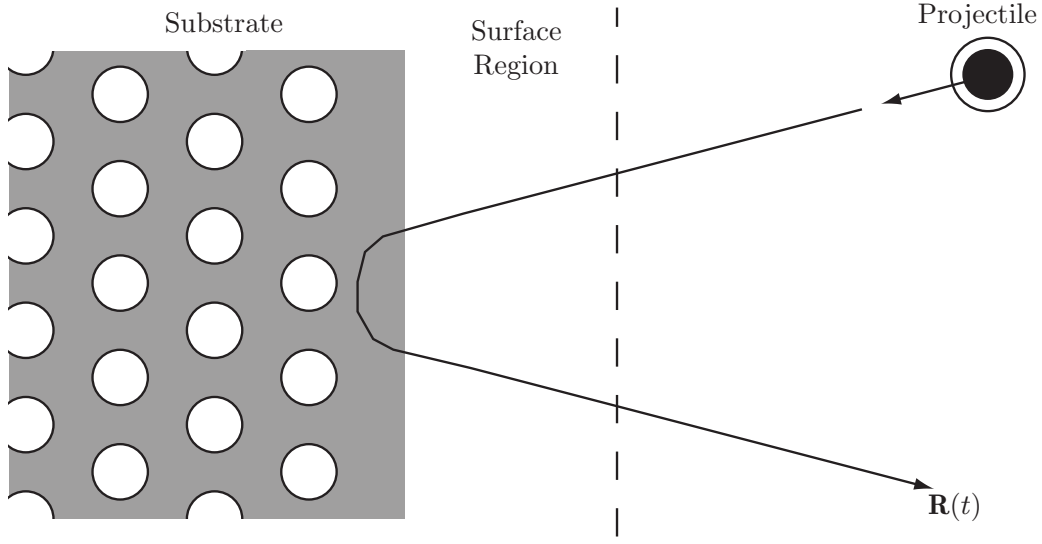


Figure 3.1: Schematic diagram of the scattering of an 10^2 eV ion on a smooth metal surface: in the substrate region the projectile is reflected by the strongly repulsive potential due to the inner orbitals of target atoms. The valence orbital of the adatom completely loses its identity, and makes part of the conduction band of the substrate. In the surface region, the ion trajectory is almost straight, and the interaction between the substrate electronic band and the valence level decreases quickly (approximately exponentially) as the adatom moves away. Outside the surface region, the electron exchange between the projectile and the substrate effectively vanishes, but the energy shift of the atomic level, due to dielectric screening, may still be large.

where

$$\hat{V}_{\text{QM}}[\mathbf{R}_a, \mathbf{R}_b] = \hat{V}_A[\mathbf{R}_a] + \hat{V}_A[\mathbf{R}_b] \quad (3.4)$$

is the potential of the diatomic system, made of (a) and (b) atoms, while

$$\Delta V_{\text{QM}}[\mathbf{R}_a, \mathbf{R}_b] = \Delta \hat{V}_A[\mathbf{R}_a] + \Delta \hat{V}_A[\mathbf{R}_b] \quad (3.5)$$

accounts for the change in the surface potential, due to the effective action of all electrons and protons in the quasi molecule. It follows that the corrected one-body Hamiltonian reads

$$\hat{H}'_1[\mathbf{R}_a, \mathbf{R}_b] = \frac{\hat{p}^2}{2} + \hat{V}_E[\mathbf{R}_a, \mathbf{R}_b]. \quad (3.6)$$

3.1.1 The surface potential

The knowledge of the interaction of an electron with a metal surface plays an essential role in the quantitative description of many phenomena other than surface-barrier tunneling, such as low-energy electron diffraction, field emission, photoemission and inverse photoemission. For this reason, the variation of $V_s(\mathbf{r})$ near the metal-vacuum interface has been central to discussions of the electron-surface interaction for many years. It is well known, from classical electrostatics, that an electron at distance z from an ideal metal surface is attracted to its image, with a potential function of the form $-1/(4z)$, with the substrate in the halfspace $z \leq 0$. This solution is clearly unsatisfactory near the surface, where the electron image potential tends to infinity. The first quantum-mechanical attempt to go beyond this idealized picture was given by Bardeen [?], who examined the potential barrier for the “jellium” model of a simple metal, where the ionic charges are represented by a uniform positive background. Neglecting the dependence of the surface potential on the surface plane coordinates, $V_s(\mathbf{r}) = V_s(z)$, he showed that the electron-surface interaction, far outside the surface ($z \rightarrow \infty$), is described by the image term $-1/(4z)$, but there are large deviations as the electron approaches the surface. Within a few atomic units of the surface, the corrections can be comparable to the image term itself, and the potential goes over smoothly to a constant value inside the metal. More detailed calculations on the same model have been performed by Lang and Kohn [?], who used selfconsistent density-functional, with a local density description of exchange and correlation, to determine charge densities and effective potentials for an electron in the surface region. When considering the response of the surface to an external electric field, they found that the potential far from the surface had the classical image form, but with the reference plane shifted outwards from the edge of the jellium background:

$$V_s(z) \stackrel{z \gg 1 \text{ au}}{=} -\frac{1}{4(z - z_{\text{IM}})}. \quad (3.7)$$

The position of this “image plane” z_{IM} , lying 1 – 3 au beyond the jellium edge, was identified with the center of mass of the induced surface charge. Subsequently, other authors [?] found values of z_{IM} closer to the jellium edge than that obtained by Lang and

Kohn. Based on these considerations, a basic form for the the surface potential is given by the combination of the conduction-band potential, inside the bulk, and the electron self-image potential far outside the surface:

$$V_s^0(z) = -\varepsilon_0 \Theta(z_{\text{IM}}^0 - z) - \frac{1}{4z} \Theta(z - z_{\text{IM}}^0). \quad (3.8)$$

Here, the image plane is fixed at $z_{\text{IM}}^0 = 1/(4\varepsilon_0)$, by the condition that $V_s^0(\mathbf{r})$ is continuous at $z = z_{\text{IM}}$ [28, 82]. The former case of the step potential plus the electronic self-image potential should be a crude approximation to any ab initio surface potential derived from a more sophisticated density functional approach. To study these differences, Jennings, Jones, and Weinert [62] used a full-potential linearized augmented-plane-wave method and computed the effective electronic surface potentials for various metals, such as W, Ni, Cu, and Ag. They averaged the ab initio potential over the surface plane and fitted analytic functions in order to obtain the closed-form expression:

$$V_s(z) = -\frac{\varepsilon_0}{A e^{-B(z-z_{\text{IM}})} + 1} \Theta(z_{\text{IM}} - z) - \frac{1 - e^{-\lambda(z-z_{\text{IM}})}}{4(z - z_{\text{IM}})} \Theta(z - z_{\text{IM}}), \quad (3.9)$$

where $A = -1 + 4\varepsilon_0/\lambda$ and $B = 2\varepsilon_0/A$ constrain continuity and differentiability at the image plane. Eq. (3.9) depends on the parameters λ and z_{IM} , reported in table 3.1; it smoothly interpolates the two asymptotic behaviors of the basic potential (??), with a smearing out governed by λ .

Crystal plane	z_{IM}	λ	ε_0
W(001)	-2.90	0.90	0.500
W(110)	-3.10	0.90	0.525
Ni(001)	-2.30	0.90	0.525
Ni(110)	-2.4	0.9	0.425
Cu(001)	-2.35	1.05	0.425
Cu(110)	-2.4	0.9	0.425
Cu(111)	-2.60	1.10	0.45

Table 3.1: Empirical values of the parameters z_{IM} , λ , and ε_0 , determined in ref.[jennings], by fitting LEED fine-structure, photoemission, and inverse-photoemission data (au).

An improved version of the Jennings' potential has been derived by Chulkov, Silkin and Echenique [63], who used pseudopotential local density calculations to include the periodic oscillations of the bulk component of (3.9), in the z -direction. Specifically, they introduced a lattice parameter, a_s , to account for the separation between two crystal planes, along the surface normal, and corrected (3.9), within the metal, as

$$V_s(z) = A_{10} + A_1 \cos\left(\frac{2\pi z}{a_s}\right), \quad z < 0, \quad (3.10a)$$

in which $A_{10} = -\varepsilon_0$ is the energy of the bottom of the conduction band, in the bulk, and A_1 reproduces the width of the “projected band gap” of the metal. In the solid-vacuum interface region, $0 \leq z < z_{\text{IM}}$, they used the oscillating function

$$V_s(z) = A_{20} + A_2 \cos(\beta z), \quad 0 \leq z < z_1, \quad (3.10b)$$

where A_{20} is the energy of the bottom of the conduction band, at the surface, A_2 , β determine the energies of surface and image states, respectively, and $z_1 = 5\pi/(4\beta)$ is an intermediate point which converts the potential function into a smooth exponential

$$V_s(z) = A_3 e^{-\alpha(z-z_1)}, \quad z_1 \leq z < z_{\text{IM}}, \quad (3.10c)$$

that interpolates the bulk component (3.10) with the Jennings' potential in the Vacuum:

$$V_s(z) = \frac{e^{-\lambda(z-z_{\text{IM}})} - 1}{4(z - z_{\text{IM}})}, \quad z \geq z_{\text{IM}}. \quad (3.10d)$$

The Chulkov's potential, defined by eqs. (3.10a-d) and shown in Fig. ??, depends on ten parameters which are completely determined by fixing A_{10} , A_1 , A_2 , β and constraining continuity and differentiability everywhere in the space. The main features of this potential are that it accounts for a portion of the energy spectrum, i.e., the projected band gap, in the range $(\varepsilon_1, \varepsilon_2)$, where bulk states are absent. Furthermore, due to the symmetry breaking at the surface of the solid, it generates localized electronics states that can be classified as intrinsic surface states and image potential states. The intrinsic surface states appear as a consequence of the termination of the surface and are mainly located at the top-most atomic layer. On the other hand, electrons with energies close

to the vacuum level and within a range forbidden by an energy gap may be trapped in a Rydberg-like series due to the attractive Coulomb-like potential created by the polarization charge induced at the surface region.

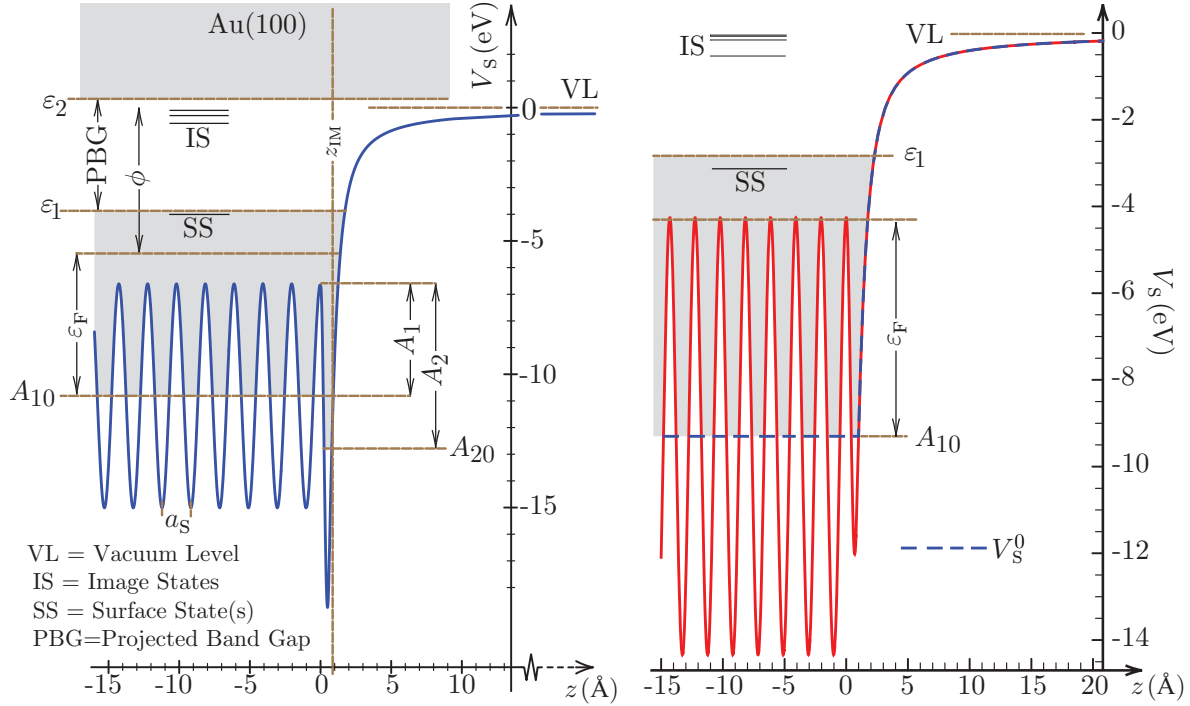


Figure 3.2: Self consistent surface potential (3.10) for Au(100) and Ag(100) surfaces. The shaded area represents the projected bulk bands, with the projected band gap lying in the range $\epsilon_1 - \epsilon_2$. Image and surface states are indicated by discrete lines. In the left panel, we also show the basic step-image potential (3.10)

3.1.2 Metal States

The bulk states of the Chulkov's potential (3.10) are denoted by $\{|k\rangle\}$ and calculated from the diagonalization of the surface Hamiltonian

$$\hat{H}_s = \frac{\hat{p}^2}{2} + \hat{V}_s, \quad (3.11)$$

i.e., from the Schrödinger equation $\hat{H}_s |k\rangle = \epsilon_k |k\rangle$, with $\{\epsilon_k\}$ the band spectrum. Due to the cylindrical symmetry of $V_s(z)$, the metal wave function $\{\langle \mathbf{r} | k \rangle\}$ are plane waves along

the surface plane. Thus, each $\langle \mathbf{r} | k \rangle$ can be factored as

$$\langle \mathbf{r} | k \rangle = \frac{e^{i\mathbf{r}_{\parallel} \mathbf{k}_{\parallel}}}{L} \psi_{k_{\perp}}(z), \quad (3.12)$$

where L is the thickness of the solid, $\mathbf{k} = (\mathbf{k}_{\parallel}, k_{\perp})$ the electron wavevector and $\psi_{k_{\perp}}(z)$ obeys to the eigenvalue equation

$$\left[-\frac{\partial_z^2}{2} + V_s(z) \right] \psi_{k_{\perp}}(z) = \left(\varepsilon_k - \frac{k_{\parallel}^2}{2} \right) \psi_{k_{\perp}}(z). \quad (3.13)$$

Applying the Born-von Karman periodic boundary conditions, the wavevector becomes quantized, meaning that we can write: $\mathbf{k} = 2\pi \mathbf{n}/L$, with $\mathbf{n} \in \mathbb{N}^3$. Therefore, to each choice of L there corresponds a different discretization of the band spectrum $\{\varepsilon_k\}$ and, then, a different number of metal states, solution of (3.13).

In the step-barrier approximation, i.e., when $V_s(z)$ is replaced with the bulk component of (3.8), each eigenfunction of (3.13), denoted $\psi_{k_{\perp}}^0(z)$, results from the superposition of an incident bulk term, proportional to $e^{ik_{\perp}z}$, a reflected bulk term, proportional to $e^{-ik_{\perp}z}$, and a reflected vacuum term, proportional to $e^{-\lambda_{\perp}z}$, with a decay rate $\lambda_{\perp} = \sqrt{-k_{\perp}^2 + 2\varepsilon_0}$. The self-consistent Chulkov's potential requires to numerically solve eq. (3.13) with the boundary conditions $\psi_{k_{\perp}}(\pm L) = \psi_{k_{\perp}}^0(\pm L)$. We consider the ideal flat surfaces of Aluminum, Copper, Silver and Gold. In particular, we examine the Al(111), Cu(100), Ag(100), and Au(100) cases, with the parameters reported in table 3.2

Surf.	A_{10} (eV)	A_1 (eV)	A_2 (eV)	β (au)	ε_1 (eV)	ε_2 (eV)	z_{IM} (au)	ϕ (eV)*
Al(111)	-15.70	0.30	1.95	5.73	-8.89	-8.64	3.49	4.24
Au(100)	-10.810	4.20	6.0690	3.3626	-3.87	0.33	2.06	5.47
Ag(100)	-9.300	5.04	3.8808	2.4222	-2.83	2.21	1.62	4.43

Table 3.2: Key parameters of the Chulkov's potential (3.10) for Al(111), Au(100) and Ag(100). Energies are measured from to the vacuum level, while z_{IM} is measured from the surface plane. The work function is taken from the experiments of ref.

To construct the band states for Al(111) we fix L to $\sim 10^3 \text{ \AA}$ so that the maximum energy spacing between two band states, at $\mathbf{k}_{\parallel} = 0$, is smaller than $\sim 0.05 \text{ eV}$. Thus, we

consider ~ 500 perpendicular wavevectors to reproduce the continuum spectrum up to $\varepsilon_k = 10$ eV. Fig. 3.3(A) shows the spatial probability density $p_{k_F}(z) = |\psi_{k_F}(z)|^2$ for an

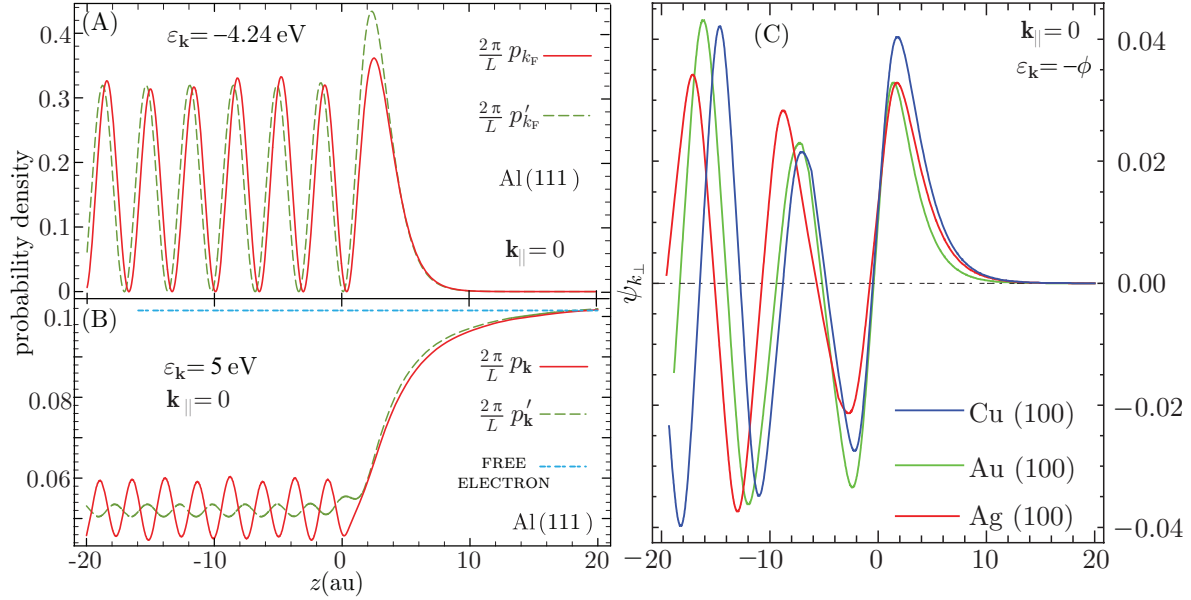


Figure 3.3: (A) Spatial probability densities $p_{k_F}(z)$ and $p'_{k_F}(z)$, spanned by the potentials (3.10) and (3.9), respectively, for an Al(111) state at the Fermi energy with $\mathbf{k}_{\parallel} = 0$; (B) spatial probability densities $p_{k_{\perp}}(z)$ and $p'_{k_{\perp}}(z)$ for an Al(111) state of the continuous spectrum above the vacuum level ($\mathbf{k}_{\parallel} = 0$, $\varepsilon_k = 5$ eV). The probability density for a free electron is also shown. (C) normalized wavefunctions $\psi_{k_{\perp}}(z)$, for an electron at the Fermi energy of Cu(100), Ag(100) and Ag(111) with $k_{\perp} = k_F$ and $\mathbf{k}_{\parallel} = 0$.

electron of Al(111) at the Fermi level with parallel momentum $\mathbf{k}_{\parallel} = 0$; Fig. 3.3(B) shows $p_{k_{\perp}}(z) = |\psi_{k_{\perp}}(z)|^2$ for an electronic state of the continuum spectrum of Al(111), above the vacuum level (with $\mathbf{k}_{\parallel} = 0$ and $\varepsilon_k = 5$ eV). For comparison, we report to the corresponding quantities, $p'_{k_F}(z)$ and $p'_{k_{\perp}}(z)$, calculated from the Jennings' potential (3.9). The two bases are significantly different at atomic distances from surface, which reflects in the calculation of the local density of states. Nevertheless, the use of eigenfunctions of the Jennings' potential to reproduce the conduction band and the continuous spectrum of Al(111) is still a reasonable approximation, because of the narrow projected band gap in the conduction band, well below the Fermi surface.

On the other hand, Cu(100), Ag(100) and Ag(111) have a large band gap around the Fermi energy, which extends above the vacuum level (Fig. ??). In this case L is chosen in order to have a maximum energy spacing between two band states, at $\mathbf{k}_{\parallel} = 0$, smaller

than ~ 0.025 eV. In this way, about ~ 250 perpendicular wave-vectors are used to reproduce the continuum spectrum below ε_1 . Fig. 3.3(C) shows the normalized wave-functions $\psi_{k_\perp}(z)$, for an electron at the Fermi energy of Cu(100), Ag(100) and Ag(111) with $k_\perp = k_F$ and $\mathbf{k}_\parallel = 0$.

3.1.3 Atomic Potential

As we discussed in chapter 2, we shall focus on ion-metal systems where the atomic particle (adatom) has one active level capable of exchanging electrons with the substrate. Accordingly, the modelling of the atomic potential depends on whether we are considering positive or negative ionization/neutralization processes. In the first case, the atomic level is specified by a valence orbital and an instantaneous ionization energy. In the latter case, we have an affinity orbital and an instantaneous affinity energy.

In the case of positive ionization, which applies, for example, to AN and RN processes, we consider an adatom, of atomic number Z , in which the outer electron (valence state) is attracted by the effective central field of all other $(Z - 1)$ electrons. The corresponding state-dependent potential is written in the local form

$$V_A(r) = \langle \mathbf{r} | \hat{V}_A[\mathbf{R} = \mathbf{0}] | \mathbf{r} \rangle = -\frac{(Z - 1)\sigma(r) + 1}{r}, \quad (3.14)$$

where $\sigma(r)$ is a screening function accounting for the average effect of all the inactive atomic electrons. Therefore, the effective ion charge is $Q_{\text{EFF}}(r) = (Z - 1)\sigma(r) + 1$. Such an approximation works quite well for single-valenced adatoms, such as Li, Na, or Cs, while it is a crude approximation for noble gas ions, such as Ar^+ . Several types of screening functions can be found in literature [?], starting from the constant value $\sigma(r) = \sigma_0$ that reduces the atomic particle to a Hydrogenoid atom. An exponential screening function, of the form $\sigma(r) = \sigma_0 e^{-\mu_0 r}$, is suitable for alkali atoms. A more self-consistent type of screening was obtained by Green, Sellin and Zachor [64] who, using Hartree-Fock calculations, proposed the three-parameter interpolating function

$$\sigma(r) = \frac{1}{\alpha d (Z - 1)^\nu (e^{\frac{r}{d}} - 1) + 1}, \quad (3.15)$$

and showed that, for most elements of the periodic table, the parameters ν and α can be fixed to $\nu = 0.4$ and $\alpha = 1.05$, so that (3.14) depends basically on the screening length d . We notice that when the electron is close to the nucleus, at $r \rightarrow 0$, eq. (3.15) tends to 1 and the pseudopotential (3.14) becomes the bare Coulomb potential $-Z/r$. On the other hand, when the electron is far from the nucleus, at $r \rightarrow \infty$, the pseudopotential (3.14) tends to $-1/r$, i.e., the electron sees the atomic nucleus plus the remaining $Z-1$ electrons as an effective proton charge

Z	Symb.	d (au)	I'_a (eV)	I_a (eV)	Z	Symb.	d (au)	I_{TH} (eV)	I_{EXP} (eV)
3	Li	0.563	5.0775	5.3917	11	Na	0.561	4.94629	5.1391
18	Ar	0.862	15.3062	15.7596	55	Cs	1.022	3.5002	3.8939

Table 3.3: Values of d entering eq. (3.15) taken from ref. [Green] for some alkali atoms and for Ar. I'_a denotes the theoretical ionization energy, calculated from the self-consistent potential (3.14), while I_a is taken from the NIST website [www.nist.gov]

The study of negative ions requires the determination of the bound states of electrons in the dipolar potential of neutral atomic particles. A simple way to establish this interaction is to use a separable, non local potential [65, 66]

$$\hat{V}_A[\mathbf{R} = \mathbf{0}] = \eta |\phi\rangle \langle\phi|, \quad (3.16)$$

spanned by the normalized state $|\phi\rangle$ which is related to the affinity state of the atomic system. The advantage with this approach is that the calculated wave function is accurately described also in the inner region of the atom. The separable potential has been very successful for the description of negative ion states with zero angular momentum, such as H^- and Li^- [?]

3.1.4 Atomic States

The localized orbital of the adatom, at position \mathbf{R} , is generated by the atomic Hamiltonian

$$\hat{H}_A[\mathbf{R}] = \frac{p^2}{2} + \hat{V}_A[\mathbf{R}], \quad (3.17)$$

via the Schrödinger equation $\hat{H}_A[\mathbf{R}]|a(\mathbf{R})\rangle = \varepsilon_a^0|a(\mathbf{R})\rangle$. The state $|a(\mathbf{R})\rangle$ follows the motion of the adatom, yielding the localized wavefunction

$$\langle \mathbf{r}|a(\mathbf{R})\rangle = \langle \mathbf{r} - \mathbf{R}|a\rangle, \quad (3.18)$$

where $|a\rangle$ is the atomic state calculated from the ion's reference frame ($\mathbf{R} = \mathbf{0}$). This means that we can calculate $|a\rangle$ from $\hat{V}_A[\mathbf{R} = \mathbf{0}]$ and then set back the reference frame to the topmost surface layer. In positive ionization/neutralization, we use the potential function (3.15) so that the atomic energy ε_a^0 coincides with the ionization energy $-I_a$. In negative ionization/neutralization, we consider the separable potential (3.16) and ε_a^0 denotes the affinity energy $-A_a$.

Positive ion states

We begin with the valence state of a positive ion, observing that the function (3.15) is spherically symmetric. Then, the ionization orbital is specified by definite angular momentum quantum numbers, say l_a and m_a . Hence, we use the factorization

$$\langle \mathbf{r}|a\rangle = R_a(r) Y_{l_a}^{m_a}(\Omega), \quad (3.19)$$

where R_a is the unknown radial wavefunction, solution of the radial Schrödinger equation

$$\left[-\frac{1}{2} \frac{d^2}{dr^2} - \frac{1}{r} \frac{d}{dr} + \frac{l_a(l_a+1)}{2r^2} + V_A(r) \right] R_a(r) = -I_a R_a(r) \quad (3.20)$$

and $Y_{l_a}^{m_a}(\Omega) = \langle \Omega|l_a m_a\rangle$ is the spherical harmonic for the quantum numbers (l_a, m_a) . Fig. 3.4(A) shows the numerical probability densities $p_a(r) = 4\pi r^2 |R_a(r)|^2$, for the

valence states of Li, Na and Cs, calculated from (3.20) with the parameters reported in table 3.3. In order to improve the validity of the pseudopotential method, we assume a radial wave function of the shape

$$R_a(r) = \frac{f_a(r) e^{-\lambda_a r}}{r \sqrt{\langle l_a m_a | l_a m_a \rangle}}, \quad (3.21)$$

where the decreasing exponential has a decay rate related to the ionization energy as $\lambda_a = \sqrt{2I_a}$. Eq. (3.20) becomes

$$\left\{ \frac{d^2}{dr^2} - 2\lambda_a \frac{d}{dr} - \left[\frac{l_a(l_a+1)}{r^2} + 2V_A(r) \right] \right\} R_a(r) = 0. \quad (3.22)$$

Unlike ref. [64], we impose that the experimental value $-I_a$ is the eigenvalue for the potential (3.14). Therefore, we solve (3.22) numerically optimizing the parameters $H = \alpha d (Z-1)^\nu$ and d in order to obtain a normalizable radial function $R_a(r)$ on a very large interval on the atomic scale. Then, we analytically continue (3.21) by interpolating its behavior with the exponential function $e^{-\lambda_a r}$.

For example, in the case of Argon, the valence state we are looking for lies the $3p$ -shell, which contains six electrons. The experimental ionization energy is $I_a = 15.76$ eV, while the theoretical value is $I'_a = 15.30$ eV. So, the screening function takes into account the asymmetry of charge due to the existence of other electrons in the remaining subshells. The initial condition is given by the analytical wavefunction $R_{3p}^0(r)$ of the bare Coulomb potential $-18/r$, with eigenenergy $-I_a$. Parameter optimization yields

$$H = 2.62296 \pm 0.00001, \quad d = 0.74001 \pm 0.00001, \quad (3.23)$$

which prevents $R_{3p}(r)$ to explode in the range $0 \leq r \leq 50$ Å. For $r > 50$ Å, we interpolate the behavior of R_{3p} with the exponential $e^{-0.761 r}$. Fig. 3.4(B) shows the numerical probability densities $p_{3p}(r) = 4\pi r^2 |R_{3p}(r)|^2$ calculated either from eq. (3.22), with the parameters (3.23), or from eq. (3.20) with the parameters reported in table 3.3. For comparison, we also show the Hydrogenoid probability density $p_{3p}^H(r)$, generated by the Coulomb potential $-3.22874/r$, and corresponding to an analytical bound state with eigenenergy $-I_a$. We observe that slight differences are detected in the two numerical

solutions whose peak position and asymptotic behavior is agreement with self-consistent Hartree-Fock calculations on Argon [?].

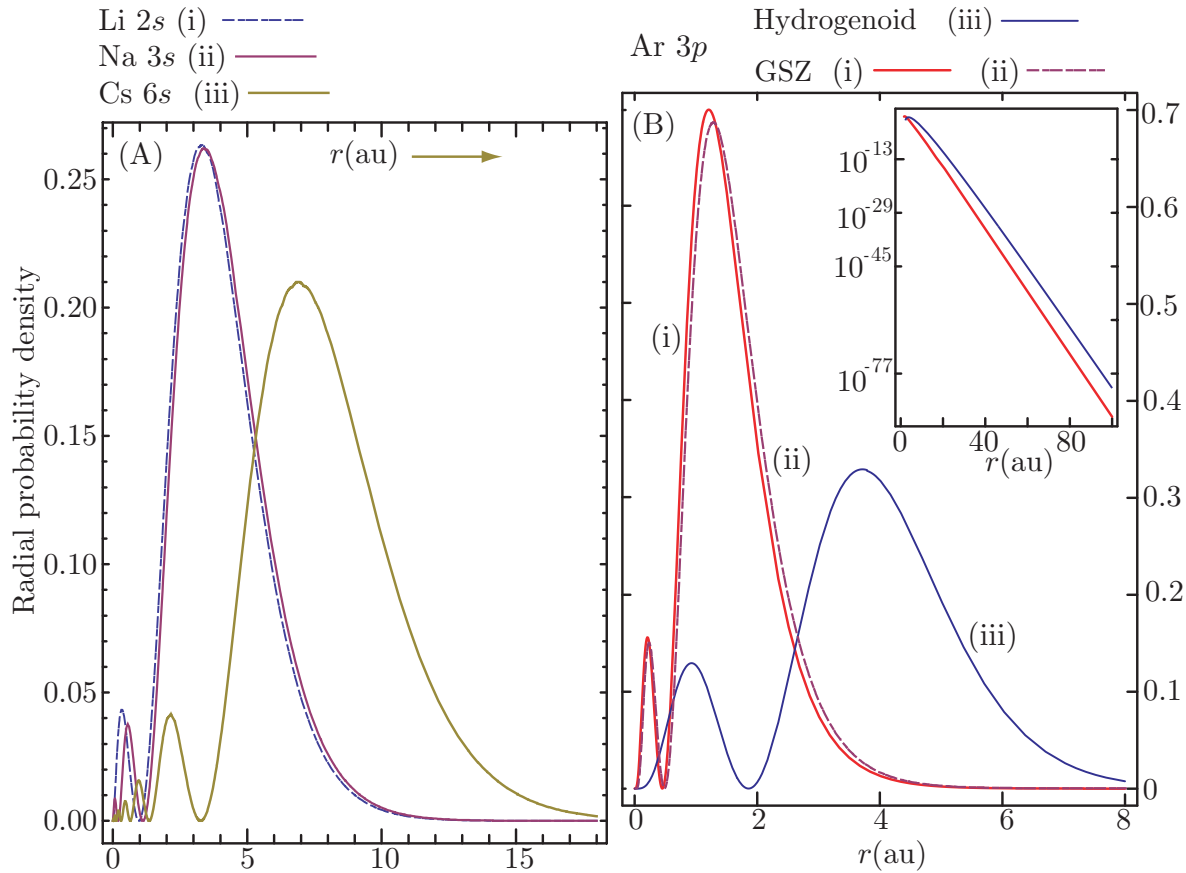


Figure 3.4: (A) Radial probability density $p_a(r)$ for the valence states of Li (i), Na (ii) and Cs (iii) Atoms. Eq. (3.20) has been used, with the parameters reported in table 3.3. (B) Radial probability density for the $3p$ state of Ar, with the numerical methods explained in the text: curve (i) corresponds to the numerical solution of eq. (3.22), with the parameters (3.23); curve (ii) is obtained from eq. (3.20) with the parameters of table 3.3; curve (iii) corresponds to the analytical hydrogenoid orbital

Negative ion states

For a correct description of the physical properties of negative ions, it is important that the calculated electron wave functions have the right asymptotic behavior

$$\langle \mathbf{r} | a \rangle \rightarrow \sqrt{2\lambda_a} B_a \frac{e^{-\lambda_a r}}{r} Y_{l_a}^{m_a}(\Omega), \quad (3.24)$$

where the affinity energy of the state is $A_a = \lambda_a^2/2$ and the asymptotic parameter B_a has been calculated tabulated for different negative ions [66]. The asymptotic tail of the wave function determines many of its physical properties such as the polarizability, cross sections for electron attachment and detachment. In addition it plays a crucial role in the determination of the probabilities for charge transfer in collisions between negative ions and atoms. The state $|\phi\rangle$, in the potential operator (3.16), can be obtained from the affinity state of the negative-ion through

$$|\phi\rangle = \frac{1}{\eta \langle \phi|a\rangle} \left(\frac{\hat{p}^2}{2} - \frac{\lambda_a^2}{2} \right) |a\rangle \quad (3.25)$$

and the coupling constant η is calculated through

$$\eta = \frac{\langle \phi| (\hat{p}^2 - \lambda_a^2) |a\rangle}{2 \langle \phi|a\rangle}. \quad (3.26)$$

An accurate analytical form for negative ions of s -simmetry, like Ag^- and Au^- , is

$$\langle \mathbf{r}|a\rangle = B_a \sqrt{2\alpha} \frac{e^{-\lambda_a r} - e^{-\mu_a r}}{r} Y_0^0(\Omega), \quad (3.27)$$

where $\mu_a > \lambda_a$. The coefficient B_a is obtained from the asymptotic form of the exact wave function. Normalization of the wave function uniquely determines μ_a

$$\mu_a = \frac{\lambda_a B_a^2 + \frac{\lambda_a}{2}}{B_a^2 - 1} + \sqrt{\frac{(\lambda_a B_a^2 + \frac{\lambda_a}{2})^2}{(B_a^2 - 1)^2} - \frac{B_a^2 \lambda_a^2}{B_a^2 - 1}} \quad (3.28)$$

The normalized ‘‘inner function’’ $\langle \mathbf{r}|\phi\rangle$, spanning the affinity orbital (3.27), has the form

$$\langle \mathbf{r}|\phi\rangle = \sqrt{\frac{\mu_a}{2\pi}} \frac{e^{-\mu_a r}}{r}, \quad (3.29)$$

yielding, by eq. (3.26), the coupling constant

$$\eta = -\frac{1}{2} (\lambda_a + \mu_a)^2. \quad (3.30)$$

Ion	B_a (au)	λ_a (au)	μ_a (au)	A_a (eV)
H ⁻	1.67	0.236	0.752	0.7577
Li ⁻	1.90	0.212	0.556	0.6114
Cu ⁻	2.93	0.301	0.526	1.2327
Ag ⁻	3.79	0.309	0.469	1.2991
Au ⁻	3.94	0.412	0.613	2.3095

Thus, the potential operator for a negative ion at position \mathbf{R} reads

$$\hat{V}_A[\mathbf{R}] = -\frac{(\lambda_a + \mu_a)^2}{2} |\phi[\mathbf{R}]\rangle \langle\phi[\mathbf{R}]|, \quad (3.31)$$

with $\langle\mathbf{r}|\phi[\mathbf{R}]\rangle = \langle\mathbf{r} - \mathbf{R}|\phi\rangle$. The parameters N_A , λ_a and μ_a for some negative ions are reported in ??.

3.1.5 Image potential

The third term in (3.2) describes the effect of the variation of the electron density, in the surface region, due to the ion-surface interaction. To describe $\Delta\hat{V}_{AS}[\mathbf{R}]$, we express the ion position vector as

$$\mathbf{R} = \mathbf{R}_{\parallel} + Z \mathbf{u}_z, \quad (3.32)$$

where, in a reference frame centered at the surface of the solid, \mathbf{R}_{\parallel} denotes the component of \mathbf{R} parallel to the surface plane, Z is the ion-surface distance, and \mathbf{u}_z is the versor of the perpendicular direction to the surface. Fig. (3.5) shows the ion-surface coordinate system.

In the region where the overlap between the atom and the surface electrons is small ($Z \gtrsim 10$ au), $\Delta\hat{V}_{AS}[\mathbf{R}]$ is proportional to the classical potential due to the image charges of all inactive electrons and all protons within the atom, i.e., $\Delta\hat{V}_{AS}[\mathbf{R}] \approx -\hat{V}_A[\mathbf{R}'(z_{\text{IM}})]$, where

$$\mathbf{R}'(z_{\text{IM}}) = \mathbf{R}_{\parallel} - (Z - 2z_{\text{IM}}) \mathbf{u}_z \quad (3.33)$$

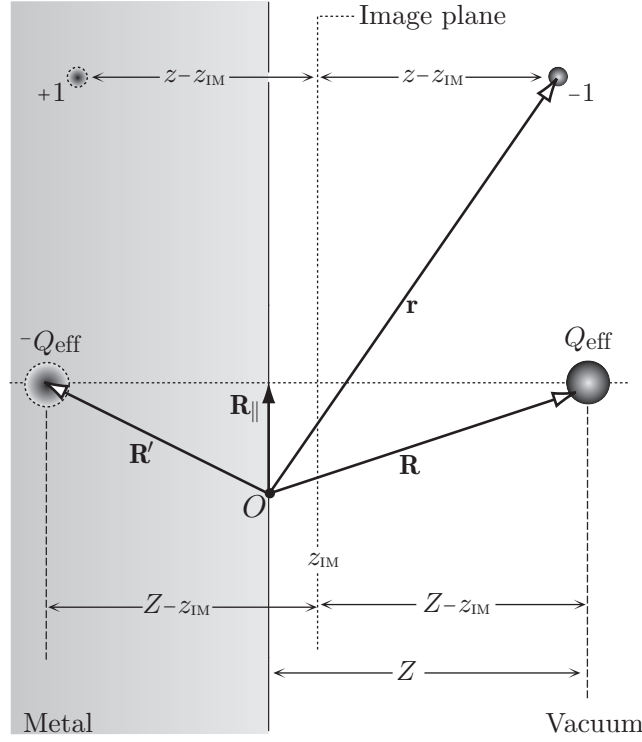


Figure 3.5: Coordinate system for an ion, of charge Z , approaching a metal surface.

denotes the position of the image charge. More specifically, for positive ions the screening function (3.15) induces an effective image charge

$$-Q_{\text{EFF}}(r, \mathbf{R}, z_{\text{IM}}) = (Z - 1) \sigma(|\mathbf{r} - \mathbf{R}'(z_{\text{IM}})|) + 1, \quad (3.34)$$

due to the nuclear charge and to other electrons not participating to the process. Then, the $\Delta\hat{V}_{\text{AS}}[\mathbf{R}]$ terms yields the potential function

$$\Delta V_{\text{AS}}(\mathbf{r}, \mathbf{R}) = \langle \mathbf{r} | \Delta\hat{V}_{\text{AS}}[\mathbf{R}] | \mathbf{r} \rangle \stackrel{Z \gtrsim 10 \text{ au}}{=} \frac{Q_{\text{EFF}}(r, \mathbf{R}, z_{\text{IM}})}{|\mathbf{r} - \mathbf{R}'(z_{\text{IM}})|}. \quad (3.35)$$

For negative ionization, $\Delta\hat{V}_{\text{AS}}[\mathbf{R}]$ has the form of a van der Waals interaction, which can be obtained from the state $|\phi\rangle$ as

$$\Delta\hat{V}_{\text{AS}}[\mathbf{R}] \stackrel{Z \gtrsim 10 \text{ au}}{=} -\frac{(\lambda_a + \mu_a)^2}{2} |\phi[\mathbf{R}'(z_{\text{IM}})]\rangle \langle \phi[\mathbf{R}'(z_{\text{IM}})]|. \quad (3.36)$$

It turns out that the effect of image charges is stronger in positive ionization. When the ion is at short atomic distances from the surface, between the surface $\Delta\hat{V}_{\text{AS}}[\mathbf{R}]$ tends to

an approximate constant value and then it switches off inside the metal [12, 19, 29]. To model such a behavior, we interpolate the expressions for $\Delta V_{\text{AS}}(\mathbf{r}, \mathbf{R})$, in eq. (3.35), and $\langle \mathbf{r} | \phi[\mathbf{R}'(z_{\text{IM}})] \rangle$, in eq. (3.36), at large atom-surface distances with the smooth decreasing function $A z \exp[-B(z - z_{\text{IM}})^2]$. Finally we constrain $\Delta \hat{V}_{\text{AS}}[\mathbf{R}] = \hat{0}$, for $Z < 0$. Fig. (3.6) shows the surface potential function (3.10), corrected by the effect of $\Delta \hat{V}_{\text{AS}}[\mathbf{R}]$, in the case of 100 eV Ar^+ ion impinging on Al(111).

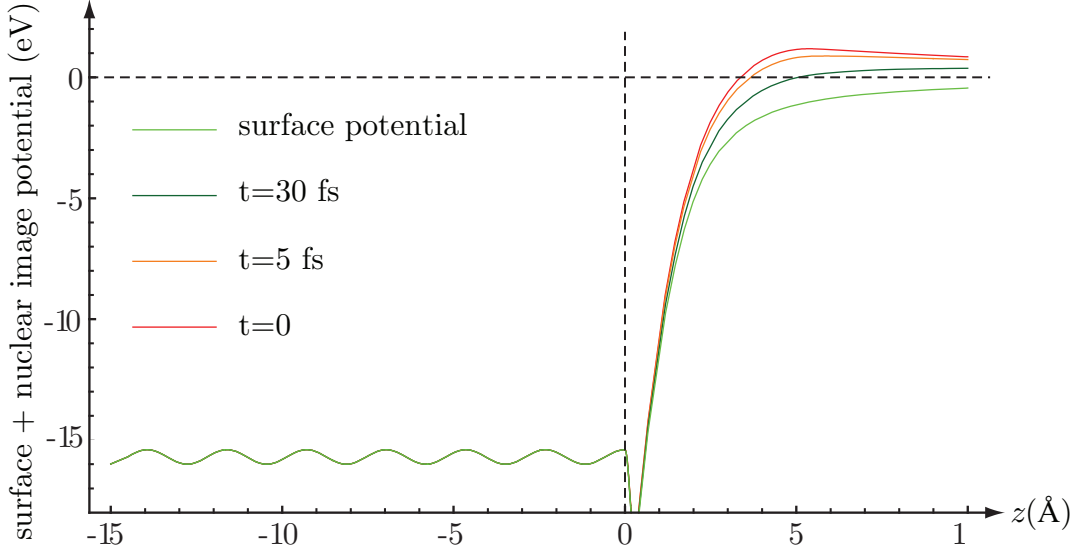


Figure 3.6: Surface potential plus nuclear image potential $V_s(z) + \Delta V_{\text{AS}}(z, \mathbf{R})$ for a 100 eV Ar^+ ion impinging on Al(111). A rectilinear trajectory is used for the impinging particle, with incidence angle of 10° . The instant $t = 0$, corresponds to an atom-surface distance of 4.5 Å.

3.1.6 Field Operator: selection of a truncated basis

In order to express the Hamiltonians (3.1), or (3.6), in a second quantized form, we need introduce the field operator $\Psi(\mathbf{r}; \mathbf{R})$, or $\Psi(\mathbf{r}; \mathbf{R}_a, \mathbf{R}_b)$, for the many electron system which depends parametrically on the positions of the moving particles. In the coordinate space representation, either $\Psi(\mathbf{r}; \mathbf{R})$ or $\Psi(\mathbf{r}; \mathbf{R}_a, \mathbf{R}_b)$ obey to the the ordinary anticommutation

rules of fermion operators

$$[\Psi(\mathbf{r}), \Psi^\dagger(\mathbf{r}')]_+ = \Psi(\mathbf{r})\Psi^\dagger(\mathbf{r}') + \Psi^\dagger(\mathbf{r}')\Psi(\mathbf{r}) = \delta(\mathbf{r} - \mathbf{r}') \quad (3.37a)$$

$$[\Psi(\mathbf{r}), \Psi(\mathbf{r}')]_+ = [\Psi^\dagger(\mathbf{r}), \Psi^\dagger(\mathbf{r}')]_+ = 0. \quad (3.37b)$$

For notational convenience, we introduce a generalized field operator $|\Psi[\mathbf{R}]\rangle$, or $|\Psi[\mathbf{R}_a, \mathbf{R}_b]\rangle$, defined by the property that its projection on a generical single particle bra $\langle\alpha|$ gives the annihilation operator of an electron in the state $|\alpha\rangle$, i.e.,

$$\langle\alpha|\Psi\rangle = c_\alpha, \quad \langle\Psi^\dagger|\alpha\rangle = c_\alpha^\dagger, \quad \langle\mathbf{r}|\Psi\rangle = \Psi(\mathbf{r}), \quad \langle\Psi^\dagger|\mathbf{r}\rangle = \Psi^\dagger(\mathbf{r}). \quad (3.38)$$

The algebraic rules (3.37) are easily extended to any set of fermion operators $\{c_\alpha\}$, $\{c_\alpha^\dagger\}$ as

$$[c_\alpha, c_{\alpha'}^\dagger]_+ = \delta_{\alpha\alpha'}, \quad [c_\alpha, c_{\alpha'}]_+ = [c_\alpha^\dagger, c_{\alpha'}^\dagger]_+ = 0. \quad (3.39)$$

It follows that the second quantized version of the Hamiltonians (3.1) and (3.6) are, respectively,

$$\begin{aligned} \mathcal{H}_1[\mathbf{R}] &= \langle\Psi^\dagger[\mathbf{R}]|\hat{H}_1[\mathbf{R}]|\Psi[\mathbf{R}]\rangle = -\frac{1}{2} \int d^3r \Psi^\dagger(\mathbf{r}; \mathbf{R}) \nabla^2 \Psi(\mathbf{r}; \mathbf{R}) \\ &\quad + \int d^3r \int d^3r' \Psi^\dagger(\mathbf{r}; \mathbf{R}) \langle\mathbf{r}|\hat{V}_E[\mathbf{R}]|\mathbf{r}'\rangle \Psi(\mathbf{r}'; \mathbf{R}) \end{aligned} \quad (3.40a)$$

and

$$\begin{aligned} \mathcal{H}'_1[\mathbf{R}_a, \mathbf{R}_b] &= \langle\Psi^\dagger[\mathbf{R}_a, \mathbf{R}_b]|\hat{H}'_1[\mathbf{R}_a, \mathbf{R}_b]|\Psi[\mathbf{R}_a, \mathbf{R}_b]\rangle \\ &= -\frac{1}{2} \int d^3r \Psi^\dagger(\mathbf{r}, \mathbf{R}_a, \mathbf{R}_b) \nabla^2 \Psi(\mathbf{r}, \mathbf{R}_a, \mathbf{R}_b) \\ &\quad + \int d^3r \Psi^\dagger(\mathbf{r}, \mathbf{R}_a, \mathbf{R}_b) \langle\mathbf{r}|\hat{V}_E[\mathbf{R}_a, \mathbf{R}_b]|\mathbf{r}'\rangle \Psi(\mathbf{r}, \mathbf{R}_a, \mathbf{R}_b). \end{aligned} \quad (3.40b)$$

A more detailed specification of the one-electron processes occurring when one, or two, moving atomic particles interact with a metal surface, requires the definition of a complete orthonormal set. In general, the electron field operator of a many particle system

can be expanded into a one-particle basis $\{|\alpha\rangle\}$ as

$$|\Psi\rangle = \sum_{\alpha} |\alpha\rangle \langle\alpha|\Psi\rangle = \sum_{\alpha} |\alpha\rangle c_{\alpha}, \quad (3.41)$$

then a one-electron Hamiltonian \hat{H}_1 is converted into the second quantized operator

$$\mathcal{H}_1 = \sum_{\alpha\alpha'} \langle\alpha|\hat{H}_1|\alpha'\rangle c_{\alpha}^{\dagger} c_{\alpha'}. \quad (3.42)$$

In our application, the diagonalization of the surface Hamiltonian (3.11) provides a basis of one-electron states ($B_s = \{|k\rangle\}$), which includes both the band states and the projected states above the vacuum level. In practice, however, the calculation of each wavefunction $\langle\mathbf{r}|k\rangle$ come from the numerical solution of eq. (3.13). Thus, we can calculate only a subset B'_s , of the basis B_s . On the other hand, we have at our disposal the atomic Hamiltonian (3.17), which provides one or two additional states, i.e., $|a(\mathbf{R})\rangle$, or $|a(\mathbf{R}_a)\rangle$ and $|a(\mathbf{R}_b)\rangle$. It follows that, we can represent the many electron system into an approximated basis, made of:

- (i) the truncated, orthonormal set B'_s and the orthonormalized atomic state

$$|\alpha(\mathbf{R})\rangle = \frac{|a(\mathbf{R})\rangle - \sum_{k \in B'_s} |k\rangle \langle k|a(\mathbf{R})\rangle}{\sqrt{N_{\alpha}(\mathbf{R})}}, \quad (3.43)$$

where $N_{\alpha}(\mathbf{R})$ is a real normalization constant;

- (ii) The truncated, orthonormal set B'_s , the orthonormalized atomic state

$$|\alpha(\mathbf{R}_a)\rangle = \frac{|a(\mathbf{R}_a)\rangle - \sum_{k \in B'_s} |k\rangle \langle k|a(\mathbf{R}_a)\rangle}{\sqrt{N_{\alpha}(\mathbf{R}_a)}}, \quad (3.44a)$$

and the orthonormalized quasi-molecular state

$$|\beta(\mathbf{R}_a, \mathbf{R}_b)\rangle = \frac{|a(\mathbf{R}_b)\rangle - |\alpha(\mathbf{R}_a)\rangle \langle\alpha(\mathbf{R}_a)|a(\mathbf{R}_b)\rangle - \sum_{k \in B'_s} |k\rangle \langle k|a(\mathbf{R}_b)\rangle}{\sqrt{N_{\beta}(\mathbf{R}_a, \mathbf{R}_b)}}, \quad (3.44b)$$

where $N_{\alpha}(\mathbf{R}_a)$, $N_{\beta}(\mathbf{R}_a, \mathbf{R}_b)$ are real normalization constants.

It can be easily verified that both $B'_s \cup \{|\alpha(\mathbf{R})\rangle\}$, which describes one moving atomic particle and the metal surface, and $B'_s \cup \{|\alpha(\mathbf{R}_a)\rangle, |\beta(\mathbf{R}_a, \mathbf{R}_b)\rangle\}$, dealing with two moving atoms, are orthonormal, since they have been obtained via the Gram-Schmidt orthonormalization procedure. These two sets allow to expand the generalized electron field as

$$|\Psi[\mathbf{R}]\rangle = \sum_k |k\rangle c_k + |\alpha[\mathbf{R}]\rangle c_\alpha(\mathbf{R}), \quad (3.45a)$$

and

$$|\Psi[\mathbf{R}_a, \mathbf{R}_b]\rangle = \sum_k |k\rangle c_k + |a[\mathbf{R}_a]\rangle c_\alpha(\mathbf{R}_a) + |\beta(\mathbf{R}_a, \mathbf{R}_b)\rangle c_\beta(\mathbf{R}_a), \quad (3.45b)$$

where the k -summation runs over the truncated set B'_s .

3.1.7 Second quantized Hamiltonian for resonant electron transfer

Substituting the expansion of eq. (3.45b) in the Hamiltonian (3.40a), we obtain the one body operator

$$\begin{aligned} \mathcal{H}_1[\mathbf{R}] &= \langle\alpha(\mathbf{R})|\hat{H}_1[\mathbf{R}]|\alpha(\mathbf{R})\rangle c_\alpha^\dagger(\mathbf{R}) c_\alpha(\mathbf{R}) + \sum_{k,k'} \langle k|\hat{H}_1[\mathbf{R}]|k'\rangle c_k^\dagger c_{k'} \\ &+ \sum_k \left[\langle\alpha(\mathbf{R})|\hat{H}_1[\mathbf{R}]|k\rangle c_\alpha^\dagger(\mathbf{R}) c_k + \text{HC} \right] \end{aligned} \quad (3.46)$$

We let

$$\varepsilon_\alpha(\mathbf{R}) \equiv \langle\alpha(\mathbf{R})|\hat{H}_1[\mathbf{R}]|\alpha(\mathbf{R})\rangle \quad (3.47a)$$

be the energy of the ion level and

$$\varepsilon_k(\mathbf{R}) \equiv \langle k|\hat{H}_1[\mathbf{R}]|k\rangle \quad (3.47b)$$

the energy of a metal state $|k\rangle$, when the ion is at position \mathbf{R} . Next, we introduce the coupling matrix elements

$$V_{\alpha k}(\mathbf{R}) \equiv \langle \alpha(\mathbf{R}) | \hat{H}_1[\mathbf{R}] | k \rangle = V_{k\alpha}^*(\mathbf{R}), \quad \text{and} \quad V_{kk'}(\mathbf{R}) \equiv \langle k | \hat{H}_1[\mathbf{R}] | k' \rangle \quad (3.47c)$$

that describe, respectively, the hopping of an electron between the orthonormalized atomic level and the selected band states, and the intraband scattering of a metal electron induced by the atomic particle. The Hamiltonian (3.46) is written

$$\mathcal{H}_1[\mathbf{R}] = \varepsilon_\alpha(\mathbf{R}) c_\alpha^\dagger(\mathbf{R}) c_\alpha(\mathbf{R}) + \sum_k \varepsilon_k(\mathbf{R}) c_k^\dagger c_k + \quad (3.48)$$

$$+ \sum_k [V_{ak}(\mathbf{R}) c_a^\dagger(\mathbf{R}) c_k + \text{HC}] + \sum_{k \neq k'} V_{kk'}(\mathbf{R}) c_k^\dagger c_{k'}. \quad (3.49)$$

Neglecting the effect of distortion of the ion motion on the metal wavefunction, i.e., approximating $\varepsilon_k(\mathbf{R}) \approx \varepsilon_k$ and $V_{kk'}(\mathbf{R}) \ll V_{ak}(\mathbf{R})$, the latter reduces to the TDAN Hamiltonian (2.75)

$$\mathcal{H}_1[\mathbf{R}] = \mathcal{H}_0[\mathbf{R}] + \mathcal{V}_H[\mathbf{R}], \quad (3.50)$$

where

$$\mathcal{H}_0[\mathbf{R}] = \varepsilon_\alpha(\mathbf{R}) c_\alpha^\dagger(\mathbf{R}) c_\alpha(\mathbf{R}) + \sum_k \varepsilon_k c_k^\dagger c_k \quad (3.51a)$$

describes the unperturbed many-electron system and

$$\mathcal{V}_H[\mathbf{R}] = \sum_k [V_{ak}(\mathbf{R}) c_a^\dagger(\mathbf{R}) c_k + \text{HC}] \quad (3.51b)$$

denotes the hopping potential.

In order to obtain the generalized hamiltonian for the double-ion metal system (3.40b), we use the field expansion eq. (3.45b). Then, we extend the definitions (3.47) and introduce: (i) the adiabatic energy of the atomic

$$\varepsilon_\alpha(\mathbf{R}_a, \mathbf{R}_b) \equiv \langle \alpha(\mathbf{R}_a) | \hat{H}'_1[\mathbf{R}_a, \mathbf{R}_b] | \alpha(\mathbf{R}_a) \rangle, \quad (3.52a)$$

and orthonormalized quasi-molecular state

$$\varepsilon_\beta(\mathbf{R}_a, \mathbf{R}_b) \equiv \langle \beta(\mathbf{R}_a, \mathbf{R}_b) | \hat{H}'_1[\mathbf{R}_a, \mathbf{R}_b] | \beta(\mathbf{R}_a, \mathbf{R}_b) \rangle; \quad (3.53a)$$

(ii) the hopping matrix element between the localized levels and a metal band level

$$V_{k\alpha}(\mathbf{R}_a, \mathbf{R}_b) \equiv \langle k | \hat{H}'_1[\mathbf{R}_a, \mathbf{R}_b] | \alpha(\mathbf{R}_a) \rangle = V_{\alpha k}^*(\mathbf{R}_a, \mathbf{R}_b), \quad (3.53b)$$

$$V_{k\beta}(\mathbf{R}_a, \mathbf{R}_b) \equiv \langle k | \hat{H}'_1[\mathbf{R}_a, \mathbf{R}_b] | \beta(\mathbf{R}_a, \mathbf{R}_b) \rangle = V_{\beta k}^*(\mathbf{R}_a, \mathbf{R}_b); \quad (3.53c)$$

(iii) the hopping matrix element between the two localized states

$$V_{\alpha\beta}(\mathbf{R}_a, \mathbf{R}_b) \equiv \langle \alpha(\mathbf{R}_a) | \hat{H}'_1[\mathbf{R}_a, \mathbf{R}_b] | \beta(\mathbf{R}_a, \mathbf{R}_b) \rangle = V_{\beta\alpha}^*(\mathbf{R}_a, \mathbf{R}_b); \quad (3.53d)$$

(iv) the intraband scattering term

$$V_{kk'}(\mathbf{R}_a, \mathbf{R}_b) \equiv \langle k | \hat{H}'_1[\mathbf{R}_a, \mathbf{R}_b] | k' \rangle. \quad (3.53e)$$

Finally, we neglect the effect of the ion on the energy of the metal states to obtain

$$\mathcal{H}'_1[\mathbf{R}_a, \mathbf{R}_b] = \mathcal{H}'_0[\mathbf{R}_a, \mathbf{R}_b] + \mathcal{V}_H[\mathbf{R}_a, \mathbf{R}_b] + \sum_{k,k'} V_{kk'}(\mathbf{R}_a, \mathbf{R}_b) c_k^\dagger c_{k'}, \quad (3.54a)$$

in which the unperturbed system is now described by the Hamiltonian

$$\mathcal{H}'_0[\mathbf{R}_a, \mathbf{R}_b] = \varepsilon_\alpha(\mathbf{R}_a) c_\alpha^\dagger(\mathbf{R}_a) c_\alpha(\mathbf{R}_a) + \sum_k \varepsilon_k c_k^\dagger c_k \quad (3.54b)$$

$$+ \varepsilon_\beta(\mathbf{R}_a, \mathbf{R}_b) c_\beta^\dagger(\mathbf{R}_a, \mathbf{R}_b) c_\beta(\mathbf{R}_a, \mathbf{R}_b) \quad (3.54c)$$

and the hopping potential becomes

$$\mathcal{V}_H[\mathbf{R}_a, \mathbf{R}_b] = \sum_k [V_{\alpha k}(\mathbf{R}_a) c_\alpha^\dagger(\mathbf{R}_a) c_k + \text{HC}] \quad (3.54d)$$

$$+ \sum_k [V_{\beta k}(\mathbf{R}_a, \mathbf{R}_b) c_\beta^\dagger(\mathbf{R}_a, \mathbf{R}_b) c_k + \text{HC}] \quad (3.54e)$$

$$+ [V_{\alpha\beta}(\mathbf{R}_a, \mathbf{R}_b) c_\alpha^\dagger(\mathbf{R}_a) c_\beta(\mathbf{R}_a, \mathbf{R}_b) + \text{HC}]. \quad (3.54f)$$

If we neglect the coupling of the atomic and quasimolecular states, the Hamiltonian (3.54a) reduces to the Hamiltonian (2.117).

3.2 Hamiltonian for one and two-electron processes.

One-electron processes leading to positive ionization of a moving particle in front of a metal surface have been described by a local Hamiltonian $\hat{H}_1(\mathbf{R})$ with coordinate representation

$$\langle \mathbf{r} | \hat{H}_1(\mathbf{R}) | \mathbf{r}' \rangle = \delta(\mathbf{r} - \mathbf{r}') H_1(\nabla, \mathbf{r}; \mathbf{R}), \quad H_1(\nabla, \mathbf{r}; \mathbf{R}) = \frac{-\nabla^2}{2} + V_E(\mathbf{r}; \mathbf{R}) \quad (3.55)$$

where the potential function (3.2) is involved. In dealing with two-electron processes, we need to consider the conjugate operators, namely $(\hat{\mathbf{r}}, \hat{\mathbf{p}})$ and $(\hat{\mathbf{r}}', \hat{\mathbf{p}}')$, for the electrons. Thus, the unperturbed, two-electron Hamiltonian is defined by the operator $\hat{H}_{11}[\mathbf{R}]$ with coordinate representation

$$H_{11}(\nabla, \mathbf{r}, \nabla', \mathbf{r}'; \mathbf{R}) = H_1(\nabla, \mathbf{r}; \mathbf{R}) + H_1(\nabla', \mathbf{r}'; \mathbf{R}), \quad (3.56)$$

while the total Hamiltonian reads

$$\hat{H}_2[\mathbf{R}] = \hat{H}_{11}[\mathbf{R}] + \hat{V}_{\text{sc}}(|\mathbf{r} - \mathbf{r}'|).$$

Here, the electron-electron potential operator $\hat{V}_{\text{sc}}(|\hat{\mathbf{r}} - \hat{\mathbf{r}}'|)$ takes into account the screening of the other electrons in the medium.

3.2.1 Electron screening.

There are several shapes for screened potential. Indeed, in an interacting system the Coulombic interaction introduces correlations between the electrons that cannot be easily treated. To get around this difficulty, one considers a fictitious system of independent particles moving in an average potential, such as (3.2). We will study the response of all the other electrons of the system to the perturbing potential $V_{\text{sc}}(|\mathbf{r} - \mathbf{r}'|)$, generated

by the interaction of two electrons. Following the treatment of [9, 38], we can define the unperturbed charge density

$$\delta n_0(\mathbf{r}, t) = \int d^3\mathbf{r}' \chi_0(\mathbf{r}, \mathbf{r}', t) V_{\text{sc}}(\mathbf{r}', t), \quad (3.57)$$

where $\chi_0(\mathbf{r}, \mathbf{r}', t)$ is the independent particle response. In the random phase approximation we can write $V_{\text{sc}}(\mathbf{r}, t)$ as the sum of two terms, the first is the response of the system and the second one is the pure Coulomb potential

$$V_{\text{sc}}(\mathbf{r}, t) = V_{\text{sy}}(\mathbf{r}, t) + V_{\text{el}}(\mathbf{r}, t), \quad (3.58)$$

where $V_{\text{el}}(\mathbf{r}, t)$ satisfies the Poisson's equation

$$-\nabla^2 V_{\text{el}}(\mathbf{r}, t) = -4\pi \delta n_0(\mathbf{r}, t) \quad (3.59)$$

and $V_{\text{sy}}(\mathbf{r}, t)$ satisfies

$$\delta n(\mathbf{r}, t) = \int d^3\mathbf{r}' \chi(\mathbf{r}, \mathbf{r}', t) V_{\text{sy}}(\mathbf{r}', t), \quad (3.60)$$

in which $\delta n(\mathbf{r}, t)$ is the induced charge density. Thus,

$$V_{\text{sc}}(\mathbf{r}, t) = V_{\text{sy}}(\mathbf{r}, t) - \int d^3\mathbf{r}' \frac{\delta n_0(\mathbf{r}', t)}{|\mathbf{r} - \mathbf{r}'|}. \quad (3.61)$$

Approximating the induced density of the interacting system with $\delta n_0(\mathbf{r}, t)$ and using Eqs. (3.60), (3.57) and (3.61), we obtain the response function

$$\chi(\mathbf{r}, \mathbf{r}', t) = \chi_0(\mathbf{r}, \mathbf{r}', t) + \int d^3\mathbf{r}'' \int d^3\mathbf{r}''' \chi_0(\mathbf{r}, \mathbf{r}''', t) \frac{\chi(\mathbf{r}'', \mathbf{r}', t)}{|\mathbf{r}'' - \mathbf{r}'''|}, \quad (3.62)$$

which accounts selfconsistently for the screening of the many electron system [67]. A simpler treatment is provided by the Yukawa potential function

$$V_{\text{sc}}(|\mathbf{r} - \mathbf{r}'|) = \frac{e^{-\mu|\mathbf{r} - \mathbf{r}'|}}{|\mathbf{r} - \mathbf{r}'|} \quad (3.63)$$

where the effect of the screening is contained in the phenomenological parameter μ that can be interpreted as the inverse screening length of the electron gas [68]. In what follows a specific model for the electron-electron interaction is not required, however, in chapter 4, we shall limit our study to projectile/target combinations where the screened potential can be approximated to the form (3.63)

3.2.2 Second quantized two-electron potential: collective excitations

Now we can calculate the second quantized Hamiltonian \mathcal{H}_2 , which describes two body Coulomb interactions. It is obtained, in the second quantization formalism, considering as starting point the tensor product

$$|\Psi[\mathbf{R}]\rangle |\Psi[\mathbf{R}]\rangle = \left[\sum_k |k\rangle c_k + |\alpha(\mathbf{R})\rangle c_\alpha(\mathbf{R}) \right] \otimes \left[\sum_{k'} |k'\rangle c_{k'} + |\alpha(\mathbf{R})\rangle c_\alpha(\mathbf{R}) \right] \quad (3.64)$$

$$= \sum_k [|k\rangle |\alpha(\mathbf{R})\rangle - |\alpha(\mathbf{R})\rangle |k\rangle] c_k c_\alpha(\mathbf{R}) + \sum_{k,k'} |k\rangle |k'\rangle c_k c_{k'}. \quad (3.65)$$

The general expression for the two-body Hamiltonian is [67],

$$\mathcal{H}_2(\mathbf{R}) = \frac{1}{2} \langle \Psi^\dagger[\mathbf{R}] | \langle \Psi^\dagger[\mathbf{R}] | \hat{V}_{\text{sc}}(|\mathbf{r} - \mathbf{r}'|) | \Psi[\mathbf{R}] \rangle | \Psi[\mathbf{R}] \rangle \quad (3.66)$$

$$= \frac{1}{2} \int d^3r \int d^3r' \Psi^\dagger(\mathbf{r}, \mathbf{R}) \Psi^\dagger(\mathbf{r}', \mathbf{R}) \hat{V}_{\text{sc}}(|\mathbf{r} - \mathbf{r}'|) \Psi(\mathbf{r}', \mathbf{R}) \Psi(\mathbf{r}, \mathbf{R}) \quad (3.67)$$

From the former two equations, we obtain

$$\mathcal{H}_2(\mathbf{R}) = \mathcal{V}_{\text{AU}}(\mathbf{R}) + \mathcal{V}_{\text{IE}}(\mathbf{R}) + \mathcal{V}_{\text{FE}}(\mathbf{R}), \quad (3.68)$$

where each potential correspond to a different physical process. Specifically,

$$\mathcal{V}_{\text{AU}}(\mathbf{R}) = \sum_{k,k',k''} \left[V_{kk'}^{\alpha k''}(\mathbf{R}) c_\alpha^\dagger(\mathbf{R}) c_k^\dagger c_{k'} c_{k''} + \text{HC} \right] \quad (3.69a)$$

denotes the usual Auger potential of matrix element

$$V_{kk'}^{\alpha k''}(\mathbf{R}) = \langle k | \langle \alpha(\mathbf{R}) | \hat{V}_{\text{sc}}(|\mathbf{r} - \mathbf{r}'|) | k'' \rangle | k' \rangle. \quad (3.69b)$$

It contains three fermion operators which refer to electrons of the valence band and a fermion operator related to the atomic state. Two electrons are destroyed in the states $|k'\rangle$ and $|k''\rangle$, while two electrons are created; one of these is the neutralizing electron, in the atomic state $|\alpha(\mathbf{R})\rangle$, and the other is the excited electron, in a state $|k\rangle$. The usual electron-electron interaction in the metal [67] is contained in

$$\mathcal{V}_{\text{IE}}(\mathbf{R}) = \frac{1}{2} \sum_{k,k',k'',k'''} V_{k'k''}^{kk'''}(\mathbf{R}) c_k^\dagger c_{k'}^\dagger c_{k''} c_{k'''} \quad (3.69c)$$

where

$$V_{kk'''}^{k'k''}(\mathbf{R}) = \langle k | \langle k' | \hat{V}_{\text{sc}}(|\mathbf{r} - \mathbf{r}'|) | k'' \rangle | k''' \rangle. \quad (3.69d)$$

This potential, containing fermion operators acting on the valence band states, may be responsible collective excitations, such as surface or bulk plasmons. The last term in (3.68),

$$\mathcal{V}_{\text{FE}}(\mathbf{R}) = \sum_{k,k'} V_{kk'}^\alpha(\mathbf{R}) c_k^\dagger c_{k'} c_\alpha^\dagger(\mathbf{R}) c_\alpha(\mathbf{R}) \quad (3.69e)$$

is a new interaction, of matrix element

$$V_{kk'}^\alpha(\mathbf{R}) = \langle k | \langle \alpha(\mathbf{R}) | v_{\text{sc}}(|\mathbf{r} - \mathbf{r}'|) | \alpha(\mathbf{R}) \rangle | k' \rangle, \quad (3.69f)$$

that derives naturally from the representation of the Hamiltonian into the basis $\{c_k, c_\alpha(\mathbf{R})\}$.

It describes the sudden change of charge due to neutralization of the incident ion and injection of a band hole. It is a collective excitation of the metal target, known as Fermi Edge singularity, due to the singular behavior of electrons at the Fermi level. It has the same structure of the MND potential, where $c_\alpha^\dagger c_\alpha$ is the number operator of the core hole [78, 79]. The Fock space is, therefore, partitioned into two subspaces: on the one hand, many electron states with the ion state empty are still constructed by antisymmetrizing the unperturbed set $\{\langle \mathbf{r} | k \rangle\}$; on the other hand, many electron states with the ion state occupied need to be calculated from the set $\{\langle \mathbf{r} | k_\alpha(\mathbf{R}) \rangle\}$, in which each

$\langle \mathbf{r} | k_\alpha(\mathbf{R}) \rangle$ diagonalizes the unperturbed metal Hamiltonian 3.11 plus the edge potential

$$\int d^3r' V_{sc}(|\mathbf{r} - \mathbf{r}'|) |\langle \alpha(\mathbf{R}) | \mathbf{r}' \rangle|^2. \quad (3.70)$$

It turns out that the final states of Auger neutralization are not orthogonal with the initial states. The sudden change of charge of the projectile, as a consequence of Auger neutralization, leads to a rearrangement (many body shake-up) of the ground state of conduction electrons on a long time scale, causing a permanent deformation in the conduction band; this final state effect parallels the creation of a core-hole absorption of a soft x-ray photon and reflects in the broadening of the distributions of ejected electrons with kinetic energy E , for a given incident ion velocity. Indeed some experiments [12] on the Ar^+/Al system have shown that the behavior of the kinetic energy distribution of ejected electrons is characterized by exponential tails. This means that the spectra do not follow a strict Lorentzian broadening trend, as discussed in § 2.1.5.

3.2.3 Total Hamiltonian

From eqs. (3.51a) and (3.68), we can introduce a universal Hamiltonian that describes either resonant or non resonant charge transfer processes, in the ion-surface interaction, and accounts for many-body electron excitations:

$$\mathcal{H}(\mathbf{R}) = \mathcal{H}_1(\mathbf{R}) + \mathcal{H}_2(\mathbf{R}) \quad (3.71)$$

$$= \mathcal{H}_0(\mathbf{R}) + \mathcal{V}_H(\mathbf{R}) + \mathcal{V}_{\text{AU}}(\mathbf{R}) + \mathcal{V}_{\text{IE}}(\mathbf{R}) + \mathcal{V}_{\text{FE}}(\mathbf{R}). \quad (3.72)$$

This operators generalizes previous formulations [69] and will be used in the applications proposed in the following chapter.

3.3 Parametric time-dependence

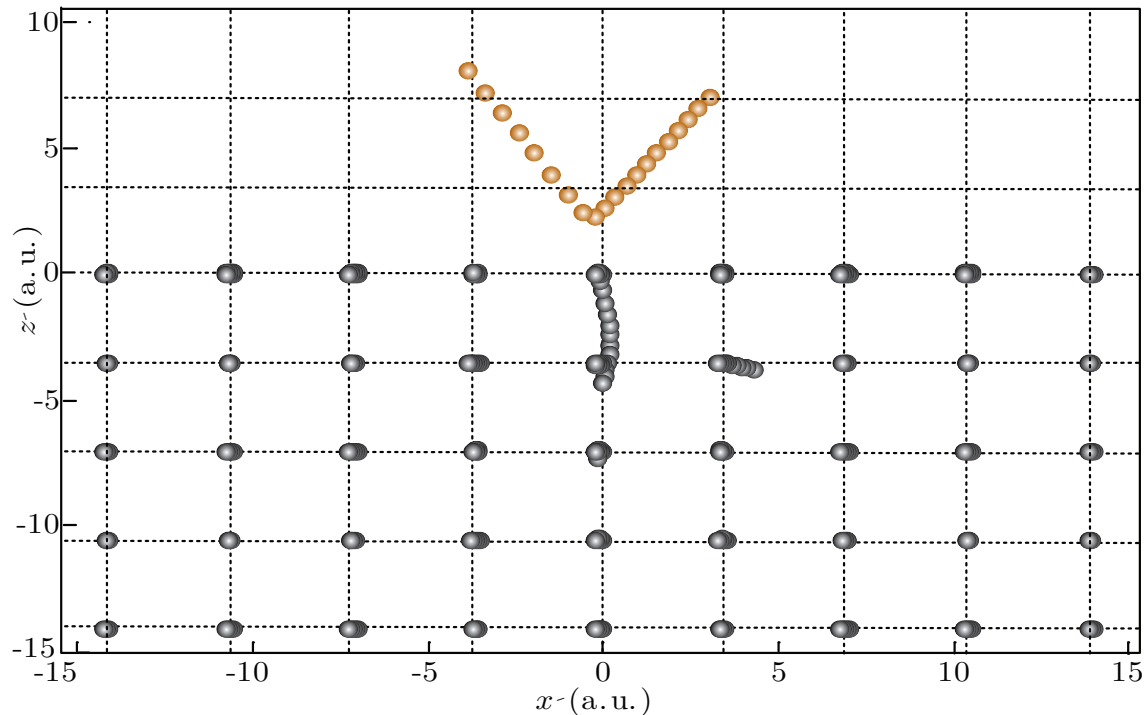
So far, we have seen that the Hamiltonian operators depend parametrically on the positions of the moving atomic particles interacting with the surface. In the case of a single

atom scattering from a metal surface, a description of the trajectory followed by the projectile is a crucial point for a quantitative analysis of the electron transfer processes. The simplest possibility is to assume that the impinging particle reflects elastically from the sample; then the position vector \mathbf{R} , in (3.71), takes the parametric time dependence

$$\mathbf{R} = \mathbf{v}_{\parallel} t + (Z_{\text{T}} - v_{\perp} |t|) \mathbf{u}_z, \quad (3.73)$$

in which \mathbf{v}_{\parallel} is the parallel component, and v_{\perp} the perpendicular component, of the impact projectile velocity, and Z_{T} is an ideal distance where the ion is reflected. Indeed, Molecular Dynamics (MD) simulations seem to confirm such an assumption, at least for incident ion energies larger than ~ 50 eV.. For example, MD was used by Sroubek in some works, where he treated Na^+ ions scattered from a Cu(100) surface [?]. From Fig. ?? we can see that trajectories are well approximated by a linear law.

Figure 3.7: 50 eV Na^+ scattering from Cu(100), with $\theta_i = 30^\circ$ and $\theta_f = 35^\circ$, with respect to the surface normal. The final kinetic energy of Na along the surface normal is $E_{k,f} = 15$ eV [?].



In secondary atomic emission, the problem of finding reasonable analytical trajectories for emitted atoms is rather cumbersome. It can be shown [70, 57, 12] that, under some crude assumptions on the collision dynamics, the motion of sputtered atoms outside the surface region is nearly rectilinear. In particular, for a diatomic system, such as the one described by the Hamiltonian (3.54a), the following approximation can be made: (i) The two atoms are initially placed outside the collision cascade area; (ii) Their interaction is given by a Morse potential; (iii) All interactions with other surface atoms are neglected. The resulting classical problems gives an analytical time dependence for \mathbf{R}_a and \mathbf{R}_b , being such that \mathbf{R}_a follows the law of a uniform rectilinear motion at distances from the surface larger than ~ 5 au..

To confirm such qualitative predictions, we have tested different type of numerical trajectories calculated from MD simulations on two-dimensional clusters of Silver and Gold atoms, containing about 250 particles. We thus considered two-(100) surfaces covering the region $(-60$ to $60)$ au, along the surface plane, and $(-60, 0)$ au along the surface perpendicular direction. We used both 1 – 15 keV Ar and 1 – 15 keV Cs projectiles, at 0° incident angles from the surface normal. The interaction potential between two target particles is given the form of the many body tight binding potential of ref. [71], while the projectile target interaction is modelled by a Moliere function [72]. Indeed, sputtering simulations typically employ composite potentials. These consist of a repulsive short-range screened Coulomb potential which is splined to an attractive potential at internuclear separations somewhat below the first neighbor distance.

The tight-binding potentials, used to describe the interaction of two target atoms, is based on an effective pair potential $V_{ij}(r_{ij})$ acting between two atoms i and j . In ref. [71], this potential has the form

$$V_{ij}(r_{ij}) = 2U_{ij}(r_{ij}) - \frac{\phi(r_{ij})}{G} + \frac{[\phi(r_{ij})]^2}{4G^3}, \quad r < r_0 \quad (3.74)$$

$$= 0, \quad r \geq r_0 \quad (3.75)$$

where: (i) $U_{ij}(r_{ij})$ is the repulsive pair potential

$$U_{ij}(r_{ij}) = A \exp \left[-p \left(-1 + \frac{r}{R_0} \right) \right], \quad (3.76)$$

depending on the equilibrium distance R_0 ; (ii) $\phi(r_{ij})$ represents the cohesive band energy term:

$$\phi(r_{ij}) = B^2 \exp \left[-2q \left(-1 + \frac{r}{R_0} \right) \right].$$

Other parameters, i.e., G , A , B , p , q and r_0 , are also tabulated in ref. [71] for a variety of crystal planes. The Moliere potential [72], is obtained from the pair potential function $W_i(r)$, acting between a target atom i and the projectile, at distance r :

$$\begin{aligned} W_i(r) &= \frac{A}{r} \left[0.35e^{-\frac{0.3r}{B}} + 0.55e^{-\frac{1.2r}{B}} + 0.1e^{-\frac{6r}{B}} \right], & r < r_a & \quad (3.77) \\ &= C_0 + C_1r + C_2r^2 + C_3r^3, & r_a \leq r < r_b \\ &= D \left[e^{-2\beta(r-r_c)} - 2e^{-\beta(r-r_c)} \right], & r_b \leq r < r_c \\ &= 0, & r \geq r_c. \end{aligned}$$

All the parameters in this equation can be found in ref. [72] for some projectile target combinations.

Fig. 3.8 shows a simulation on the Cs/Au(100) system, computed with the Verlet algorithm [73] and implemented on Mathematica5.2 [74], using a time step of ~ 1 au. Particles emitted from Au(100) clusters, bombarded with 2 keV Cs projectiles, mainly come out as monomers and dimers outside the collision cascade area. In either cases, when the ejected atoms are at distances of about 5 – 10 au from the surface, their interactions with other surface atoms are negligible. Furthermore, the binding energy in a dimer is small compared to its center of mass kinetic energy, at interatomic distances larger than $\sim 6 - 7$ au. Indeed the kinematic model predicted nearly straight trajectories for a-atoms. These considerations let us assume that a and b atoms still possess strong electronic interactions when their binding forces tend to 0, moving with approximately constant velocities from the instant $t = 0$, when both particles are outside the image plane (3.8b).

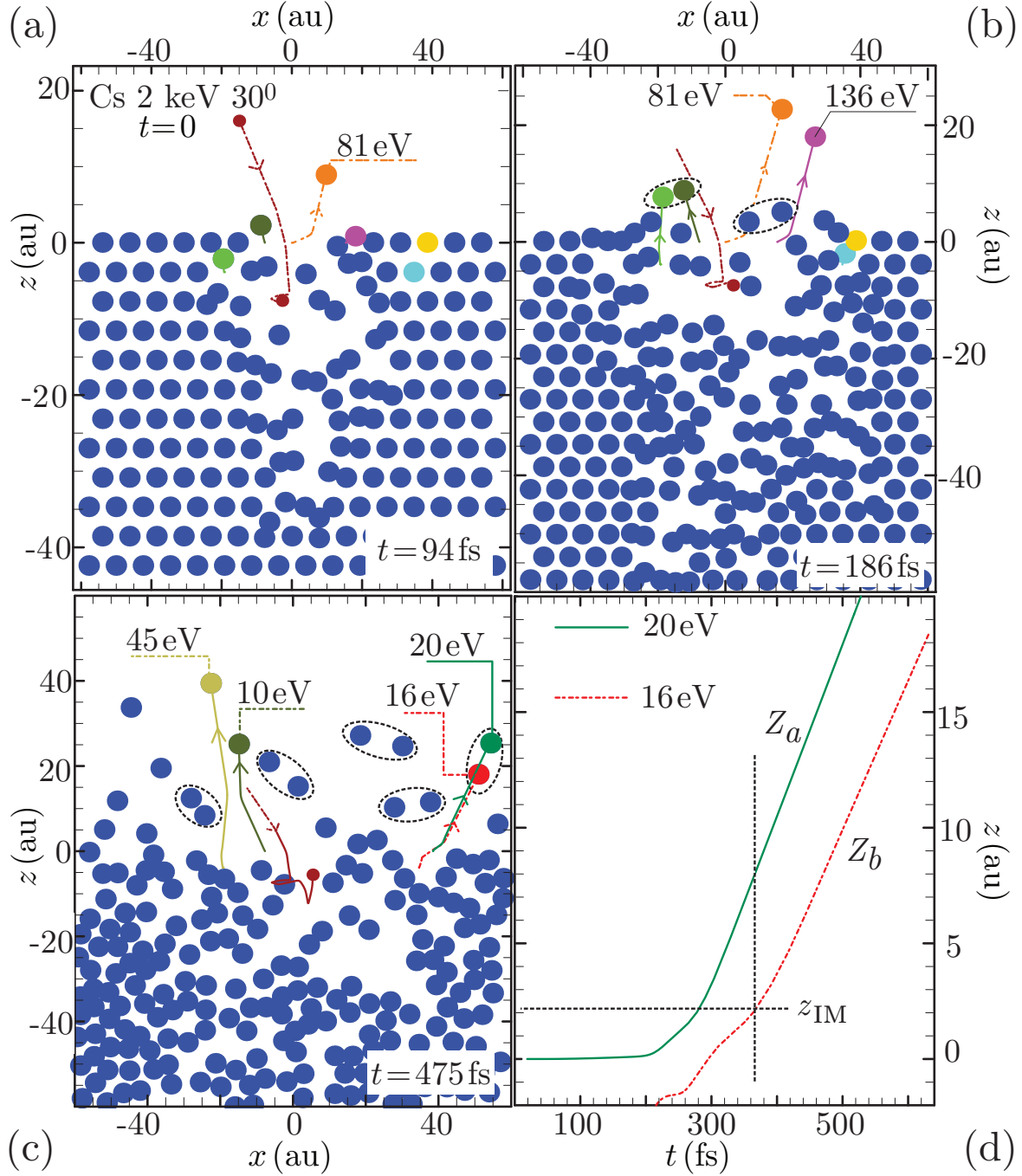


Figure 3.8: (a)-(c): MD simulation of 2 keV *Cs* projectiles incident at 30° from the perpendicular direction of a two-dimensional FCC *Au*(100) cluster. The trajectories of some of these atoms are drawn in the plot. (d): time laws, $Z_a(t)$ and $Z_b(t)$ of two possible candidates for *a* and *b* atoms.

Applications and results.

In the first part of this chapter we are going to obtain the kinetic energy distribution of emitted electrons due to Auger neutralization of Ar^+ ions on an $Al(111)$ surface, and we will parallel it with previous results and with the experimental spectrum. In the second part of the chapter we are going to calculate the ionization probability for the orthonormalized affinity states in the resonant charge transfer induced by sputtering. We will use two techniques for achieve our goal: the spectral method and the wave packet method.

4.1 Fermi's golden rule formulation.

We can write the Auger Hamiltonian of Eq. (3.26) in a more compact form:

$$\mathcal{H}(R) = \mathcal{H}_{\text{EG}}(\mathbf{R}) + \mathcal{V}_{\text{H}}(\mathbf{R}) + \mathcal{V}_{\text{AU}}(\mathbf{R}) + \mathcal{V}_{\text{FE}}(\mathbf{R}) \quad (4.1)$$

The unperturbed exactly solvable part of the Hamiltonian is $\mathcal{H}_{\text{r}}(\mathbf{R}) = \mathcal{H}_{\text{EG}}(\mathbf{R}) + \mathcal{V}_{\text{FE}}(\mathbf{R})$, which contains the electron gas and the Fermi Edge. It follows that shake-

up electrons are approximately generated by the contact perturbation

$$\bar{V}_{\mathbf{k}\mathbf{k}'}^a(t) = \begin{cases} V_{k_F}^a(t), & \text{if } |\varepsilon_{\mathbf{k}} - \varepsilon_{\mathbf{k}'}| \leq \varepsilon_0(v_{\perp}) \\ 0, & \text{otherwise} \end{cases}, \quad (4.2)$$

where $\varepsilon_0(v_{\perp})$ is a cut-off parameter, that depends on the projectile perpendicular velocity [12], and $V_{k_F}^a(t)$ denotes the average coupling of two metal states at the Fermi surface

$$V_{k_F}^a(t) = \int \frac{d^2\Omega_{\mathbf{k}}}{4\pi} \int \frac{d^2\Omega_{\mathbf{k}'}}{4\pi} \langle k_F\Omega_{\mathbf{k}} | v_{\text{FE}}^a(\mathbf{r}, t) | k_F\Omega_{\mathbf{k}'} \rangle. \quad (4.3)$$

We have seen that this introduces a partition of the Fock space in two subspaces. In fact many electron states with the ion state empty are still constructed by antisymmetrizing the unperturbed set $\{|\mathbf{r}|k\rangle\}$. On the other hand many electron states with the ion state occupied need to be calculated from the eigenfunctions $\{|\mathbf{r}|k_a(\mathbf{R})\rangle\}$ of the final state Hamiltonian $\hat{h}'_{\text{M}}(z) = \hat{h}_{\text{M}}(z) + \hat{v}_{\text{FE}}(\mathbf{r}, \mathbf{R})$, with the same spectrum of the unperturbed operator $\hat{h}_{\text{M}}(z)$. The local potential activated by neutralization reads

$$v_{\text{FE}}(\mathbf{r}, \mathbf{R}) = \langle a[Z(t)] | \hat{v}_{\text{SC}}(|\mathbf{r} - \mathbf{r}'|) | a[Z(t)] \rangle \quad (4.4)$$

and we have seen that this is the matter why the final states of Auger Neutralization are not orthogonal because the sudden switching modifies significantly the final state of the metal band. $\mathcal{V}_{\text{FE}}(\mathbf{R})$ effect is dominant at the edge of AN, when both electrons of the initial state that participate to the process lie close to the Fermi energy. We wrote in the previous chapter that the trajectory followed by projectile is handled classically, thus the dynamic of the system is parametrically time dependent. In the simplest case, the ion can be assumed to reflect elastically from a plane at distance z_{IM} from surface of the target, moving along a straight line $\mathbf{R} = \mathbf{R}(t)$ of incident velocity $\mathbf{v} = (\mathbf{v}_{\parallel}, v_{\perp})$, parallel component $\mathbf{R}_{\parallel}(t) = \mathbf{v}_{\parallel}t$ and perpendicular component $Z(t) = v_{\perp}|t| + Z_0$. Since complete knowledge of the eigenfunctions of both $\hat{h}_{\text{M}}(z)$ and $\hat{h}'_{\text{M}}(z)$ is available, we work in the interaction picture spanned by $\mathcal{H}'_{\text{R}}[\mathbf{R}(t)]$ and treat the Auger potential $\mathcal{V}_{\text{AU}}(\mathbf{R})$ as a small perturbation, as in Eq. (3.10). The key quantity in our study is the transition rate

$\frac{1}{\tau}(\varepsilon_k, \mathbf{v})$, from the unperturbed ground state of the conduction band $|0\rangle_N$, composed of N band electrons with the ion state empty, to all possible excited states $|f[\varepsilon_k, \mathbf{R}(t)]\rangle_N$, with $N - 2$ electrons below the Fermi energy, the ion state occupied and an excited electron with energy $\varepsilon_k > \varepsilon_F$. The initial state is the ground state of $\mathcal{H}_{\text{EG}}[\mathbf{R}(t)]$, with eigenenergy $E_0 = \sum_k \varepsilon_k \Theta(\varepsilon_k - \varepsilon_F)$; each final state diagonalizes $\mathcal{H}_{\text{R}}[\mathbf{R}(t)]$ with eigenenergy $E_f[\mathbf{R}(t)]$. By Fermi's golden rule we have

$$\frac{1}{\tau}(\varepsilon_k, \mathbf{v}) = 2\pi \int_{-\infty}^{\infty} dt \sum_f e^{i \int_0^t dt' \{E_f[\mathbf{R}(t')] - E_0\}} |V_{f0}(t)|^2, \quad (4.5)$$

where $V_{f0}(t)$ is the element matrix $V_{f0}(t) = {}_N \langle f[\varepsilon_k, \mathbf{R}(t)] | \mathcal{V}_{\text{AU}}[\mathbf{R}(t)] | 0 \rangle_N$. Golden rule is a result of time depending perturbation theory at first order in the interaction potential. The potential \mathcal{V}_{FE} modifies significantly the many electron states of the metal when the atomic state is occupied, while it acts as a weak perturbation on single-particle states, due to the operator $\hat{c}_a^\dagger(\mathbf{R}) \hat{c}_a(\mathbf{R})$ contained in it. The Fermi edge singularity is very important to explain the trend of tails in experimental electron energy distribution above the magic energy. It is convenient evaluating the Fermi edge singularity at the edge of AN, where both the electrons participating to the process lie next to Fermi energy. The matter is that in this case both the atomic and the excited electron are negligibly perturbed by the one-electron potential of Eq. (4.4), because their energy relative to the Fermi energy are large on the eV scale. So we can approximate the final state as

$$|f[\varepsilon_k, \mathbf{R}(t)]\rangle_N \approx c_k^\dagger c_a^\dagger[\mathbf{R}(t)] |f[\mathbf{R}(t)]\rangle_{N-2}, \quad (4.6)$$

where $|f[\mathbf{R}(t)]\rangle_{N-2}$ is an exact state of the metal, with time-independent energy E_f , that involves the $N - 2$ band electron that do not participate to AN. If we replace Eq. (4.6) in Eq. (4.5), and approximating the energy of the band holes created by AN to ε_F we have

$$\frac{1}{\tau_a}(\varepsilon_{\mathbf{k}}, \mathbf{v}) = 2 \times 2\pi \rho(\varepsilon_{\mathbf{k}}) \int d^2 \Omega_k \sum_{k', k''} \int_{-\infty}^{\infty} dt \left| V_{kk'}^{ak''}[\mathbf{R}(t)] \right|^2 F_a(t, \mathbf{v}) e^{i \int_0^t dt' [\varepsilon_{\mathbf{k}} + \varepsilon_a[\mathbf{R}(t')] - \varepsilon_{\mathbf{k}'} - \varepsilon_{\mathbf{k}'}]}, \quad (4.7)$$

where the factor 2 takes into account spin multiplicity; $\rho(\varepsilon_k)$ is the density of the final states available to excited electrons; $d^2\Omega_k$ is the element of solid angle in the direction of the excited electron; $F_a(t, \mathbf{v}) =_{N-2} \langle 0 | c_a[\mathbf{R}(0)] \mathcal{U}(\mathbf{v}; 0, t) c_a^\dagger[\mathbf{R}(t)] | 0 \rangle_{N-2}$ is the inner product between the initial and final states of the $N - 2$ metal electrons that do not participate to AN and it is responsible of nonorthogonality between their initial and final states, and of broadening of tails above the magic energy; $\mathcal{U}(\mathbf{v}; 0, t)$ is the time-development operator for the singular potential \mathcal{V}_{FE} in the interaction picture spanned by the free electron gas Hamiltonian. Transition rate in Eq. (4.7) is proportional to the distribution of electrons excited at energy $\varepsilon_{\mathbf{k}}$ above the Fermi level by the incident ion. We express Eq. (4.7) in the reference frame moving with the constant parallel velocity of the projectile

$$\frac{1}{\tau_a}(\varepsilon_{\mathbf{k}}, \mathbf{v}) = 2 \times 2\pi\rho(\varepsilon_{\mathbf{k}}) \int d^2\Omega_k \sum_{k', k''} \int_{-\infty}^{\infty} dt \left| V_{kk'}^{ak''}(t) \right|^2 F_a(t, v_{\perp}) e^{i \int_0^t dt' [\varepsilon_{\mathbf{k} + \varepsilon_a(t')} - \varepsilon_{\mathbf{k}'} - \varepsilon_{\mathbf{k}''} - \mathbf{q} \cdot \mathbf{v}_{\parallel}]}, \quad (4.8)$$

where $\mathbf{q} = \mathbf{k} - \mathbf{k}' - \mathbf{k}''$ labels the momentum exchanged in a single excitation process and the factor $e^{-i\mathbf{q} \cdot \mathbf{v}_{\parallel}}$ accounts for the shift of the Fermi surface in the moving frame. In the exponential of Eq. (4.8) is also included the energy shift of the atomic level. We have to consider now broadening not included in the golden rule's formulation, first of all the finite lifetime of initial and final states. Then we have to consider broadening due to the electron-phonon interaction at room temperature. We introduce the probability that the ion ground state survives neutralization due to both Auger and resonant transitions

$$P_a(t, v_{\perp}) = e^{-\int_{-\infty}^t dt' \{w_a(t') + 2\Delta_a(t')\}}, \quad (4.9)$$

where

$$w_a(t) = 4\pi \sum_{k, k', k''} \left| V_{kk'}^{ak''}(t) \right|^2 \delta(\varepsilon_a(t) + \varepsilon_{\mathbf{k}} - \varepsilon_{\mathbf{k}'} - \varepsilon_{\mathbf{k}''}) \quad (4.10)$$

is the total AN transition rate [8, 34, 35] and

$$\Delta_a(t) = \sum_k |V_{ak}(t)|^2 \delta[\varepsilon_{\mathbf{k}} - \varepsilon_a(t)] \quad (4.11)$$

is the virtual width of the atomic state due to Hopping (tunnelling) processes [13, ?]. We take an exponential law, $e^{-\Gamma_0|t|}$, with average lifetime Γ_0 for the probability that the band holes created by AN survive recombination [8]. It does not depend nor by holes states or by ion trajectory. We model the electron-phonon interaction by a Gaussian function, $e^{-\sigma_{\text{PH}}^2 t^2/2}$, of width σ_{PH} [81]. With these prescriptions we can write

$$\begin{aligned} N_I(\mathbf{k}, \mathbf{v}) &= N_0 \rho(\varepsilon_{\mathbf{k}}) \sum_{k', k''} \int_{-\infty}^{\infty} dt \left| V_{kk'}^{ak''}(t) \right|^2 \\ &\times F_a(t, \mathbf{v}_{\perp}) P_a(t, \mathbf{v}_{\perp}) e^{-\Gamma_0 t} e^{-\frac{\sigma_{\text{PH}}^2}{2} t^2} \\ &\times e^{i \int_0^t dt' [\varepsilon_{\mathbf{k}+\varepsilon_a(t')} - \varepsilon_{\mathbf{k}'} - \varepsilon_{\mathbf{k}''} - \mathbf{q} \cdot \mathbf{v}_{\parallel}]}, \end{aligned} \quad (4.12)$$

where N_0 is the normalization factor. Thanks to Eq. (4.12), we can write the internal spectrum as the convolution integral

$$N_I(\mathbf{k}, \mathbf{v}) = \int_{-\infty}^{\infty} d\varepsilon N_I^0(\varepsilon_{\mathbf{k}} - \varepsilon, \mathbf{k}, \mathbf{v}) B(\varepsilon, \mathbf{v}_{\perp}) \quad (4.13)$$

of a *pure* spectrum, $N_I^0(\varepsilon, \mathbf{k}, \mathbf{v})$, and a broadening function, $B(\varepsilon, \mathbf{v}_{\perp})$. The pure spectrum is the number of excited electrons, per unit of time, by a projectile with constant ionization energy $\varepsilon_a^0 = \varepsilon_a(Z_0)$ in the Fermi golden rule approximation:

$$N_I^0(\varepsilon, \mathbf{k}, \mathbf{v}) = N_0 \rho(\varepsilon_k) \sum_{k', k''} \int_{-\infty}^{\infty} dt \left| V_{kk'}^{ak''}(t) \right|^2 e^{i(\varepsilon_{\mathbf{k}} + \varepsilon_a^0 - \varepsilon_{\mathbf{k}'} - \varepsilon_{\mathbf{k}''} - \mathbf{q} \cdot \mathbf{v}_{\parallel})}. \quad (4.14)$$

Indeed, in the simplest approximation the time dependence of the matrix element $V_{kk'}^{ak''}(t)$ is modelled by an exponential function independent on electron momenta, that is $V_{kk'}^{ak''}(t) = V_{kk'}^{ak''}(0) e^{-\frac{\lambda_a v_{\perp} |t|}{2}}$ and the effect of the parallel projectile is neglected. This gives rise just to Hagstrum's self-convolution model [8] where $N_I^0(\varepsilon, \mathbf{k}, \mathbf{v})$ results from the convolution of a pure spectrum with a Lorentzian of broadening $\lambda_a v_{\perp}$ scaling linearly with the ion perpendicular velocity.

The broadening function

$$B(\varepsilon_{\mathbf{k}}, \mathbf{v}_{\perp}) = \int_{-\infty}^{\infty} dt e^{i\varepsilon_{\mathbf{k}}t} P_a(t, \mathbf{v}_{\perp}) e^{i \int_0^t dt' [\varepsilon_a[Z(t')] - \varepsilon_a^0]} e^{-\Gamma_0|t|} e^{-\frac{\sigma_{\text{th}}^2 t^2}{2}} F_a(t, \mathbf{v}_{\perp}) \quad (4.15)$$

mainly describes those many body effects that are outside the golden rule identified by Hagstrum [8, ?], plus the effect of many body shake-up. The broadening function is shifted by the variation of the ion energy, with the change of the projectile-target distance. $F_a(t, \mathbf{v}_{\perp})$ is given the form of the Mahan-Nozieres-De Dominicis function:

$$F_a(t, \mathbf{v}_{\perp}) = [1 + i\varepsilon_0(\mathbf{v}_{\perp})t]^{-\alpha(\mathbf{v}_{\perp})}. \quad (4.16)$$

Its Fourier transform defines the distribution of shake-up electrons

$$\tilde{F}_a(\varepsilon, \mathbf{v}_{\perp}) = \frac{\Theta(\varepsilon)}{\Gamma[\alpha(\mathbf{v}_{\perp})]} \frac{1}{\varepsilon} \left(\frac{\varepsilon}{\varepsilon_0(\mathbf{v}_{\perp})} \right)^{\alpha(\mathbf{v}_{\perp})} e^{-\frac{\varepsilon}{\varepsilon_0(\mathbf{v}_{\perp})}}, \quad (4.17)$$

with $\Theta(\varepsilon)$ the step function and $\Gamma[\alpha(\mathbf{v}_{\perp})]$ the Euler Gamma function. Eqs. (4.16) and (4.17) depend on two parameters: $\varepsilon_0(\mathbf{v}_{\perp})$ is the width of the distribution, corresponding to the energy range where the sudden perturbation, activated by projectile neutralization, is non vanishing; $\alpha(\mathbf{v}_{\perp})$ is a singularity index that, in the MND formulation, depends on the phase-shifts of the (static) core-hole potential, activated by the X-ray field, at the Fermi surface of the target [78, 79]. We deal with a time-dependent shake-up potential in this work, so we need the Fourier transform of the instantaneous phase shift $\Phi(\mathbf{v}_{\perp}, \varepsilon)$ of the average coefficient $V_{k_F}^a(t)$ [46]. Eqs. (4.14) and (4.15) turn the calculation of N_I into a formidable problem that depends either on the choice of a basis for the ion/metal system or on the model used to simulate the screened electron-electron interaction. We want to calculate $N(E, \mathbf{v})$, the distribution of electrons ejected from the target with a kinetic energy E , following Auger Neutralization of the projectile with impact velocity $(\mathbf{v}_{\parallel}, v_{\parallel})$. To do this we need, a part the internal distribution, the transmission function $P(E, \Omega_{\mathbf{k}})$ too. It represents the probability that an excited electron with kinetic energy E and wavevector \mathbf{k} , of solid angle $\Omega_{\mathbf{k}}$, escapes the metal barrier. In

this approach we refer to the quantum-mechanical derivation of [36], yielding to

$$P(E, \Omega_{\mathbf{k}}) = \frac{p_z}{k_z} |T(k_z, p_z)|^2. \quad (4.18)$$

$P(E, \Omega_{\mathbf{k}})$ depends on the surface perpendicular wavevectors of the electron far inside the metal, $k = \sqrt{2(E + \xi)}$, and far outside the metal, $p = \sqrt{2E}$; moreover it depends on the transmission coefficient of the metal wavefunctions $\langle \mathbf{r} | \mathbf{k} \rangle$ at the image plane, $T(k_z, p_z)$. It is calculated numerically. The kinetic energy distribution of ejected electrons is

$$N(E, \mathbf{v}) = \int d^2\Omega_{\mathbf{k}} P(E, \Omega_{\mathbf{k}}) N_I(\mathbf{k}, \mathbf{v}). \quad (4.19)$$

In previous works [12], the angular dependence of the electron escape probability was neglected, so the internal distribution was first resolved in angle, $\bar{N}_I(E, \mathbf{v}) = \int d^2\Omega_{\mathbf{k}} N_I(E, \Omega_{\mathbf{k}}, \mathbf{v})$, and then multiplied by the transmission function, to obtain the distribution of electrons excited to a state of kinetic energy E

$$\bar{N}(E, \mathbf{v}) = T(E) \bar{N}_I(E, \mathbf{v}), \quad (4.20)$$

where $T(E) = \frac{E}{E + \xi}$ is the well known spherical surface transmission function.

4.2 Experimental distribution.

Experimental distributions we have analyzed in the study of Auger Neutralization refer to electrons emitted by a polycrystalline target of $Al(111)$, bombarded by Ar^+ ions. The ions were produced in an electron bombardment source operated at low electron energies (30 eV) to prevent significant contamination of the ion beam with doubly charged ions. The incident beam energy ranges from 130 to 430 eV. The high purity polycrystalline Al surfaces were sputter cleaned by 4 keV Ar^+ ions at 12° glancing incidence. The experiment was conducted in UHV atmosphere. The surface of the samples were normal to the axis of the spectrometer and at 12° with respect to the ion beam direction. The

spectrometer was operated at a constant pass energy of 50 eV and with a resolution of 0.2 eV. The spectra were acquired with the sample biased at -2.5 eV to separate the contribution of electrons emitted directly from the sample (and accordingly shifted to higher energies) from a spurious peak of low energy electrons, mainly arising from the grounded entrance grid of the analyzer, that tails exponentially and can be easily subtracted.

In Fig. (4.1), we show experimental spectra of electrons ejected from *Al* by 130–430 eV Ar^+ ions. We can see the characteristic features of AN spectra [5, 8, 4]: constant areas, total electron emission yields and a magic energy. At emission energies larger than the 5.3 eV magic value, each spectrum follows an exponential trend. This behavior cannot be ascribed to electrons ejected by kinetic energy transfer from the projectile, since previous measurements, of 1 keV Ar^+ impact on *Al* surfaces at varying incident angle [76], have shown that their contribution does not affect significantly the high energy broadening of the electron spectra. Furthermore the exponential tailing can be explained just in terms of Fermi edge singularity.

4.3 Results compared with experimental spectra and with other models.

In the previous chapter we were arrived at the calculation of the Auger matrix elements. The next step consists in the calculation of the pure spectrum $N_I^0(\varepsilon, \mathbf{k}, \mathbf{v})$ through a Monte-Carlo integration over \mathbf{k}' and \mathbf{k}'' . Using Eqs. (4.19) and (4.14) we obtained the final spectrum $N(E, \mathbf{v})$, using a FFT (Fast Fourier Transformation) algorithm. Then we introduce the distribution of electrons excited to a state $|\mathbf{k}\rangle$ of energy $\varepsilon_{\mathbf{k}}$, in the Fermi golden rule approximation, neglecting the momentum dependence of the static matrix element of Auger potential $V_{kk'}^{ak''}(0) = V_0^a$. This distribution is obtained according to previous works, and it is already integrated in the solid angle

$$\bar{N}_I^0(\varepsilon_{\mathbf{k}}, \mathbf{v}) = \int d^2\Omega_{\mathbf{k}} N_I^0(\varepsilon_{\mathbf{k}}, \mathbf{k}, \mathbf{v}). \quad (4.21)$$

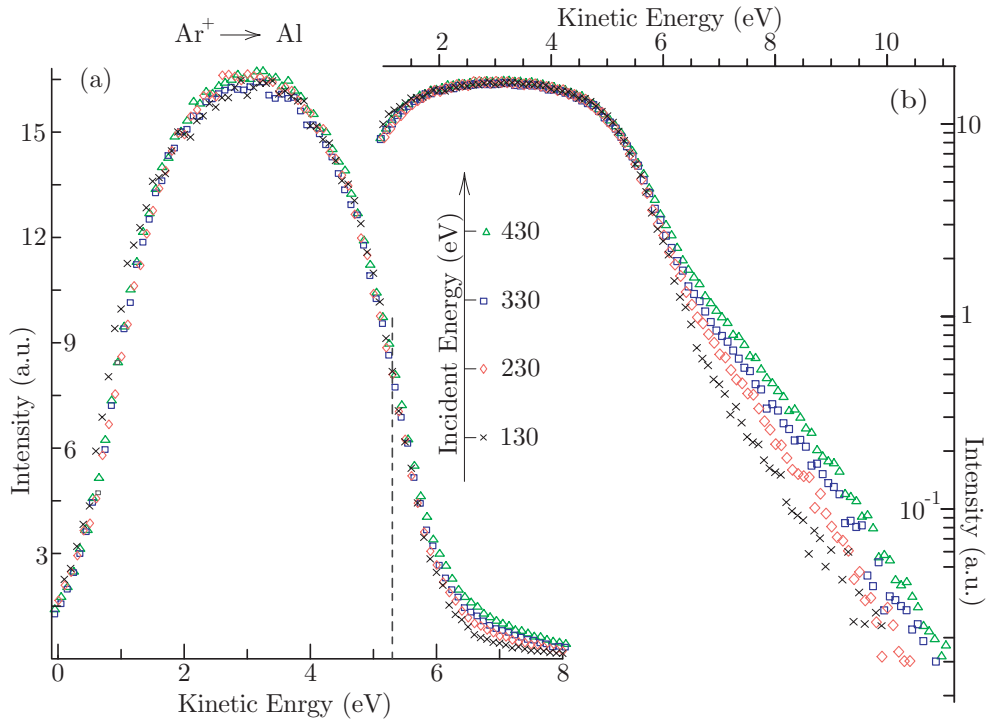
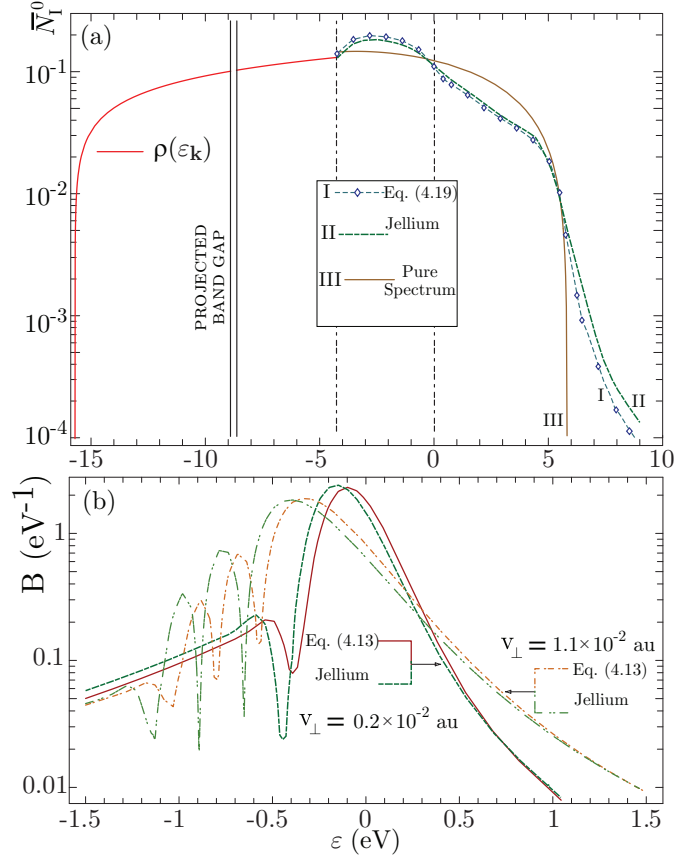


Figure 4.1: a) Kinetic energy distributions of electrons ejected from Al by 130–430 eV Ar⁺ ions. b) logarithmic scale for the same distribution.

This quantity we allows to visualize the broadening due to the long-time exponential decay of $V_{kk'}^{ak''}(t)$ by comparison with the pure spectrum, analytically derived from

Hagstrum's self-convolution model. We report in Fig. (??) the two curves calculated from Eqs. (4.19) (labelled with I in the picture) and (4.21) (labelled with III), where we display the curve $\bar{N}_i^0(\varepsilon_{\mathbf{k}}, \mathbf{v})$ obtained for Jellium too (labelled with II) [12].

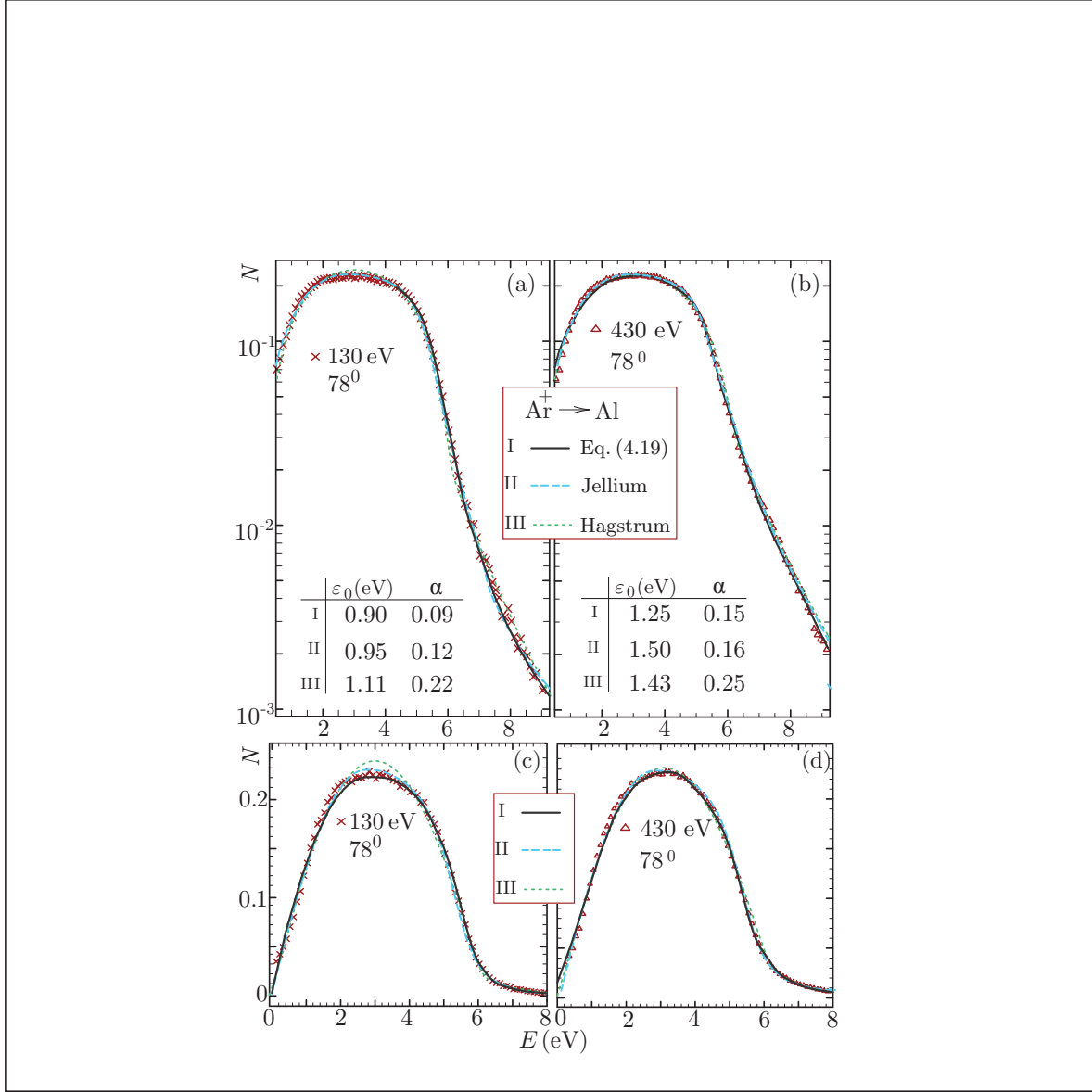
Figure 4.2: a) Energy distribution of electrons excited from $Al(111)$ by $130 \text{ eV } Ar^+$ ions at an incidence angle of 78° . The spectrum calculated from Eq. (4.19) is compared with the Jellium calculation of Ref. [] and the pure spectrum of Ref. []; b) broadening function of Eq. () for the models I and II of panel a). Two perpendicular velocities, $v_\perp = 0.2 \times 10^{-2} \text{ au}$ and $v_\perp = 1.1 \times 10^{-2} \text{ au}$, are used.



First of all we obtain the differences between the pseudopotential calculations used in this thesis (I) and the Jellium prescription (II [12]) of Al . The distribution II has a larger broadening to higher energy than the distribution I, because of the different decaying rates of corresponding metal wavefunctions within the surface regions, in the corresponding models. This reflects in the calculation of the energy shift and the ion survival probability, which affect the shape of the broadening function of Eq. (4.15), as reported in Fig. (4.2,b)). You can note an important difference in the trend of tails for the three curves in Fig. (4.2,a)). In Fig. (??) we show the theoretical distributions

$N(E, \mathbf{v})$ in comparison with the distributions acquired from Al by (130 – 430) eV Ar^+ ions [12].

Figure 4.3: Fig. 3. Kinetic energy distributions of electrons ejected from Al by 130 and 430 eV Ar^+ ions, with an incident angle of 78° relative to the surface normal. Comparison is made with the theoretical distributions obtained from Eqs. (4.19), Jellium of Ref. [12] and calculations of Ref. [12].



In models I and II, the parameters of the broadening function of shake-up electrons, Eq. (4.16) were adjusted to experiments. All other parameters were fixed, since for σ_{PH} we used the same value of X-ray studies on Al at room temperature, $\sigma_{PH} \sim 0.1$ eV [81]; Γ_0 is set to 0.01 eV, [8, 12]. As for the model III of self-convolution, we obtain the

average rate of electron decay outside the solid, fitting to experiments: $\lambda_a = 1$ au. It is interesting to note the excellent agreement of curves with experimental data. Even for model III there is a good experimental agreement, but in this case the number of parameters fitted has been increased with respect to models I and II. Furthermore, the projectile parallel velocities take values in the range $\mathbf{v}_{\parallel} = 0.01 - 0.02$ au, while the Fermi velocity of $Al(111)$ is $v_F = 0.91$ au. This means that the shift of the Fermi surface with \mathbf{v}_{\parallel} is small. In either model, the optimized values for α and ε_0 increase with increasing the projectile perpendicular velocity, which clearly manifests the non negligible effect of shake-up electrons in AN. As a further evidence, we report in Fig. (4.4) the theoretical distributions calculated for an incidence energy of 1 keV, and incidence angles in the range $0^\circ - 70^\circ$, in comparison with the experiments of [11]. The latter show a low energy peak due to kinetic electron emission, that is empirically fitted out with a Gaussian function. The effect of the parallel component of the impact velocity is still of second-order, since \mathbf{v}_{\parallel} takes values in the range $0 - 0.03$ au. Even if the results are more qualitative, owing to the absence of a reliable model to reproduce the raising front of the signals, we continue to observe an increase of the parameters of $F_a(t, \mathbf{v}_{\perp})$. More importantly, the tail of the distributions clearly show a non Lorentzian behavior with a superimposed Gaussian trend due to the decreased resolution of the analyzer.

The behavior of the best fitted values of α and ε_0 vs v_{\perp} is reported in Fig. 5, for all the experimental distributions of [11, 12]. The singularity index takes values in the range $\sim 0.1 - 0.3$, typical of x-ray studies on metal samples [81], and increases with increasing v_{\perp} . In fact, owing to the small perturbation, the instantaneous phase-shift of the contact potential can be approximated to $V_{k_F}^a(t)$, which decreases exponentially, in the long time limit, with a rate proportional to v_{\perp} . It follows that $\Phi(v_{\perp}, \varepsilon)$ depends on ε with a nearly Lorentzian structure. Its broadening increases with increasing v_{\perp} , together with $\Phi(v_{\perp}, \varepsilon_F)$. The other parameter, $\varepsilon_0(v_{\perp})$, enters the exponential part of $\tilde{F}_a(v_{\perp}, \varepsilon)$. Its increase, with increasing v_{\perp} , is clearly observed in the increase of the exponential tailing of the experimental kinetic energy distributions. We believe that this is a consequence of the increase of the efficiency of the singular response of the metal band to the sudden neutralization, as attested by the increase of the neutralization rates.

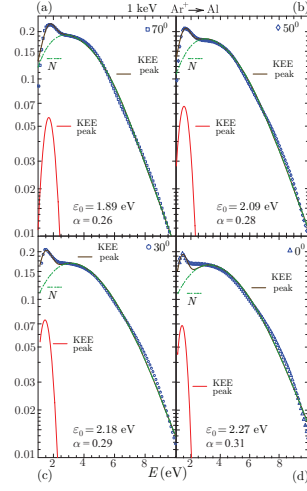


Figure 4.4: Kinetic energy distributions of electrons ejected from Al by 1 keV Ar^+ -ions, with an incident angle of 70° , 50° , 20° and 0° , relative to the surface normal. Comparison is made with the theoretical distributions obtained from Eqs. (4.13) and (4.19). The low energy peak, due to KEE, is empirically fitted with a Gaussian function.

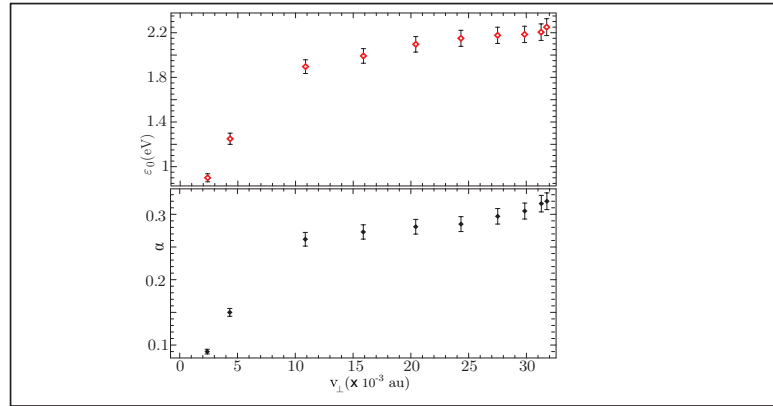


Figure 4.5: Best fitted values of α and ϵ_0 vs v_{\perp} , for the experiments of Refs. [?, ?, ?].

4.4 Resonant charge transfer: spectral method.

Now we are going to speak about applications and results for negative resonant charge transfer. In the previous chapter we have introduced the atomic energies $\epsilon_a(t)$ and $\epsilon_b(t)$

with their shifts, Eqs. (3.86) and (3.87); the Hopping potentials $\hat{V}_{\mathbf{a}\mathbf{k}}(t)$ and $\hat{V}_{\mathbf{b}\mathbf{k}}(t)$, Eqs. (3.89) and (3.90). Now we introduce interatomic charge exchanges allowed by

$$\hat{V}_{\mathbf{a}\mathbf{b}}(t) = -I\sigma_{\mathbf{a}\mathbf{b}}(t) + \langle \mathbf{a}(t) | \hat{v}_{\mathbf{S}}^i(\hat{\mathbf{r}}, \mathbf{R}_{\mathbf{a}}(t), \mathbf{R}_{\mathbf{b}}(t)) | \mathbf{b}(t) \rangle + \langle \mathbf{a}(t) | \hat{v}_{\mathbf{A}}(|\hat{\mathbf{r}} - \mathbf{R}_{\mathbf{a}}(t)|) | \mathbf{b}(t) \rangle. \quad (4.22)$$

A measure of the energy exchanges brought by $\hat{V}_{\mathbf{a}\mathbf{k}}(t)$ and $\hat{V}_{\mathbf{b}\mathbf{k}}(t)$, at any band energy $\varepsilon_k = \varepsilon$, is given by the instantaneous broadenings $\Delta_{\mathbf{a}(\mathbf{b})}(\varepsilon, t)$

$$\Delta_{\mathbf{a}(\mathbf{b})}(\varepsilon, t) = \pi \sum_{\mathbf{k}} \left| \hat{V}_{\mathbf{a}(\mathbf{b})\mathbf{k}}(t) \right|^2 \delta(\varepsilon - \varepsilon_k) \quad (4.23)$$

of the state $|\mathbf{a}(\mathbf{b})(t)\rangle$.

The renormalized energy of the orthogonalized state $|\beta(t)\rangle$ reads

$$\varepsilon_{\beta}(t) = \varepsilon_{\beta}^0(t) + \varepsilon_m(t). \quad (4.24)$$

$\varepsilon_{\beta}^0(t)$ is the molecular energy

$$K_{\beta}(t)^2 \varepsilon_{\beta}^0(t) = \varepsilon_{\beta}(t) - 2\sigma_{\mathbf{a}\mathbf{b}}(t) \hat{V}_{\mathbf{a}\mathbf{b}}(t) + \sigma_{\mathbf{a}\mathbf{b}}(t)^2 \varepsilon_{\mathbf{a}}(t), \quad (4.25)$$

and $\varepsilon_m(t)$ encloses the effect of metal states

$$K_{\beta}(t)^2 \varepsilon_m(t) = \sum_{\mathbf{k}} \left\{ |\sigma_{\mathbf{k}\mathbf{b}}(t)|^2 \varepsilon_k + 2 \operatorname{Re} \left[\sigma_{\mathbf{b}\mathbf{a}}(t) \hat{V}_{\mathbf{a}\mathbf{k}}(t) \sigma_{\mathbf{k}\mathbf{b}}(t) - \hat{V}_{\mathbf{b}\mathbf{k}}(t) \sigma_{\mathbf{k}\mathbf{b}}(t) \right] \right\}. \quad (4.26)$$

$\varepsilon_{\beta}^0(t)$ takes values outside the Fermi surface, at short times, $t \lesssim 30$ fs, and it tends quite rapidly to $\varepsilon_{\mathbf{b}}(t)$, as the interatomic distance increases. $\varepsilon_m(t)$ has an oscillating behavior after ejection and it damps to zero in the time scale of the motion of the substrate atom. As a result, $\varepsilon_{\beta}(t)$ is initially promoted to positive values, above the vacuum level. At $10 \lesssim t \lesssim 30$ fs, it crosses $\varepsilon_{\mathbf{F}}$, facing the occupied band states. At $t \gtrsim 30$ fs, it crosses $\varepsilon_{\mathbf{a}}(t)$ and goes below the bottom of the conduction band, reaching

asymptotically the unperturbed value $-I$, as fast as $\varepsilon_b(t)$. Even at short times, at $t \approx 20$ fs, the ionization channel $|a(t)\rangle \rightarrow |\beta(t)\rangle \rightarrow |k\rangle$ is at least competitive with the direct Hopping $|a(t)\rangle \rightarrow |k\rangle$.

With these ingredients, and keeping in mind chapter 2, we calculate the negative ionization probability, $R_-(t)$, of a-atoms, i.e., the probability that affinity state $|a(t)\rangle$, initially empty at $t = t_0$, is occupied when the secondary ion lies at large distances from the surface- $Z_a(t) \gg z_{\text{IM}}$ - and its charge state is detected. The instant $t = 0$, corresponds to the time when both particles are outside the image plane and move with approximately constant velocity. Then, the problem is analytically continued to negative times, through Gellmann and Low's adiabatic theorem Ref. [59], assuming $\hat{h}_{\text{EFF}}(t < 0) = \hat{h}_{\text{EFF}}(0)$, $|a(b)(t < 0)\rangle = |a(b)(0)\rangle$. Previous derivations [56, 17, 57, 58, 46, 50] have shown that $R_-(t)$ may be written as the weighted sum

$$R_-(t) = \sum_{\mathbf{k}} |G_{\mathbf{a}\mathbf{k}}^+(t, t_0)|^2 n(\varepsilon_{\mathbf{k}}, t_0) \quad (4.27)$$

of the probability amplitudes, $G_{\mathbf{a}\mathbf{k}}^+(t, t_0) = -i \langle a(t) | \hat{u}(t, t_0) | \mathbf{k} \rangle$, that an electron, in the state $|\mathbf{k}\rangle$, will eventually be captured by the emitted atom, by the Fermi-Dirac occupation numbers $n(\varepsilon_{\mathbf{k}}, t_0) = \Theta(\varepsilon_{\text{F}} - \varepsilon_{\mathbf{k}})$, at the time t , when $Z_a(t) \gg z_{\text{IM}}$. By definition, $G_{\mathbf{a}\mathbf{k}}^+(t, t_0)$ is a retarded Green's function and $\hat{u}(t, t_0)$ the time-development operator for the evolution spanned by $\hat{h}(t)$. Complementarily, $G_{\beta\mathbf{k}}^+(t, t_0)$ denotes the probability amplitude for electron transfer to the orthonormalized molecular state. We introduce the retarded Green's functions

$$\begin{pmatrix} G_{\alpha\mathbf{k}}^+(t, t_0) \\ G_{\beta\mathbf{k}}^+(t, t_0) \end{pmatrix} = -i \begin{pmatrix} \langle \alpha(t) | \\ \langle \beta(t) | \end{pmatrix} \hat{u}(t, t_0) | \mathbf{k} \rangle \theta(t - t_0), \quad (4.28)$$

and

$$G_{\mathbf{k}'\mathbf{k}}^+(t, t_0) = -i \langle \mathbf{k}' | \hat{u}(t, t_0) | \mathbf{k} \rangle \theta(t - t_0), \quad (4.29)$$

where the initial condition $\hat{u}(t, t_0) = 1$ implies $G_{\alpha\mathbf{k}}^+(t_0, t_0) = G_{\beta\mathbf{k}}^+(t_0, t_0) = 0$ and $G_{\mathbf{k}'\mathbf{k}}^+(t_0, t_0) = -i\delta_{\mathbf{k}'\mathbf{k}}$. The Schrödinger equation for the time development operator, and the expansion of $\hat{u}(t, t_0)|\mathbf{k}\rangle$ into $\{|\alpha(t)\rangle, |\beta(t)\rangle, |\mathbf{k}'\rangle\}_{\varepsilon_{\mathbf{k}'} \leq 0}$, yields

$$[i\partial_t - H_{\text{QM}}(t)] \begin{pmatrix} G_{\alpha\mathbf{k}}(t, t_0) \\ G_{\beta\mathbf{k}}(t, t_0) \end{pmatrix} = \sum_{\mathbf{k}'} \begin{pmatrix} V_{\alpha\mathbf{k}'}(t) \\ V_{\beta\mathbf{k}'}(t) \end{pmatrix} G_{\mathbf{k}'\mathbf{k}}(t, t_0), \quad (4.30)$$

and

$$[i\partial_t - \varepsilon_{\mathbf{k}'}] G_{\mathbf{k}'\mathbf{k}}(t, t_0) = V_{\mathbf{k}'\alpha}(t)G_{\alpha\mathbf{k}}(t, t_0) + V_{\mathbf{k}'\beta}(t)G_{\beta\mathbf{k}}(t, t_0), \quad (4.31)$$

where

$$H_{\text{QM}}(t) = \begin{pmatrix} \varepsilon_{\alpha}(t) & V_{\alpha\beta}(t) \\ V_{\beta\alpha}(t) & \varepsilon_{\beta}(t) \end{pmatrix} \quad (4.32)$$

is the QM Hamiltonian and the adiabatic derivatives $\langle\alpha(t)|\partial_t|\beta(t)\rangle$ are neglected, together with the coupling between different band states. H_{QM} has the (real) matrix elements of $\hat{h}(t)$ into the states $|\alpha(t)\rangle$ and $|\beta(t)\rangle$. Its diagonal components, $\varepsilon_{\alpha}(t)$ and $\varepsilon_{\beta}(t)$, are the instantaneous energies of the orthonormalized affinity states. Eq. (4.31) is eliminated using the semiclassical approximation [Shao], that, in the present context, can be formulated as

$$\begin{aligned} & \sum_{\mathbf{k}'} \int_{t_0}^t dt' \begin{pmatrix} V_{\alpha\mathbf{k}'}(t) \\ V_{\beta\mathbf{k}'}(t) \end{pmatrix} e^{-i\varepsilon_{\mathbf{k}'}(t-t')} V_{\mathbf{k}'\alpha(\beta)}(t') G_{\alpha(\beta)\mathbf{k}}(t', t_0) \\ & \approx \sum_{\mathbf{k}'} \int_{t_0}^t dt' \begin{pmatrix} V_{\alpha\mathbf{k}'}(t) \\ V_{\beta\mathbf{k}'}(t) \end{pmatrix} e^{i\int_{t'}^t d\tau [\varepsilon_{\alpha(\beta)}(\tau) - \varepsilon_{\mathbf{k}'}]} V_{\mathbf{k}'\alpha(\beta)}(t') G_{\alpha(\beta)\mathbf{k}}(t, t_0), \end{aligned} \quad (4.33)$$

so that

$$[i\partial_t - H'_{\text{QM}}(t)] \begin{pmatrix} G_{\alpha\mathbf{k}}(t, t_0) \\ G_{\beta\mathbf{k}}(t, t_0) \end{pmatrix} = -ie^{-i\varepsilon_{\mathbf{k}}(t-t_0)} \begin{pmatrix} V_{\alpha\mathbf{k}}(t) \\ V_{\beta\mathbf{k}}(t) \end{pmatrix} \quad (4.34)$$

Here, the time evolution is governed by the (non Hermitian) dissipative Hamiltonian $H'_{\text{QM}}(t) = H_{\text{QM}}(t) + \Sigma_{\text{QM}}(t)$, in which

$$\Sigma_{\text{QM}}(t) = -i \sum_{\mathbf{k}} \int_{t_0}^t dt' \begin{pmatrix} V_{\alpha\mathbf{k}}(t) \\ V_{\beta\mathbf{k}}(t) \end{pmatrix} \otimes \begin{pmatrix} e^{i \int_{t'}^t d\tau [\varepsilon_{\alpha}(\tau) - \varepsilon_{\mathbf{k}}]} V_{\alpha\mathbf{k}}(t') \\ e^{i \int_{t'}^t d\tau [\varepsilon_{\beta}(\tau) - \varepsilon_{\mathbf{k}}]} V_{\beta\mathbf{k}}(t') \end{pmatrix} \quad (4.35)$$

behaves as a damping potential, \otimes denoting the tensor product of two column vectors. This dissipative term is the complex self-energy matrix. $V_{\alpha(\beta)\mathbf{k}}(t) = \langle \alpha(\beta)(t) | \hat{h}(t) | \mathbf{k} \rangle$ are the coupling integrals of discrete and continuous states. It should be noted that the interaction with a state $|\mathbf{k}\rangle$ has the form of an external perturbation. Thus, the calculation of $G_{\alpha\mathbf{k}}(t, t_0)$, tending asymptotically to $G_{\text{ak}}(t, t_0)$, and $G_{\beta\mathbf{k}}(t, t_0)$ reduces to the solution of a (dissipative) 2-level system [56, 17, 57, 58]. The matrix elements appearing in Eq. (4.34) evolve over two different time scales, related to the different motions of a and b atoms. This is shown, for example, in the study of the renormalized energies of the orthonormalized affinity states, reported in Figs. (4.6)a and b for $Ag^-/Ag(100)$ and $Au^-/Au(100)$, respectively. Indeed, $\varepsilon'_\alpha(t) = \text{Re}[H'_{\text{QM}}(t)]_{\alpha\alpha}$ and $\varepsilon'_\beta(t) = \text{Re}[H'_{\text{QM}}(t)]_{\beta\beta}$, the effective energies, are corrected by the effect real part of the self energy matrix (4.35) inducing short time oscillations, which are more clearly observed in Fig. (4.6)b, where QM interaction are stronger. $\Delta_{\alpha(\beta)}(t) = -\text{Im}[\Sigma_{\text{QM}}(t)]_{\alpha\alpha(\beta\beta)}$ are the broadenings of the orthonormalized QM states, coupled by the off-diagonal terms $V'_{\alpha\beta(\beta\alpha)}(t) = V_{\alpha\beta}(t) + [\Sigma_{\text{QM}}(t)]_{\alpha\beta(\beta\alpha)}$. In general, $\varepsilon'_\alpha(t)$ changes faster than $\varepsilon'_\beta(t)$, although both terms are slow on the femtosecond scale of the electronic transitions, which justifies the use of the semiclassical approximation. At short times after the instant of ejection, $\varepsilon'_\alpha(t)$ is shifted negatively, with respect to its unperturbed value, due to the dominant effect of the electron-surface interaction (\hat{v}_s), while $\varepsilon'_\beta(t)$ is promoted above the vacuum level, since the substrate atom is initially closer to the image plane where the leading effect is due to the image

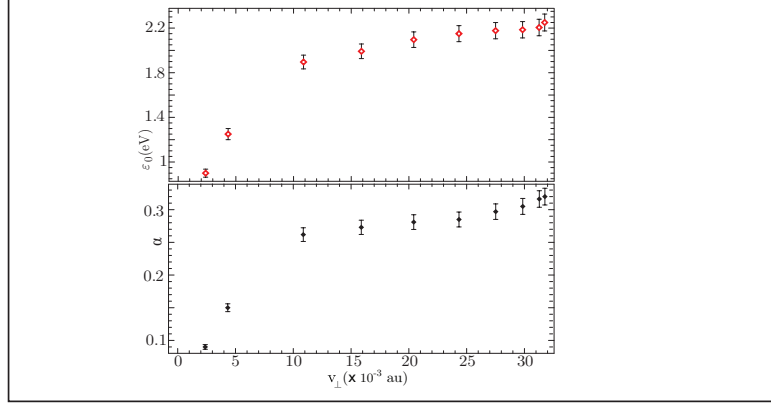


Figure 4.6: Instantaneous energies (ε_{\pm}) and broadenings (Δ_{\pm}) of the bonding and antibonding orbitals of the QM, made of a- and b-atoms, with the parameters of $\text{Ag}^-/\text{Ag}(100)$ and $\text{Au}^-/\text{Au}(100)$. In panel (a), (b), the renormalized affinity energies (ε'_{α} and ε'_{β}) are reported for comparison. In panel (b), the unrenormalized atomic energy ε_{α} is also shown to visualize the effect of the shift induced by the self-energy matrix (4.35).

potential ($\Delta\hat{v}_{\text{QM}}$). At larger times, $\varepsilon'_{\alpha}(t)$ tends to the unperturbed affinity energy as fast as $1/Z_{\text{a}}(t)$, while $\varepsilon'_{\beta}(t)$ behave as $1/Z_{\text{b}}(t)$. $\varepsilon'_{\beta}(t)$ crosses $\varepsilon'_{\alpha}(t)$ and reaches a minimum, because of the competing action of the repulsive ($\Delta\hat{v}_{\text{QM}}(t)$) and attractive ($\hat{v}_{\text{s}}(t) + \hat{v}_{\text{QM}}(t)$) components of $\hat{v}_{\text{EFF}}(t)$. $\Delta_{\alpha}(t)$ and $\Delta_{\beta}(t)$ drop off to zero, with an oscillating exponential behavior, at $t \gtrsim 10$ fs and $t \gtrsim 100$ fs, respectively; the monotonic behavior of $\varepsilon'_{\alpha}(t)$ reflects in the maximum of $|\Delta_{\alpha}(t)|$, occurring at $t \leq 0$, when the a-atom is closer to the surface, while $|\Delta_{\beta}(t)|$ is maximum at the time when $\varepsilon'_{\beta}(t)$ is minimum and closer to the Fermi surface. $V'_{\alpha\beta}(t)$ and $V_{\beta\alpha}(t)$, have similar trends, taking absolute values of the order of ~ 1 eV at $t \lesssim 50$ fs that tend to zero exponentially, at larger times with an intermediate time-scale between the motions of a and b atoms. Level crossing allows resonant charge transfer processes between $|\alpha(t)\rangle$ and $|\beta(t)\rangle$, coupled by the off diagonal terms $[H'_{\text{QM}}(t)]_{\alpha\beta}$ and $[H'_{\text{QM}}(t)]_{\beta\alpha}$.

A closer insight into quasi-molecular correlations is gained by considering the instantaneous spectrum of $H'_{\text{QM}}(t)$, yielding the eigenvalues $\varepsilon_{\pm}(t) - i\Delta_{\pm}(t)$. The corresponding eigenstates, namely $|+(t)\rangle$ and $|-(t)\rangle$, are the antibonding and bonding states of the QM, obtained from linear combinations of $|\alpha(t)\rangle$ and $|\beta(t)\rangle$. Their energies, $\varepsilon_{\pm}(t)$, and their virtual broadenings, $\Delta_{\pm}(t)$, are shown in Fig. (4.6): we see that $\varepsilon_{+}(t)$ tends to $\varepsilon'_{\alpha}(t)$, while $\varepsilon_{-}(t)$ tends to $\varepsilon'_{\beta}(t)$, in the long time limit (Figs. (4.6)a and b); thus, an

electron captured in the antibonding state will be detected in a-atom. In addition, the bonding orbital is further shifted towards ε_F , compared to $\varepsilon'_\alpha(t)$ and $\varepsilon'_\beta(t)$, which enhances the probability for electron capture to the QM. From this perspective, Eq. (4.34) establishes electron transfer dynamics based on two mechanisms: one is *direct* tunnelling from each band state to the ejected atom and the other an *indirect*, two-step process, with an intermediate transition through the molecular level $\varepsilon_-(t)$.

Another crucial aspect concerns the evolution of the broadenings of the QM orbitals, shown in Figs. (4.6)c and d; both $\Delta_+(t)$ and $\Delta_-(t)$ drop off to zero with an oscillating exponential behavior, which is not surprising since the adiabatic energies of the orthonormalized affinity states take values in the projected band gap during the whole process. It follows that their adiabatic broadenings are virtually zero so that the phase factors $\exp\left\{i \int_{t'}^t d\tau [\varepsilon_{\alpha(\beta)}(\tau) - \varepsilon_{\mathbf{k}}]\right\}$, within the t' -integral in Eq. (4.35), induce oscillations in $\Sigma_{\text{QM}}(t)$. On the other hand, the exponential decrease is related to the hopping terms $V_{\alpha\mathbf{k}}(t)$ and $V_{\beta\mathbf{k}}(t)$. The sign of $\Delta_\pm(t)$ modulates electron transfer processes to the state $|\pm(t)\rangle$, whose occupation probability contains the exponential factor $\exp\left[-\int^t d\tau \Delta_\pm(\tau)\right]$.

A numerical solution for Eq. (4.34), at positive times, requires a model to estimate the electronic distribution of the metal band at the instant of ejection ($t = 0$). Recalling that the final charge fraction of the localized levels is independent on their initial occupancy in the remote past [46], we continue the problem analytically to negative times with Gellmann and Low's adiabatic prescriptions [59]:

$$\hat{h}(t \leq 0) = \hat{p}^2/2 + \hat{v}(0)e^{0^+t}. \quad (4.36)$$

In this case, both $G_{\alpha\mathbf{k}}(0, t_0)$ and $G_{\beta\mathbf{k}}(0, t_0)$ can be calculated exactly, because their evolution from the remote past is stationary. In addition, the one-electron potential is switched off at $t = t_0$, implying $G_{\alpha\mathbf{k}}^+(t_0, t_0) = G_{\beta\mathbf{k}}^+(t_0, t_0) = 0$. Then, the analytical

solution of Eq. (4.34) at $t \leq 0$ reads

$$\begin{pmatrix} G_{\alpha\mathbf{k}}(0, t_0) \\ G_{\beta\mathbf{k}}(0, t_0) \end{pmatrix} = -ie^{it_0\varepsilon_{\mathbf{k}}} \frac{T'_{\mathbf{k}}}{|T'_{\mathbf{k}}|} \begin{pmatrix} V_{\alpha\mathbf{k}}(0) \\ V_{\beta\mathbf{k}}(0) \end{pmatrix}, \quad (4.37)$$

in which

$$T'_{\mathbf{k}} = \begin{pmatrix} \varepsilon_{\mathbf{k}} - \varepsilon'_{\beta}(0) & V'_{\alpha\beta}(0) \\ V'_{\alpha\beta}(0) & \varepsilon_{\mathbf{k}} - \varepsilon'_{\alpha}(0) \end{pmatrix} \quad (4.38)$$

is a transfer Hamiltonian from the state $|\mathbf{k}\rangle$ to the affinity states. Finally, Eq. (4.37) can be used as initial condition to solve numerically Eq. (4.34), for each \mathbf{k} and $t > 0$, yielding $G_{\alpha\mathbf{k}}(t, t_0)$ and $G_{\beta\mathbf{k}}(t, t_0)$. This allows to calculate the negative ionization probability of the state $|\alpha(t)\rangle$, via Eq. (4.27). Complementary, we also calculated the negative ionization probability of the state $|\beta(t)\rangle$, denoted $R'_-(t)$, by replacement of $G_{\alpha\mathbf{k}}(t, t_0)$ with $G_{\beta\mathbf{k}}(t, t_0)$ in Eq. (4.27).

Fig. (4.7) shows the negative ionization probabilities, $R_-(t)$ and $R'_-(t)$, for the orthonormalized affinity states. We observe there exists a time t_F such that both $R_-(t)$ and $R'_-(t)$ are independent on time, for $t > t_F$, whereas they depend on the kinetic energies of a- and b-atoms. t_F increases with decreasing E_a , taking typical values in the range 10 – 200 fs at $E_a = 10 - 300$ eV. A signature of charge exchanges between $|\alpha(t)\rangle$ and $|\beta(t)\rangle$ is given by the oscillating behavior of $R_-(t)$ and $R'_-(t)$, occurring for typical times of the order of 10^2 fs, for kinetic energies $E_a \lesssim 15$ eV and $E_b \lesssim 1$ eV. The transition $|k\rangle \rightarrow |\beta(t)\rangle$ is more efficient than $|k\rangle \rightarrow |\alpha(t)\rangle$, implying that the indirect hopping mechanism $|k\rangle \rightarrow |\beta(t)\rangle \rightarrow |\alpha(t)\rangle$ plays a significant role in the dynamics of the system for large time intervals, of the order $\sim 10^2$ fs.

This conclusion is in agreement with the calculations of Fig. (4.8) where particles with emission energies below 30 eV have average lifetimes larger than ~ 100 fs. In this figure we report the probability $\langle R_-(t) \rangle$, obtained as the average ionization probability of a-atoms for a Gaussian distribution of b-atoms, with mean energy E_b and standard deviation σ_b . Plots of $\langle R_-(t_F) \rangle$ vs y_a , the inverse velocity of the emitted atom, are

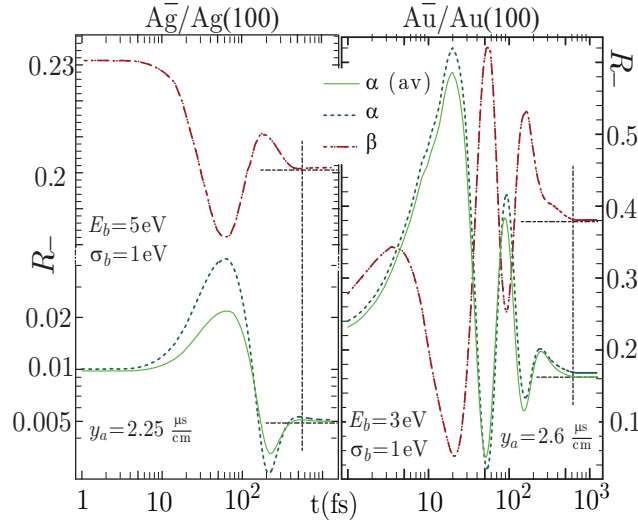


Figure 4.7: Ionization probabilities $R_-(t)$ and $R'_-(t)$ for the orthonormalized affinity states, with the parameters of $Ag^-/Ag(100)$ and $Au^-/Au(100)$ systems (Fig. 3). $\langle R_-(t) \rangle$ is obtained by averaging $R_-(t)$ over a gaussian distribution of b-particles with mean energy E_b and standard deviation σ_b .

compared with the experimentally derived distributions of Ag^- and Au^- ions sputtered from their elemental surfaces [49]. E_b is adjusted to the data, taking values in the range 1 – 7 eV, in both $Ag^-/Ag(100)$ and $Au^-/Au(100)$ systems. Fig. (4.8) shows a good agreement with data, correctly reproducing the increase in the negative ion population with increasing y_a , above $\sim 10^{-6}$ s/cm. This is explained, in the present context, with the enhancement of the probability for indirect transfers with decreasing E_a , corresponding to a longer duration of quasi molecular interactions. Conversely, the direct resonant mechanism decreases almost exponentially with increasing y_a [13, 46, 50].

4.5 Resonant charge transfer: wave packet propagation method.

In this section we present an alternative method to calculate the quantity $G_{\alpha k}^+(t, t_0)$: we have used a split operator approximation [?] for the time-development operator and a Crank–Nicholson wave-packet propagation (WPP) scheme [?] to determine the evolution- backwards in time- of the affinity orbital of the negative ion. The latter is

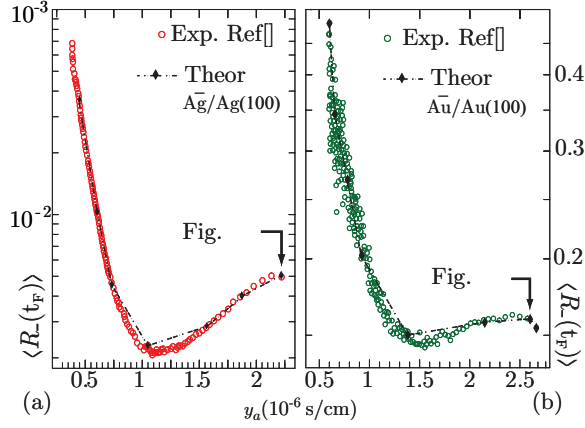


Figure 4.8: Theoretical ionization probability of negative ions for the $Ag^-/Ag(100)$ and $Au^-/Au(100)$ systems, obtained as in Fig. (4.6). Experiments are taken from Ref. [?]

isolated at distances of the order of $\sim 50 - 100$ au from the surface, so that the initial wavefunction, is set to $\langle \mathbf{r} | \alpha(t) \rangle$ at a large time t on the time-scale of the motion of the a-atom. From the spectral method [18] we have seen there exists an instant of time t_F such that the negative ionization probability is constant, Fig. (4.7). We introduce now the density probability $P_a(\varepsilon_{\mathbf{k}}, t)$

$$P_a(\varepsilon_{\mathbf{k}}, t) = \rho(\varepsilon_{\mathbf{k}}) \int d^2\Omega_{\mathbf{k}} |G_{\alpha\mathbf{k}}^+(t, -\infty)|^2 \quad (4.39)$$

that an electron in a metal state of energy $\varepsilon_{\mathbf{k}}$ will occupy the affinity state of the a-atom at the time t , being such that $R_-(t) = \int^{\varepsilon_F} d\varepsilon_{\mathbf{k}} P_a(\varepsilon_{\mathbf{k}}, t)$. In Eq. (4.39), $\rho(\varepsilon_{\mathbf{k}})$ is the unperturbed density of conduction states with Fermi energy ε_F . In Fig. (??) we show $P_a(\varepsilon_{\mathbf{k}}, t)$ calculated with the spectral method of [18], using the parameters of $Au^-/Au(100)$.

The initial distribution $P_a(\varepsilon_{\mathbf{k}}, 0)$, at the time of ejection, is derived from the analytical evolution of a stationary problem from the remote past. We verified that at times larger than $t_F \sim 700$ fs, corresponding to an atom-surface separation of 50 au, $P_a(\varepsilon_{\mathbf{k}}, t)$ remains approximately constant, with $R_-(t_F) = 0.159$ in agreement with the experiments of ??.

This demonstrates that the ejected atom is unperturbed at $t \geq t_F$, when $|a(t)\rangle$, is nearly a stationary state for the system. Then,

$$|\psi_a(t, t_F)\rangle = \hat{u}(t, t_F)|a(t_F)\rangle \quad (4.40)$$

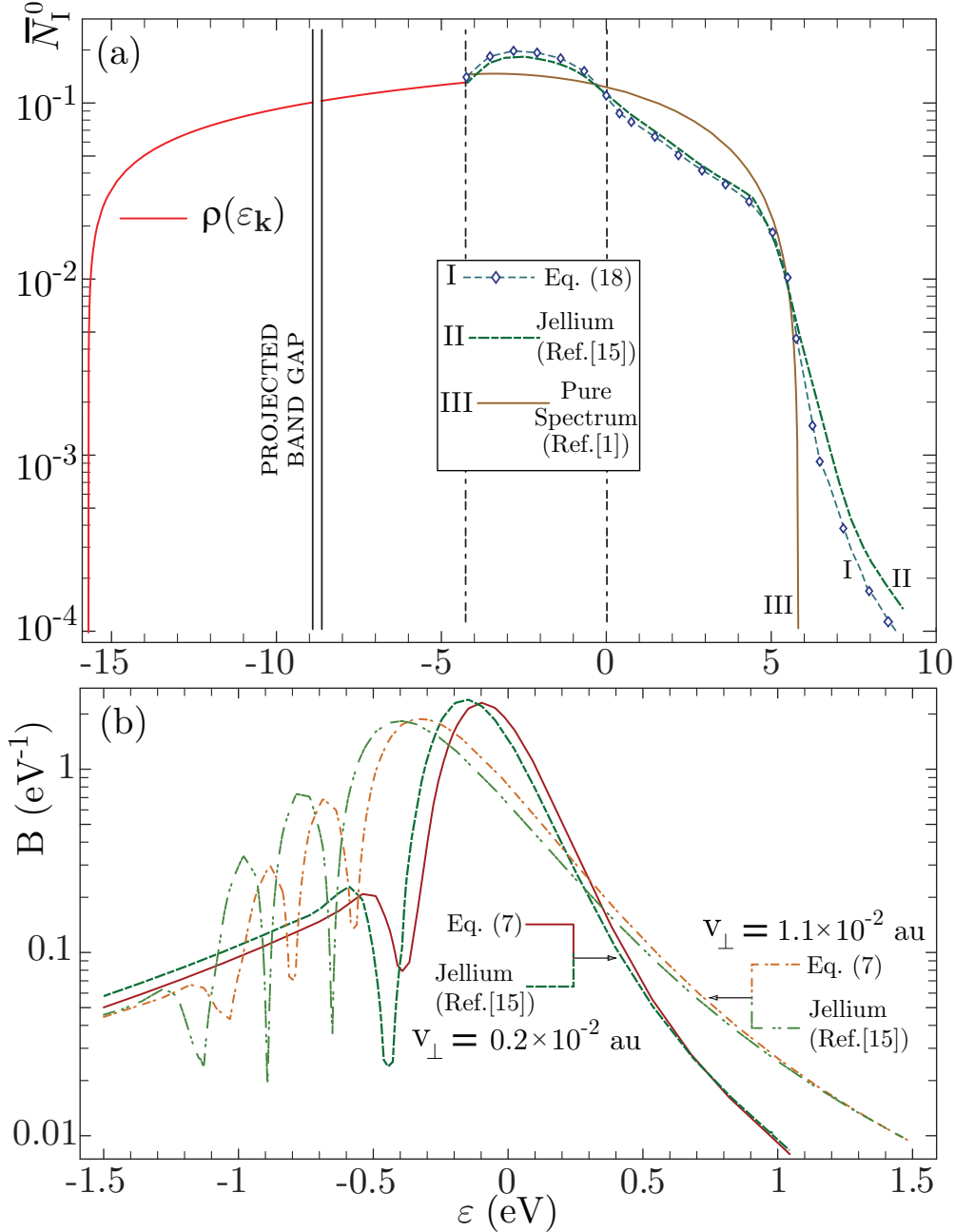


Figure 4.9: Probability density (??) for $\text{Au}^-/\text{Au}(100)$. The final emission energy of the a -particle, with initial position $Z_a^0 = 1.5 a_s$ ($a_s = 3.853 \text{ au}$), is set $E_a = 15$ eV. A gaussian distribution, peaked at $E_b = 3$ eV, with a standard deviation of 1 eV, is assumed for b -atoms with initial position $Z_b^0 = 0.5 a_s$.

determines the nonstationary evolution of the atomic state, from the (final) instant t_F to a time $t < t_F$ through the time evolution operator $\hat{u}(t, t_F)$; its representation, in the basis of coordinates, yields the atomic electron wavefunction, $\psi_a(\mathbf{r}; t, t_F) = \langle \mathbf{r} | \psi_a(t, t_F) \rangle$, whose superposition with a metal wavefunctions, $\langle \mathbf{r} | \mathbf{k} \rangle$, coincides with the retarded Green's function

$$G_{\mathbf{a}\mathbf{k}}^+(t, t_F) = -i \int d^3r \psi_a^*(\mathbf{r}; t, t_F) \langle \mathbf{r} | \mathbf{k} \rangle, \quad (4.41)$$

or the probability amplitude that a band electron, in the state $|\mathbf{k}\rangle$ at the time t , will be transferred to the a-atom. It follows that the negative ionization probability approximates to

$$R_-(t) \approx \sum_{\mathbf{k}} n(\varepsilon_{\mathbf{k}}, 0) |G_{\mathbf{a}\mathbf{k}}^+(0, t_F)|^2, \quad (4.42)$$

where

$$n(\varepsilon_{\mathbf{k}}, 0) = \sum_{\mathbf{k}'} |G_{\mathbf{k}\mathbf{k}'}^+(0, t_0)|^2 n(\varepsilon_{\mathbf{k}'}, t_0) \quad (4.43)$$

denotes the occupation number of a band level at the instant of ejection. It is obtained from the analytical solution of Eq. (4.34)

$$G_{\mathbf{k}\mathbf{k}'}^+(0, t_0) = -ie^{it_0\varepsilon_{\mathbf{k}}} \left\{ \delta_{\mathbf{k}\mathbf{k}'} + \frac{T_{\mathbf{k}\mathbf{k}'}(0)}{\varepsilon_{\mathbf{k}} - \varepsilon_{\mathbf{k}'} + i0^+} \right\} \quad (4.44)$$

and

$$T_{\mathbf{k}\mathbf{k}'}(0) = \begin{pmatrix} V_{\alpha\mathbf{k}}(0) & V_{\beta\mathbf{k}}(0) \end{pmatrix} \frac{H'_{\mathbf{k}'}}{|H'_{\mathbf{k}'}|} \begin{pmatrix} V_{\alpha\mathbf{k}'}(0) \\ V_{\beta\mathbf{k}'}(0) \end{pmatrix} \quad (4.45)$$

represents the T -matrix for electron-hole excitations produced by the hopping potentials.

Following the approach of [43], the function

$$f_a(\mathbf{r}, t) = x \psi_a(x, z; t, t_F), \quad (4.46)$$

with $x = \sqrt{r_{\parallel}}$, is obtained on a grid, in cylindric coordinates, (r_{\parallel}, ϕ, z) , which includes 50 atomic layers of bulk and extends to $z = 100$ on the vacuum side. This represents well the important surface and bulk properties along the z direction. The grid extends from $x = 0$ to $x = 10$ in the parallel direction to surface. Grid spacings $\Delta z = 0.2$ and $\Delta x = 0.02$ were found to be adequate. It should be noted that Eq. (4.46) is independent on the azimuthal angle because the initial wavefunction has the s -symmetry and the one-electron potential \hat{v}_s is invariant under spatial rotations over the z -axis.

t_F is chosen in order to have $Z_a(t_F) \approx 50$ au, yielding $t_F \approx 150 - 1000$ fs for $E_a \approx 10 - 100$ eV. The time interval $[0, t_F]$ is discretized into time steps $\delta t = 2$ au, corresponding to instants $t_n = t_F - n \delta t$. The usual composition rule $\hat{u}(t_n, t_F) = \prod_{m=1}^n \hat{u}(t_m, t_{m-1})$ allows to apply the split propagation algorithm [84]

$$\hat{u}(t_m, t_{m-1}) \approx e^{-\frac{i}{2} \int_{t_{m-1}}^{t_m} d\tau v'_{\text{EFF}}(\hat{\mathbf{r}}, \tau)} e^{-i \delta t \hat{T}_x} e^{-i \delta t \hat{T}_z} e^{-\frac{i}{2} \int_{t_{m-1}}^{t_m} d\tau v'_{\text{EFF}}(\hat{\mathbf{r}}, \tau)} \quad (4.47)$$

Here, v'_{EFF} includes the local part of Eq. (3.67), regularized in the atomic components, plus an imaginary optical potential, centered at the instantaneous position of the a-atom, that quenches all possible reflections at the grid boundaries; the kinetic energy operator is written in cylindrical coordinates with parallel component

$$\langle \mathbf{r} | \hat{T}_x = -\frac{1}{2\sqrt{r_{\parallel}}} \frac{\partial}{\partial r_{\parallel}} \left(r_{\parallel} \frac{\partial}{\partial r_{\parallel}} \right) \frac{1}{\sqrt{r_{\parallel}}} \langle \mathbf{r} |, \quad (4.48)$$

since the initial wavefunction has the symmetry of s -orbitals and orthogonal component

$$\langle \mathbf{r} | \hat{T}_z = -\partial^2 / (\partial z)^2 \langle \mathbf{r} |. \quad (4.49)$$

Both \hat{T}_x and \hat{T}_z are discretized over the grid

$$x_p = p \Delta x, z_m = m \Delta z, \quad (4.50)$$

with $1 \leq p \leq 500$, and $-700 \leq z \leq 700$ au, using a three-point differentiation formula, and the Crank–Nicholson algorithm is applied via diagonalization of a tridiagonal matrix in order to obtain $f_a(\mathbf{r}, t)$, at every time step [43]. We have calculated the spatial probability density

$$p_a(r_{\parallel}, z, t) = \int d\phi |\langle r_{\parallel}, \phi, z | \psi_a(t, t_F) \rangle|^2 \quad (4.51)$$

for the ejected atomic electron in the case of $Au^-/Au(100)$ and $Ag^-/Ag(100)$ systems. In Figs. (4.10) and (4.11) we show spatial probability densities obtained for Au and Ag .

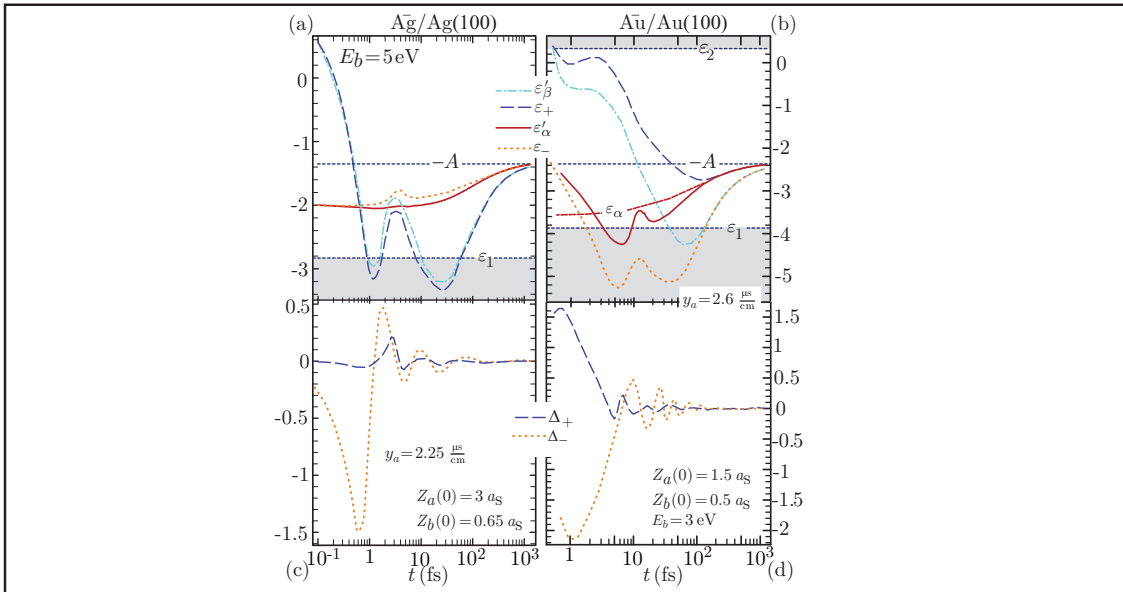


Figure 4.10: Spatial probability density (4.51) for $Au^-/Au(100)$. The contour lines are calculated at values $p_a = \eta p_{a,\max}^0$, where $p_{a,\max}^0$ denote the maximum of the spatial probability distribution associated with the unperturbed affinity wavefunction $\langle \mathbf{r} | a(t_F) \rangle$

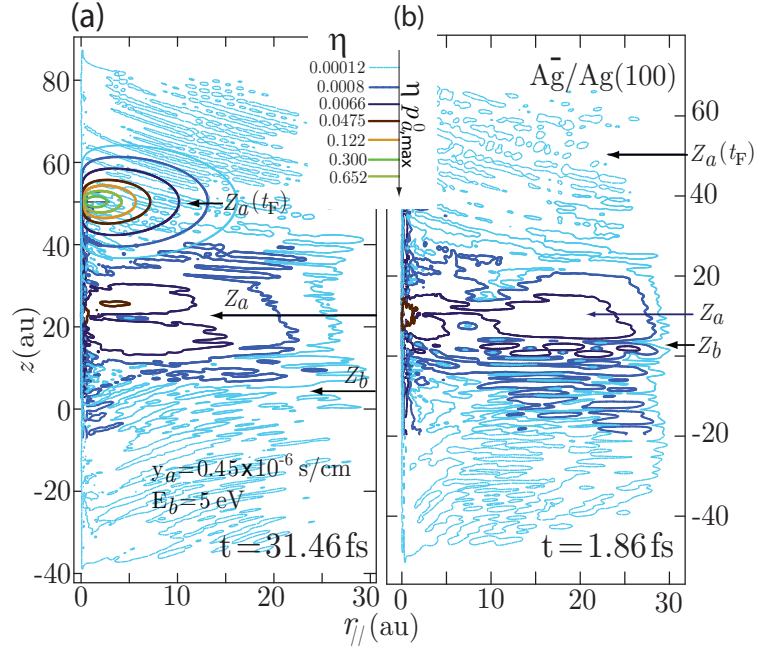


Figure 4.11: Spatial probability density (4.51) for $Ag^-/Ag(100)$, at two different time steps. The contour lines are calculated at values $p_a = \eta p_{a,\max}^0$, where $p_{a,\max}^0$ is defined as in Fig. (4.10)

From the knowledge of $f_a(\mathbf{r}, t)$, the retarded Green's function (4.41) can be determined at every time step by the following relation, numerically calculated

$$G_{\mathbf{a}\mathbf{k}}^+(t, t_F) = -2\pi i \int dz \langle z | k_{\perp} \rangle \int_0^{\infty} dr_{\parallel} f_a^*(\mathbf{r}, t) J_0(k_{\parallel} r_{\parallel}), \quad (4.52)$$

in which J_0 labels the Bessel function and k_{\perp} (k_{\parallel}) the parallel/perpendicular components of the electron wave-vector relative to the surface. This quantity allows to compare the WPP and the spectral decomposition methods via the probability density $P_a^0(\varepsilon_{\mathbf{k}})$ that a band electron occupying the unperturbed solid at the instant of ejection will be

transferred to the state $|a(t = t_F)\rangle$

$$P_a^0(\varepsilon_{\mathbf{k}}) = \rho(\varepsilon_{\mathbf{k}}) \int d^2\Omega_{\mathbf{k}} |G_{\alpha\mathbf{k}}^+(0, t_F)|^2. \quad (4.53)$$

In Fig. (4.12) we show that both approaches yield a similar trend for $P_a^0(\varepsilon_{\mathbf{k}})$, at least in the case $Au^-/Au(100)$ and $Ag^-/Ag(100)$. Thus, they can be used independently or comparatively in future applications to other double ion-surface systems.

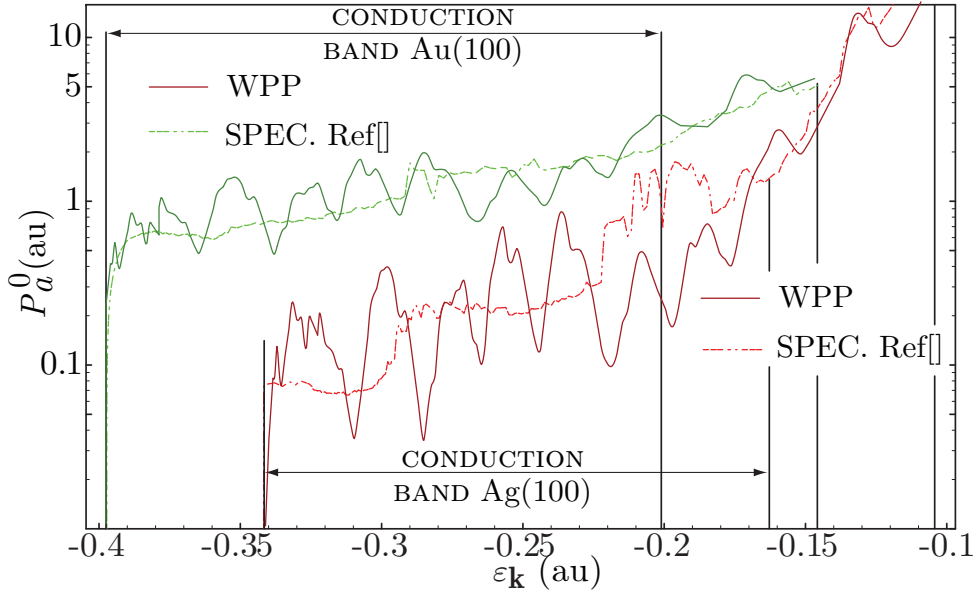


Figure 4.12: The tunnelling probability density (4.53) is calculated for $Ag^-/Ag(100)$ and $Au^-/Au(100)$ either with the WPP or with the spectral method.

Conclusions.

The thesis has covered the problem of electronic processes induced by slow ion-surface interaction. There are several motivations which induced us to develop the topic of non adiabatic excitations induced in a many electronic system, perturbed by a semiclassical probe. First of all, ion spectroscopy is a unique tool to probe the electronic structure of the first layers of the target. We can obtain information on ionization/neutralization of projectiles, the mechanisms of electron and photon emission, and the characteristics of sputtered particles from the solid. Besides, the developing of ion spectroscopy is attractive from a practical point of view. In general, the interaction of an ion impinging on a target material presents a highly dynamic many-body problem that should take into account the trajectory followed by the projectile, the geometric structure of the target material, the (multi-)electron exchange between target and projectile as well as the accompanying excitation of both collision partners. At present, most models handle the trajectories followed by the projectile classically while they combine both classical and quantum mechanical concepts in the treatment of the electronic ion-target system. The classical treatments of ion trajectories make extensive use of Molecular Dynamics codes. The electronic ion-target system is mostly treated in terms of a model Hamiltonian formalizing the interaction between the discrete electronic projectile levels and the valence bands of the material. Electron transfer occurs usually either by one electron processes, such as in resonant electron tunneling, or by two electron Auger-type processes, such as Auger neutralization or Resonant neutralization followed by Auger De-excitations.

In this work, particular attention was paid to Auger neutralization of the projectile and the kinetic energy distributions of emitted electrons due to ion neutralization. Moreover, resonant charge neutralization due to sputtering was treated.

For Auger Neutralization the starting point is the Hagstrum model. His goal consisted in obtaining the kinetic distribution of emitted electrons, rather than obtaining the transition rate from calculations of matrix elements. The kinetic energy distribution of emitted electrons, in this model, is given by the convolution of three functions: the inner spectrum of excited electrons, the probability that the ion is neutralized at a given distance from surface and the function probability that an electron can leave surface. This scheme is still valid now, in new models; just the shapes of these functions vary. A typical experimental characteristic of Auger spectra is the asymmetric shape of kinetic energy distribution of emitted electrons: there is a broadening of tails at high energies. Broadening is evident for all the possible ion-surface combinations, and becomes more and more important at higher energies. In the theory this effect is taken into account through a convolution of the pure spectrum with a broadening function characterized principally by a lorentzian trend. Considering as starting point Hagstrum model's, Monreal and Apel were able to explain an important feature of experimental spectra: the existence of a magic energy, i.e. there exists an energy for which the spectra of a given ion/surface system intersect in spite of variation of kinetic energy of projectile. However the effect of broadening in tails, could not be explained considering the classical broadening causes, such as the finite lifetime of the initial and final states, the electron-phonon interaction at room temperature, etc. The exponential trend of spectra after the magic point can be explained just if we consider many body shake-up.

In this thesis we obtained the kinetic distribution of emitted electrons starting from the Fermi's golden rule, proportional to the transition rate. We have proposed a generalized time dependent Anderson-Newns Hamiltonian. The total Hamiltonian is written in second quantization, and we calculated numerically matrix elements through algorithm implemented by the software Mathematica [74]. From this calculation, naturally derives the new interaction term of many body shake-up. It is a form of collective response of the metal target due to the abrupt change of charge of the projectile during neutralization. It causes permanent deformations in the conduction band, because the final

states of electrons which do not participate to Auger neutralization are not orthogonal to the initial states. This final-state effect is similar to the sudden creation of a core hole, by absorption of a soft X-ray photon. Many body shake-up was first observed in experiments of Ar^+ impact on Al/surfaces, in the exponential tailing of the kinetic energy distributions of ejected electrons. We have applied the formalism developed in the thesis to the $\text{Ar}^+/\text{Al}(111)$ system at varying projectile kinetic energies and incident angles. We used a semiempirical one electron potential to describe both the plane metal surface, of defined symmetry, and the impinging ion, together with its image charge, while in other works Jellium model was used for surface. In addition, we assume the electron–electron interaction to be of the Yukawa form. We discussed the variation of the broadening parameters with the projectile perpendicular velocity and show excellent agreement between theory and experiments.

We are developing models to improve the understanding of sub-threshold, kinetic electron emission processes from bombarded metal surfaces. We also intend to extend modeling of many body shake up in Auger processes to other projectile target combinations.

Our future research activity will be more devoted to the study of ion induced electron excitations in nanostructured materials. In particular, we intend to study many body effects in Auger core-valence-valence processes. The idea is to combine our Knowledge in Auger electron emission from solids with some peculiarities of the response of the band structure of nanostructured materials to a sudden perturbation.

Electron transfer and excitations phenomena in secondary atomic emission from ion-bombarded solids are subjects of continuous interest and debate. The lack of information on the physical and chemical environment within the surface region of target materials reflects in the unclear understanding of the underlying mechanisms responsible for secondary ion formation and escape. Among them, there is the problem of positive and negative ionization of secondary atoms sputtered from solid surfaces. In recent years, considerable progress has been achieved in the theoretical description of resonant electron exchanges between an atomic particle and a crystal surface, for which non-perturbation methods have been developed and applied. Some experimental and theoretical studies have tried to identify the main ionization/neutralization mechanisms active during ejection. One of these, predominating at higher emission energies ($\gtrsim 100$ eV) is well

explained by resonant electron tunneling between the ejected particle and the target. Another one was observed at lower emission energies ($\lesssim 40$ eV) and described with a model accounting for quasi molecular correlations between the secondary emitted and their nearest-neighbor substrate atoms, put in motion by the collision cascade, during ejection. In the thesis we considered resonant ionization of negatively charged, single-valence ions sputtered off (100)-metal surfaces. We treated the problem through two methods: the spectral method and the wave packet propagation one. In the first case we used the formalism of the generalized time dependent Anderson-Newns Hamiltonian, already applied to AN of Ar^+ on Al surface. We have provided an application to the $\text{Ag}^-/\text{Ag}(100)$ and $\text{Au}^-/\text{Au}(100)$ -systems. Surface effects were considered in the form of transient QM correlations in the diatomic systems formed between secondary emitted atoms and their nearest-neighbor substrate atoms both ejected in the collision cascade. We have formulated the electron problem in terms of two, spatially-correlated discrete states interacting with a continuous of metal states, reducing the calculation of the ionization probability to the numerical solution of a matrix equation. We used a pseudo-potential to describe surface, the same used for AN, which takes into account the effect of a projected band gap in the metal band structure. Besides, we modeled the motion of ejected atoms with simple analytical trajectories. We developed a theory depending on some free parameters, related to the trajectories of the di-atomic system, whose numerical solution produced excellent agreement with a series of experiments. Results suggest that the final ionization probability is weakly influenced either by the band structure of the material or by many body correlations in sputtered atomic species, while it depends on the width of the projected band gap. Another significant question relates to the analytical continuation to negative times used as a mathematical tool to determine the initial distribution of metal electrons. Different models for such a distribution change the calculation of the Hamiltonian at short times when the emitted atom is close to the surface. Thus, a more realistic model is certainly needed to better estimate the initial shifts and the broadenings of the two level system. Recently, particular attention has been devoted to the space-time evolution of the atomic wave-function of the secondary emitted particles. It has been presented a WPP study of the evolution of the affinity orbital of a secondary ion, ejected from a sputtered metal surface in presence of another

surface ion. The great advantage in using WPP consists in explicitly time-dependent Hamiltonians and emission of particles in the continuum. We have focussed on the influence of quasi molecular correlations on the spatial probability density of the ejected atomic electron. We have observed that a sort of transient covalent bonding is formed during ejection, between the two atomic particles. The latter has a long duration- on the femtosecond scale, even at relatively high emission energies, of the order of 100 eV. We have compared the WPP approach with the spectral decomposition method, specifically examining the $\text{Au}^-/\text{Au}(100)$ and $\text{Ag}^-/\text{Ag}(100)$ systems. It is the first time that the WPP was applied to these systems. From a preliminary analysis, we have found a good agreements between the two methods, although, further investigations will be devoted to this last topic. We intend to include molecular dynamics calculations for the trajectories of both projectiles and sputtered atomic species into the generalized Anderson-Newns Hamiltonian. Particular attention will be devoted to recent experiments of low energy Na bombardment of clean Cu surfaces, that have shown different charge transfer rates for different projectile trajectories.

Bibliography

- [1] H. Winter, Kinetic Electron Emission for Grazing Scattering of Atoms and Ions from Surfaces, in: H.P. Winter, J. Burgdörfer (Ed.), *Slow Heavy-Particle Induced Electron Emission from Solid Surfaces*, Springer, 2006;
- [2] E.V. Alonso, M. A. Alurralde, and R. A. Baragiola, Surf. Sci. 166, L155 (1986).
- [3] A. Duvenbeck, O. Weingart, V. Buss and A. Wucher, New J. Phys. 9 38
- [4] J. Lorincik, Z. Sroubek, H. Eder, F. Aumayr, H.P. Winter, Phys. Rev. B 62, 16116 (2000);
- [5] R.A. Baragiola, Electron Emission from Slow Ion-Solid Interaction, in: J.W. Rabalais (Ed.), *Low Energy Ion-Surface Interactions*, John Wiley & Sons Ltd, 1994; R.A. Baragiola, Nucl. Instr. and Meth. B 78, 223 (1993);
- [6] F. Aumayr and H.P. Winter, 3 Potential Electron Emission from Metal and Insulator Surfaces, in: H.P. Winter, J. Burgdörfer (Ed.), *Slow Heavy-Particle Induced Electron Emission from Solid Surfaces*, Springer, 2006;
- [7] R.A. Baragiola and C. Monreal, Electron Emission from Surfaces Mediated by Ion-Induced Plasmon Excitation, in: H.P. Winter, J. Burgdörfer (Ed.), *Slow Heavy-Particle Induced Electron Emission from Solid Surfaces*, Springer, 2006;
- [8] H.D. Hagstrum, Phys. Rev. 96, 336 (1954); Phys. Rev. 96, 325 (1954); Phys. Rev. 122, 83 (1961); J. Appl. Phys. 32, 1015 (1961); J. Appl. Phys. 32, 1020 (1961);

- [9] M.A. Cazalilla, N. Lorente, R. Díez Muiño, J.P. Gauyacq, D. Teillet-Billy, P.M. Echenique, Phys. Rev. B 58, 13991 (1998);
- [10] R.A. Baragiola, C.A. Dukes, Phys. Rev. Lett. 76, 2547 (1996);
- [11] P. Riccardi, P. Barone, A. Bonanno, A. Oliva, R.A. Baragiola, Phys. Rev. Lett. 84, 378 (2000);
- [12] A. Sindona, R.A. Baragiola, G. Falcone, A. Oliva and P. Riccardi, Phys. Rev. A 71, 052903 (2005); A. Sindona, R.A. Baragiola, S. Maletta, G. Falcone, A. Oliva and P. Riccardi, Nucl. Instr. and Meth. B 230, 298 (2005);
- [13] P.W. Anderson, Phys. Rev. 124, 41 (1961); D.M. Newns, Phys. Rev. 178, 1123 (1969);
- [14] J.K. Nørskov, B.I. Lundqvist, Phys. Rev. B 19, 5661 (1979);
- [15] Z. Sroubek, Surf. Sci. 44, 47 (1974);
- [16] Z. Sroubek, Phys. Rev. B 25, 6046 (1982);
- [17] A. Sindona, G. Falcone, Surf. Sci. 423, 99 (1999);
- [18] A. Sindona, P. Riccardi, S. Maletta, S.A. Rudi, G. Falcone, Nucl. Instr. and Meth. B 256, 468 (2007);
- [19] A. Sindona, S.A. Rudi, S. Maletta, R.A. Baragiola, G. Falcone, P. Riccardi, Nucl. Instr. and Meth. B 257, 438 (2007); A. Sindona, S.A. Rudi, S. Maletta, R.A. Baragiola, G. Falcone, P. Riccardi, Surf. Sci. 601, 1205 (2007);
- [20] M.L.E. Oliphant, Proc. Roy. Soc. (Lond.) A 124, 228 (1929);
- [21] M.L.E. Oliphant and P.B. Moon, Proc. Roy. Soc. (Lond.) A 127, 388 (1930);
- [22] H.S.W. Massey, Proc. Cambridge Phil. Soc. 26, 386 (1930); Proc. Cambridge Phil. Soc. 27, 469 (1931);
- [23] S.S. Shekhter, J. Exp. Theoret. Phys. (USSR) 7, 750 (1937);
- [24] A. Cobas and W.E. Lamb Jr., Phys. Rev. 65, 327 (1944);

- [25] H.D. Hagstrum, Y. Takeishi, and D.D. Pretzer, Phys. Rev. 139, A526 (1965); Y. Takeishi and H. D. Hagstrum, Phys, Rev. 137, A641 (1965); Y. Takeishi and H.D. Hagstrum, Surface Sci. 3, 175 (1965); D.D. Pretzer and H.D. Hagstrum, Surface Sci. 4, 265 (1966); H.D. Hagstrum and G.E. Becker, Phys. Rev. Lett. 16, 230 (1966); H.D. Hagstrum, Phys. Rev. 150, 495 (1966); H.D. Hagstrum, Science 178, 275 (1972); H.D. Hagstrum and G.E. Becker, Phys. Rev. B 4, 4187 (1971);
- [26] N.W. Ashcroft, N.D. Mermin, *Solid State Physics*, Saunders, Philadelphia, 1976;
- [27] P. A. Tipler and R. A. Llewellyn, *Modern Physics*, 3rd Ed., W.H. Freeman, 1999;
- [28] M. Remy, J. Chem. Phys. 53, 2487 (1970);
- [29] P. Nordlander, J.C. Tully, Phys. Rev. B 42, 5564 (1990);
- [30] J.W. Gadzuk, Phys. Rev. B 9, 1978 (1974);
- [31] T. Fonden and A. Zwartkruis, Phys. Rev. B 48, 15603 (1993);
- [32] B. Barbiellini and P.M. Platzman, New J. Phys. 8, 20 (2006);
- [33] J.A. Appelbaum and D.R. Hamann, Phys. Rev. B 12, 5590 (1975);
- [34] R. Monreal, S.P. Apell, Nucl. Instr. and Meth. B 83, 459 (1993);
- [35] N. Lorente, R. Monreal, M. Alducin, Phys. Rev. A 49, 4716 (1994); R. Monreal, N. Lorente, Phys. Rev. B 52, 4760 (1995);
- [36] N. Lorente, R. Monreal, M. Alducin, Phys. Rev. A 49, 4716 (1994);
- [37] R. Monreal, Surf. Sci. 388, 231 (1997);
- [38] N. Lorente, R. Monreal, Surf. Sci. 370, 324 (1997);
- [39] P. Sigmund, Phys. Rev. 184, 383 (1969);
- [40] G. Falcone, Rivista del Nuovo Cimento 13, 1 (1990);
- [41] P. Sigmund, A. Oliva, G. Falcone, Nucl. Instrum. Meth. 194, 541 (1982);
- [42] G. Falcone, P. Sigmund, Appl. Phys 25, 307 (1981);

- [43] A.G. Borisov, A.K. Kazansky and J.P. Gauyacq, Phys. Rev. Lett. 80, 1996 (1998);
A.G. Borisov, A.K. Kazansky, J.P. Gauyacq, Phys. Rev. B 59, 10935 (1999);
- [44] R. Brako and D.M. Newns, Surf. Sci. 108, 253 (1981);
- [45] R. Brako and D.M. Newns, J. Phys. C: Solid State Phys., 14, 3065 (1981);
- [46] R. Brako and D.M. Newns, Rep. Prog. Phys. 52, 655 (1989);
- [47] R.G. Hart, C.B. Cooper, Surf. Sci. 94, 105 (1980);
- [48] M.J. Vasile, Phys. Rev. B 29, 3785 (1984);
- [49] P.A.W. van Der Heide, Nucl. Instr. and Meth. B 157, 126 (1999);
- [50] H. Shao, D.C. Langreth, P. Nordlander, in: J.W. Rabalais (Ed.), *Low Energy Ion-Surface Interactions*, John Wiley & Sons Ltd, 1994;
- [51] A. Blandin, A. Nourtier and D.W. Hone, Le Journal de Physique (Colloque) 37, 369 (1976);
- [52] W. Bloss, D. Hone, Surf. Sci., 72, 277 (1978);
- [53] Z. Sroubek, J. Fine, Phys. Rev. B 51, 5635 (1995);
- [54] Z. Sroubek, G. Falcone, D. Aiello and C. Attanasio, Nucl. Instr. and Meth. B 88, 365 (1994);
- [55] G. Falcone and A. Sindona, Il Nuovo Cimento 20 D, 353 (1998);
- [56] A. Sindona, G. Falcone, Nucl. Instr. and Meth. B 157, 75 (1999);
- [57] A. Sindona, G. Falcone, Surf. Sci. 529, 471 (2003);
- [58] A. Sindona, P. Riccardi, G. Falcone, Nucl. Instr. and Meth. B 230, 449 (2005);
- [59] M. Gell-Mann, F. Low, Phys. Rev. 84, 350 (1951);
- [60] A. Messiah, *Quantum Mechanics*, Dover, New York, 1999;
- [61] D.V. Klushin, M.Yu. Gusev, S.A. Lysenko and I.F. Urazgil'din, Phys. Rev. B 54, 7062 (1996);

- [62] P.J. Jennings, R.O. Jones, M. Weinert, Phys. Rev. B 37, 6113 (1988);
- [63] E.V. Chulkov, V.M. Silkin, P.M. Echenique, Surf. Sci. 437, 330 (1999);
- [64] A.E.S. Green, D.L. Sellin, A.S. Zachor, Phys. Rev. 184, 1 (1969);
- [65] P. Nordlander, Phys. Rev. B 46, 2584 (1992);
- [66] B.M. Smirnov, Physics - Uspekhi 44 (3), 221 (2001);
- [67] G.D. Mahan, *Many-Particle Physics*, Plenum Press, New York, 1981; J.W. Negele, H. Orland, *Quantum Many-Particle Physics*, Addison-Wesley, 1988;
- [68] B.H. Bransden, C.J. Joachain, *Physics of Atoms and Molecules*, Longman Scientific & Technical, 1983;
- [69] M. A. Vicente Alvarez, V. H. Ponce, and E. C. Goldberg, Phys. Rev. B 57, 14919 (1998).
- [70] N.D. Lang, Phys. Rev. B 27, 2019 (1983);
- [71] M.A. Karolewski, Nucl. Instr. and Meth. B 230, 402 (2005);
- [72] M.H. Shapiro, E. Trovato, T.A. Trombello, Nucl. Instr. and Meth. B 180, 58 (2001);
- [73] L. Verlet, Phys. Rev. 159, 98 (1967); Phys. Rev. 165, 201 (1967).
- [74] *Mathematica 5.2*, Wolfram Research Inc., 2005;
- [75] P. Barone, A. Sindona, R.A. Baragiola, A. Bonanno, A. Oliva, P. Riccardi, Nucl. Instr. and Meth. B 209, 68 (2003);
- [76] M. Commisso, M. Minniti, A. Sindona, A. Bonanno, A. Oliva, R.A. Baragiola and P. Riccardi, Phys. Rev. B 72, 165419 (2005);
- [77] B.L. Burrows, A.T. Amos, Z.L. Miskovic, S.G. Davidson, Phys. Rev. B 51, 1409 (1995);
- [78] G.D. Mahan, Phys. Rev. 163, 612 (1967); Solid State Physics 29, 75 (1974);
- [79] B. Roulet, J. Gavoret, P. Nozières, Phys. Rev. 178, 1072 (1969); P. Nozières, J. Gavoret, B. Roulet, Phys. Rev. 178, 1084 (1969); P. Nozières, C.T. De Dominicis,

- Phys. Rev. 178, 1097 (1969);
- [80] S. Doniach, M. Šunjić, Proc. Phys. Soc., London (Solid State Physics) 3, 285 (1970);
- [81] P.H. Citrin, G.K. Wertheim, Y. Baer, Phys. Rev. Lett. 35, 855 (1975);
G.K. Werthaim, P.H. Citrin, Phys. Rev. B 16, 4256 (1977);
- [82] P. Kürpick, U. Thumm, Phys. Rev. A 54, 1487 (1996);
- [83] D.M. Newns and K. Makoshi, R. Brako and J.N.M. van Wunnik, Physica Scripta T6, 5 (1983); N.D. Lang and J.K. Nørskov, Physica Scripta T6, 15 (1983); J.N.M. van Wunnik and J. Los, Physica Scripta T6, 27 (1983);
- [84] R. Kosloff, J. Phys. Chem. 92, 2087 (1988);
- [85] H. Chakraborty, T. Niederhausen and U. Thumm, Phys. Rev. A 69, 052901 (2004);
- [86] V.A. Ermoshin, A.K. Kazansky, Physics. Letters A 218, 99 (1996);
- [87] A. Sindona, P. Riccardi, S. Maletta, S.A. Rudi, G. Falcone, Nucl. Instr. and Meth. B 258, 226 (2007);